MICROMECHANICAL DAMAGE THEORIES FOR BRITTLE SOLIDS WITH INTERACTING MICROCRACKS

J.W. JU

Department of Civil Engineering & Operations Research
Princeton University
Princeton, N.J. 08544

15 March 1993

Final Report

Prepared for
Air Force Office of Scientific Research
Building 410
Bolling AFB, D.C. 20332-6448

REPORT DOCUMENTATION PAGE

Form Approved
OMB No 0704-0188

1a. REPORT SECURITY CLASSIFICATION Unclassified	1b. RESTRICTIVE MARKINGS
2a. SECURITY CLASSIFICATION AUTHORITY N/A	3. DISTRIBUTION/AVAILABILITY OF REPORT Approved for public release; distribution is unlimited
2b. DECLASSIFICATION/DOWNGRADING SCHEDULE N/A	
4. PERFORMING ORGANIZATION REPORT NUMBER(S) PU/CEOR/SM-93-1	5. MONITORING ORGANIZATION REPORT NUMBER(S)
6a. NAME OF PERFORMING ORGANIZATION Princeton University 6b. OFFICE SYMBOL (If applicable)	7a. NAME OF MONITORING ORGANIZATION Air Force Office of Scientific Research
6c. ADDRESS (City, State, and ZIP Code) Dept. of Civil Engineering & Operations Research Princeton University	7b. ADDRESS (City, State, and ZIP Code) Building 410 Bolling AFB, D.C. 20332-6448
8a. NAME OF FUNDING/SPONSORING ORGANIZATION 8b. OFFICE SYMBOL (If applicable) NA	9. PROCUREMENT INSTRUMENT IDENTIFICATION NUMBER AFOSR-90-0336
8c. ADDRESS (City, State, and ZIP Code) AFOSR/NA Bolling AFB DC 20332-6448	10. SOURCE OF FUNDING NUMBERS PROGRAM ELEMENT NO: 61102F; PROJECT NO: 2302; TASK NO: CS; WORK UNIT ACCESSION NO:

11. TITLE (Include Security Classification)
Micromechanical Damage Theories for Brittle Solids with Interacting MIcrocracks

12. PERSONAL AUTHOR(S)
Ju, Jiann-Wen

13a. TYPE OF REPORT	13b. TIME COVERED	14. DATE OF REPORT (Year, Month, Day)	15. PAGE COUNT
Final	FROM 900901 TO 920831	930315	151

16. SUPPLEMENTARY NOTATION

17. COSATI CODES			18. SUBJECT TERMS (Continue on reverse if necessary and identify by block number)
FIELD	GROUP	SUB-GROUP	Micromechanical Damage Mechanics; Brittle Solids, Interacting Microcracks; Evolutionary Damage Models; Constitutive Modelling.

19. ABSTRACT (Continue on reverse if necessary and identify by block number)

Two-dimensional and three-dimensional statistical micromechanical damage models with randomly located interacting microcracks are presented to investigate the overall nonlinear mechanical responses of microcrack-weakened brittle solids. The macroscopic stress-strain relations of elastic solids with interacting micro-cracks are micromechanically derived by taking the ensemble average over all possible realizations. Several different approximate analytical solutions of a two-crack interaction model are introduced to account for micro-crack interaction among many randomly oriented and distributed microcracks. The overall elastic-damage compliances of microcrack-weakened brittle solids are also derived by further taking the volume average of the ensemble-averaged stress-strain relations over the entire material mesostructural domain. Some special examples are investigated by using the proposed framework. At variance with existing phenomenological damage models, the proposed framework does not employ any fitted"material parameters". "Cleavage 1" microcrack growth and "evolutionary damage models" within the proposed context are also presented.

20. DISTRIBUTION/AVAILABILITY OF ABSTRACT	21. ABSTRACT SECURITY CLASSIFICATION
☐ UNCLASSIFIED/UNLIMITED ☒ SAME AS RPT ☐ DTIC USERS	Unclassified

22a. NAME OF RESPONSIBLE INDIVIDUAL	22b. TELEPHONE (Include Area Code)	22c. OFFICE SYMBOL
Marlin Louis, Maj, USAF	202-767-6963	AFOSR/NA

PREFACE

This work was sponsored by the Air Force Office of Scientific Research and the Defense Nuclear Agency under Grant No. AFOSR-90-0336. This support and the interest and comments of Dr. Spencer Wu, Major Martin Lewis, Dr. Paul Senseny and Dr. Kent Goering are gratefully acknowledged.

ABSTRACT

Two-dimensional and three-dimensional statistical micromechanical damage models with randomly located interacting microcracks are presented to investigate the overall nonlinear mechanical responses of microcrack-weakened brittle solids. The macroscopic stress-strain relations of elastic solids with interacting micro–cracks are micromechanically derived by taking the *ensemble average* over all possible realizations. Several different approximate analytical solutions of a two-crack interaction model are introduced to account for micro–crack interaction among many randomly oriented and located microcracks. The overall elastic-damage compliances of microcrack-weakened brittle solids are also derived by further taking the *volume average* of the *ensemble-averaged* stress-strain relations over the entire material mesostructural domain. Some special examples are investigated by using the proposed methods. At variance with existing phenomenological damage models, the proposed framework does not employ any fitted "material parameters". "Cleavage 1" microcrack growth and "evolutionary damage models" within the proposed context are also presented.

LIST OF PUBLICATIONS AND PRESENTATIONS

[1] "Effective Elastic Moduli of Two-Dimensional Brittle Solids with Interacting Microcracks. Part I: Basic Formulations" (with T.M. Chen), *J. of Appl. Mech.*, ASME, in press.

[2] "Effective Elastic Moduli of Two-Dimensional Brittle Solids with Interacting Microcracks. Part II: Evolutionary Damage Models" (with T.M. Chen), *J. of Appl. Mech.*, ASME, in press.

[3] "A Three-Dimensional Statistical Micromechanical Theory for Brittle Solids with Interacting Microcracks" (with K.H. Tseng), *Int. J. of Damage Mechanics*, Vol. 1, No. 1, pp. 102-131, Jan. 1992.

[4] "An Improved Two-Dimensional Statistical Micromechanical Theory for Elastic Solids with Accurate Microcrack Interaction Formulations" (with K.H. Tseng), to be submitted for publication.

[5] *Damage Mechanics in Engineering Materials*, Ed. by J.W. Ju, D. Krajcinovic, and H.L. Schreyer, AMD-Vol. 109 and MD-Vol. 24, ASME Press, New York, November 1990, ISBN No. 0-7918-0554-9, 276 pages.

[6] *Recent Advances in Damage Mechanics and Plasticity*, Ed. by J.W. Ju, AMD-Vol. 132 and MD-Vol. 30, ASME Press, New York, April 1992, ISBN No. 0-7918-0902-1, 297 pages.

[7] *Damage Mechanics and Localization*, Ed. by J.W. Ju and K.C. Valanis, AMD-Vol. 142 and MD-Vol. 34 ASME Press, New York, November 1992, ISBN No. 0-7918-1086-0, 167 pages.

[8] "On Two-Dimensional Micromechanical Damage Models for Brittle Solids with Interacting Microcracks", in *Micromechanics of Failure of Quasi-Brittle Materials*, pp. 105-114, Ed. by S.P. Shah, S.E. Swartz, and M.L. Wang, Elsevier Applied Science, London and New York, 1990.

[9] "On Two-Dimensional Statistical Micromechanical Damage Models for Brittle Solids with Interacting Microcracks", in *Damage Mechanics in Engineering Materials*, pp. 17-26, Ed. by J.W. Ju, D. Krajcinovic, and H.L. Schreyer, AMD-Vol. 109 and MD-Vol. 24, ASME Press, New York, November, 1990, ISBN 0-7918-0554-9, 1990 ASME Winter Annual Meeting, held at Dallas, Texas, November 26-28, 1990.

[10] "On Statistical Micromechanical Process Damage Models for Brittle Solids with Interacting Microcracks", in "*Mechanics Computing in 1990's and Beyond*", Proceedings of the 1991 ASCE Engineering Mechanics Specialty Conference (held at the Ramada University Hotel, Columbus, Ohio, May 20-22, 1991), Vol. 2, pp. 1122-1126, ASCE Press, ISBN 0-87262-804-3.

[11] "On Statistical Micromechanical Theories for Brittle Solids with Interacting Microcracks", in "*Local Mechanics Concepts for Composite Material Systems*", edited by J.N. Reddy and K.L. Reifsnider, Proceedings of the 1991 IUTAM Symposium held at Blacksburg, Virginia, pp. 117-139, Springer-Verlag, Berlin Heidelberg 1992, ISBN 3-540-55547-1 and ISBN 0-387-55547-1.

[12] "On Statistical Micromechanical Damage Models for Brittle Solids with Interacting Microcracks", in Proceedings of the Third International Conference on Computational Plasticity: Fundamentals and Applications, (held at Univ. Politecnica de Catalunya, Barcelona, Spain, April 6-10, 1992), Part II, pp. 1467-1478, Pineridge Press, Swansea, U.K., ISBN 0-90667-479-4.

[13] "Recent Development in Two-Dimensional Micromechanical Theories for Elastic Solids with Interacting Microcracks" (with K.H. Tseng), in "*Recent Advances in Damage Mechanics and Plasticity*", pp. 91-102, Ed. by J.W. Ju, AMD-Vol. 132 and MD-Vol. 30, ASME Press, New York, April 1992, ISBN 0-7918-0902-1, 1992 ASME Summer Mechanics Conference, held at Tempe, Arizona, April 28 - May 1, 1992.

[14] "Two-Dimensional Statistical Micromechanical Models for Microcracked Brittle Solids" (with K.H. Tseng), in Proceedings of 1992 ASCE Engineering Mechanics Conference, pp. 361-364, Ed. by L.D. Lutes and J.M. Niedzwecki, ASCE Press, New York, May 1992, ISBN 0-87262-867-1, held at College Station, Texas, May 24-27, 1992.

[15] "An Improved Two-Dimensional Statistical Micromechanical Theory for Elastic Solids with Accurate Microcrack Interaction Models" (with K.H. Tseng), in *Damage Mechanics and Localization*, pp. 69-82, Ed. by J.W. Ju and K.C. Valanis, AMD-Vol. 142 and MD-Vol. 34, ASME Press, New York, November 1992, ISBN 0-7918-1086-0, 1992 ASME Winter Annual Meeting, held at Anaheim, California, November 8-13, 1992.

[16] "An improved two-dimensional statistical micromechanical theory for elastic solids with accurate microcrack interaction models", 1992 ASME Winter Annual Meeting, Symposium on *Damage Mechanics and Localization*, Anaheim, California, November 11, 1992.

[17] "An improved two-dimensional statistical micromechanical theory for brittle solids with randomly located interacting microcracks", Department of Mechanical and Industrial Engineering, New Jersey Institute of Technology, October 21, 1992.

[18] "Two-dimensional statistical micromechanical models for microcracked brittle solids", 1992 ASCE Engineering Mechanics Specialty Conference, Session on "Material Softening and Damage Mechanics", Texas A&M University, College Station, Texas, May 25, 1992.

[19] "On statistical micromechanical models for brittle solids with randomly located interacting microcracks", School of Aerospace Engineering, Georgia Institute of Technology, May 14, 1992.

[20] "Recent development in two-dimensional statistical micromechanical theories for brittle solids with interacting microcracks", 1992 ASME Summer Mechanics

Meeting, Symposium on *Computational Models and Methods in Composites*, Arizona State University, Tempe, Arizona, April 29, 1992.

[21] "On statistical micromechanical theories for brittle solids containing interacting microcracks", Third International Conference on Computational Plasticity, Session on Damage Mechanics, Univ. Politecnica de Catalunya, Barcelona, Spain, April 9, 1992.

[22] "A complete second order statistical micromechanical theory for brittle solids with microcracks", Society of Engineering Science 28th Annual Technical Meeting, Composites Symposium, University of Florida, Gainesville, November 8, 1991.

[23] "Two- and three-dimensional second order statistical micromechanical theories for brittle materials with interacting microcracks", International Union of Theoretical and Applied Mechanics Symposium on "Local Mechanics Concepts for Composite Material Systems", Virginia Polytechnic Institute and State University, Blacksburg, Virginia, October 29, 1991.

[24] "On statistical micromechanical process damage models for brittle solids with interacting microcracks", ASCE Enginnering Mechanics Specialty Conference, Session on "Micromechanics, Creep, and Rate Effects in Geomaterials", Columbus, Ohio, May 21, 1991.

[25] "On statistical micromechanical evolutionary damage models for brittle solids", Department of Theoretical and Applied Mechanics, University of Illinois at Urbana-Champaign, February 13, 1991.

[26] "On two-dimensional statistical micromechanical damage theories for brittle solids with interacting microcracks", ASME Winter Annual Meeting, Symposium on "Damage Mechanics in Engineering Materials", Dallas, Texas, November 26, 1990.

Table of Contents

PART I

Effective Elastic Moduli of Two-Dimensional Brittle Solids with Interacting Microcracks. I : Basic Formulations

I.0. Abstract

Statistical micromechanical formulations are presented to investigate effective elastic moduli of two-dimensional brittle solids with interacting *slit* microcracks. The macroscopic stress-strain relations of elastic solids with interacting microcracks are micromechanically derived by taking the *ensemble average* over all possible realizations which feature the same material microstructural geometry, characteristics, and loading conditions. Approximate analytical solutions of a two-microcrack interaction problem are introduced to account for microcrack interaction among many randomly oriented and located microcracks. The overall elastic-damage compliances of microcrack-weakened brittle solids under uniaxial and biaxial loads are also derived. Therefore, stationary statistical micromechanical formulation is completed. Moreover, some special cases are investigated by using the proposed framework. At variance with existing phenomenological continuum damage models, the proposed framework does not employ any fitted "material parameters". "Cleavage 1" microcrack growth and "evolutionary damage models" within the proposed context will be presented in Part II of this series. It is emphasized that microstructural statistical informations are already embedded in the proposed ensemble-averaged equations and, therefore, no Monte Carlo simulations are needed.

I.1. Introduction

The nonlinear mechanical responses of damaged solids due to the existence, growth, and nucleation of microdefects (such as microcracks and microvoids) are of significant importance to engineers, and have been the subject of many investigations. See Krajcinovic (1989) for a literature review on damage mechanics. For brittle materials (e.g., concrete, rocks and ceramics), in particular, microcracks often control overall deformation and failure mechanisms. To date, the only exact results derived for microcrack-weakened brittle solids are for dilute microcrack concentrations, where microcrack interactions are entirely neglected (i.e., "Taylor's models"). On the other hand, "effective medium methods" were proposed in the literature to account for interaction effects of microcracks. For example, the "self-consistent method" [Hill (1965)] was first applied to microcrack-weakened solids by Budiansky and O'Connell (1976) with special attention directed to perfectly randomly distributed and *weakly* interacting microcracks. The self-consistent method was further developed by Horii and Nemat-Nasser (1983) to take into account the effects of *closed* microcracks undergoing frictional sliding. Christensen and Lo (1979) proposed a three-phase "generalized self-consistent model". The "differential scheme" was investigated by Roscoe (1952, 1973), McLaughlin (1977), and Hashin (1988). Further, the "Mori-Tanaka method" was developed by Mori and Tanaka (1973), Benveniste (1986), and Zhao, Tandon and Weng (1989). Some comparisons and assessments for the self-consistent method, the generalized self-consistent method, the Mori-Tanaka method, and/or the differential scheme were also presented by Horii and Sahasakmontri (1990), Laws and Dvorak (1987), Nemat-Nasser and Hori (1990), and Christensen (1990, for pure shear load only). It is noted that the foregoing effective medium methods are only valid for *low* microcrack concentrations since they do **not** depend on locations of microcracks.

All of the aforementioned work can be categorized as "*stationary*" micromechanical models since all microcracks are assumed to be *stationary*; i.e., no microcracks are allowed to grow or nucleated during loading histories. For a constitutive theory to possess *predictive* capability, however, an "*evolutionary*" micromechanical damage model is warranted to account for "cleavage 1" (pre-existing) microcrack growth and/or "cleavage 2" (new) microcrack nucleation. In the current literature, there are indeed a number of micromechanical "evolutionary" damage models available. See, e.g., Krajcinovic and Fanella (1986), Fanella and Krajcinovic (1988), and Ju (1991b) by using the "Taylor's model"; as well as Sumarac and Krajcinovic (1987, 1989), Krajcinovic and Sumarac (1989), Ju (1991a), Ju and Lee (1991), and Lee and Ju (1991) by using the self-consistent method.

When microcrack concentrations are higher and microcrack spacings are closer, *strong* microcrack interactions occur and effective medium theories are no longer appropriate. Emanating from this viewpoint, excellent strong microcrack interaction models were proposed by Gross (1982), Horii and Nemat-Nasser (1985), Hori and Nemat-Nasser (1987) for two-dimensional deterministic microcracks, and by Kachanov and Montagut (1986), Kachanov (1987), Chudnovsky et al. (1987a,b), and Kachanov and Laures (1989) for two- and three-dimensional *deterministic* arbitrary microcrack arrays. The foregoing work, nevertheless, are only *stationary* strong microcrack interaction models. Moreover, the work due to Kachanov (1987), Kachanov and Laures (1989) rely on Monte Carlo simulations of deterministic microcrack arrays, and depend on heavy numerical computations of stress "transmission factors". Therefore, it is desirable to develop simple *statistical* micromechanical theories to account for interactions among many randomly located and oriented microcracks. Furthermore, "cleavage 1" microcrack growth models are needed under the condition of microcrack interaction.

The purpose of the present work (Part I and Part II) is to establish a statistical micromechanical framework for deriving "evolutionary" damage models and corresponding constitutive equations for brittle solids containing many interacting, randomly distributed *slit* microcracks. The proposed statistical framework considers the probability and conditional probability density functions of microcrack locations, orientations, lengths, and relative configurations. See Batchelor (1970), Batchelor and Green (1972), Hinch (1977), Willis and Acton (1976), Chen and Acrivos (1978a,b) for references. In addition, the *ensemble-volume* averages of stresses, strains and compliances are systematically constructed based on analytical micromechanics solutions and probability functions. It is emphasized that the proposed method is very different from that proposed by Hudson (1980, 1981, 1986). Though using the ensemble average approach, Hudson's method is based on a second-order *stiffness* theory and therefore leads to irrational behavior for solids with moderate or high microcrack concentrations [see Sayers and Kachanov (1991)]. The proposed approach is free from this anomaly.

A brief outline of this work is as follows. In Section 2, an *ensemble-average* approach to derive damaged stress-strain relations is introduced. Approximate closed-form analytical solutions are subsequently presented for the interaction problem of two arbitrarily located and oriented (but non-intersecting) microcracks. The overall elastic moduli of a statistically representative volume element are then derived. In Section 3, applications are made to a number of special cases. In particular, for the dilute microcrack concentration case, the present approach recovers the well-known

Taylor's model by neglecting interactions among microcracks. When all microcracks are *open* and perfectly randomly distributed, the proposed approach shows that the overall compliance matrix becomes isotropic. A comparison between the present method and the self-consistent method is also discussed in this isotropic damage case.

I.2. An ensemble-average approach to microcrack interaction and effective moduli

I.2.1. Background

Consider a statistical realization within a statistical RVE (in the probability space) of a microcrack-weakened solid. The volume of the statistical RVE is V, and the exterior surface is subjected to prescribed traction $\boldsymbol{\sigma}^{\infty}$. Let a and n be the average microcrack radius and the average number of microcracks per unit volume, respectively. A typical avenue to describe mechanical responses of a statistical RVE is to relate the volume-averaged strain $\bar{\boldsymbol{\epsilon}}$ to the volume-averaged stress $\bar{\boldsymbol{\sigma}}$. It is well known that

$$\bar{\boldsymbol{\epsilon}} = \mathbf{S}^{\circ} : \bar{\boldsymbol{\sigma}} + \frac{1}{V}\int_{S_I} \frac{1}{2}\left(\llbracket \mathbf{u} \rrbracket \otimes \mathbf{n} + \mathbf{n} \otimes \llbracket \mathbf{u} \rrbracket\right)\, dS_I \tag{1}$$

where $\mathbf{S}^{\circ}$ is the virgin elastic compliance tensor for the matrix material; $\llbracket \mathbf{u} \rrbracket$ and $\mathbf{n}$ are the microcrack opening displacement vector and the unit normal vector on discontinuity surface, respectively. Moreover, S_I represents the *union* of all discontinuity (microcrack) surfaces (see Fig. 1).

Following the common assumption $\bar{\boldsymbol{\sigma}} \approx \boldsymbol{\sigma}^{\infty}$, the microcrack-induced strain reads

$$\bar{\boldsymbol{\epsilon}}^{*} \approx \frac{1}{V}\int_{S_I} \frac{1}{2}\left(\llbracket \mathbf{u} \rrbracket \otimes \mathbf{n} + \mathbf{n} \otimes \llbracket \mathbf{u} \rrbracket\right)\, dS_I \tag{2}$$

I.2.2. Ensemble average of microcrack-induced strains

In this section, a systematic approach of forming the ensemble-averaged strains and microcrack interaction-induced local *stress perturbations* are presented. The basic idea behind this approach is that the *local* constitutive relation at a typical *point* within a statistical RVE of a microcrack-weakened solid should be obtained by averaging over the ensemble of all *statistical realizations*, including the locations, orientations, lengths and relative configurations of randomly distributed microcracks. This approach was first applied to the study of fluid suspensions; see Batchelor(1970), Batchelor and Green (1972), and Hinch(1977). The ensemble average approach was later applied to interacting inclusions of solid composite materials by Willis and Acton (1976), and Chen and Acrivos (1978a,b). It is emphasized that local displacements, strains and stresses vary with *positions* within a RVE. An average over the values of physical quantities occurring in a very large number of realizations is an ensemble average, which will be denoted by angle brackets.

Let us consider a two-phase composite statistical RVE (composed of a linear elastic brittle matrix and inclusions) subjected to external load $\boldsymbol{\sigma}^{\infty}$. The local constitutive law at a material point $\mathbf{x}$ may be expressed as

$$\boldsymbol{\epsilon}(\mathbf{x}) = \mathbf{S}^{\circ} : \boldsymbol{\sigma}(\mathbf{x}) + \boldsymbol{\epsilon}^{*}(\mathbf{x}, C) \tag{3}$$

where ϵ and σ are the local strain and stress, respectively. Furthermore, ϵ^* is a perturbed strain function which is *zero* if $\mathbf{x}$ is a point in the matrix and is non-zero if $\mathbf{x}$ is a point in an inclusion. Obviously, ϵ^* depends on the full configuration of all inclusions (denoted by C). The constitutive law (3) can be easily statistically (ensemble) averaged:

$$\langle\epsilon\rangle(\mathbf{x}) = \mathbf{S}^o : \langle\sigma\rangle(\mathbf{x}) + \langle\epsilon^*\rangle(\mathbf{x}) \tag{4}$$

In addition, the ensemble-average of ϵ^* at $\mathbf{x}$ (considered to be non-zero because it lies in an inclusion centered at $\mathbf{x}_1$) is (assuming inclusions do *not* intersect one another):

$$\langle\epsilon^*\rangle(\mathbf{x}) = \int_{\mathbf{x}\in\Omega_i} \langle\epsilon^*\rangle(\mathbf{x}|\mathbf{x}_1) f(\mathbf{x}_1)\, dV_1 \tag{5}$$

where Ω_i is the domain of a single inclusion and the integral is performed over the finite domain such that $\mathbf{x}$ can lie in an inclusion centered at $\mathbf{x}_1$. Further, $f(\mathbf{x}_1)$ is the probability density function (PDF) for a single inclusion being centered at $\mathbf{x}_1$, and $\langle\epsilon^*(\mathbf{x}|\mathbf{x}_1)\rangle$ is the perturbed strain at $\mathbf{x}$ averaged over the subclass of realizations having an inclusion centered at $\mathbf{x}_1$.

At this stage, it is reasonable to restrict composite solids to be *locally homogeneous* [Hinch (1977)]. That is, all PDF do not vary under small translation on a macroscopic length scale. With this assumption, $f(\mathbf{x}_1)$ in (5) may be regarded as a constant in the integration and equal to $f(\mathbf{x})$. The statistical "local homogeneity" also allows a small translation of $\mathbf{x} - \mathbf{x}_1$ in the two arguments of $\langle\epsilon^*(\mathbf{x}|\mathbf{x}_1)\rangle$. Namely, we may equate $\langle\epsilon^*(\mathbf{x}|\mathbf{x}_1)\rangle$ to $\langle\epsilon^*(\mathbf{x} + (\mathbf{x} - \mathbf{x}_1)|\mathbf{x})\rangle$. Thus, Eq. (5) becomes

$$\langle\epsilon^*\rangle(\mathbf{x}) = f(\mathbf{x}) \int_{\mathbf{x}'\in\Omega_i} \langle\epsilon^*(\mathbf{x}'|\mathbf{x})\rangle\, dV' \tag{6}$$

where $\mathbf{x}' \equiv 2\mathbf{x} - \mathbf{x}_1$, and the integral extends over all points $\mathbf{x}'$ within an inclusion centered at the position $\mathbf{x}$. By divergence theorem, we have

$$\langle\epsilon^*\rangle(\mathbf{x}) = f(\mathbf{x}) \int_{\partial\Omega_i} \frac{1}{2}\langle\mathbf{u}\otimes\mathbf{n} + \mathbf{n}\otimes\mathbf{u}\rangle(\mathbf{x}'|\mathbf{x})\, dS \tag{7}$$

In the extreme case where inclusions become line microcracks, Eq. (7) can be recast as

$$\langle\epsilon^*\rangle(\mathbf{x}) = f(\mathbf{x}) \int_{\mathcal{G}} \int_{S_i} \frac{1}{2}\langle[\![\mathbf{u}]\!]\otimes\mathbf{n} + \mathbf{n}\otimes[\![\mathbf{u}]\!]\rangle(\mathbf{x}'|\mathbf{x},\mathcal{G}) f(\mathcal{G})\, d\mathcal{G}dS \tag{8}$$

where $\mathcal{G} \equiv (a, \mathbf{n})$ characterizes the microcrack *length* and *orientation* in addition to the information on *location* $\mathbf{x}$; $f(\mathcal{G})$ is the probability function for a microcrack with geometry $\mathcal{G}$. In what follows, for simplicity of demonstration, attention will be focused on two-dimensional plane strain (or plane

stress) problems. Accordingly, $\mathcal{G}$ defines the geometric domain (a, θ), where a denotes one half of the microcrack length and θ denotes the angle between the global (reference) coordinate and the local (microcrack) coordinate with $0 \leq \theta \leq \pi$; see Fig. 2. It is well known that for a line microcrack in an infinite linear elastic isotropic solid, the *normal* and *tangential* microcrack opening displacements take the form

$$\left\{ \begin{array}{c} [\![u_2']\!] \\ [\![u_1']\!] \end{array} \right\} = \frac{4(1-\nu^2)}{E} \sqrt{a^2 - x'^2} \left\{ \begin{array}{c} p \\ q \end{array} \right\} \tag{9}$$

where E and ν are the Young's modulus and Poisson's ratio of the virgin elastic solid, respectively; p and q are the normal and shear external stresses projected on microcrack surface in local coordinate system (see Fig. 2). For plane stress problems, the factor $(1-\nu^2)$ is removed from (9).

By substituting (9) into (8) and using the Voigt's notation for strains, we arrive at

$$\langle \mathbf{e}^* \rangle(\mathbf{x}) \equiv \left\{ \begin{array}{c} \langle \epsilon_1^* \rangle \\ \langle \epsilon_2^* \rangle \\ \langle \epsilon_6^* \rangle \end{array} \right\} \equiv \left\{ \begin{array}{c} \langle \epsilon_{11}^* \rangle \\ \langle \epsilon_{22}^* \rangle \\ \langle 2\epsilon_{12}^* \rangle \end{array} \right\} = f(\mathbf{x}) \frac{\pi(1-\nu^2)}{E} \int_{\mathcal{A}} a^2 \int_{\Theta} \mathbf{g} \cdot \langle \mathbf{T} \rangle f(a, \theta)\, d\theta da \tag{10}$$

where $\mathcal{A}$ and Θ are the integration domains of microcrack lengths and orientations (for open microcracks), respectively. Further, $\mathbf{g}$ is the transformation matrix relating the global and local coordinates, and $\mathbf{T}$ is *local* stress vector:

$$[\mathbf{g}] = \left[\begin{array}{cc} 2\sin^2\theta & -\sin 2\theta \\ 2\cos^2\theta & \sin 2\theta \\ -2\sin 2\theta & 2\cos 2\theta \end{array} \right] \quad ; \quad \mathbf{T} = \left\{ \begin{array}{c} p \\ q \end{array} \right\} \tag{11}$$

Following the same arguments in deriving $\langle \mathbf{e}^* \rangle$, the ensemble-average stress field (in the local coordinates) can be shown to be

$$\langle \mathbf{T} \rangle = \left\{ \begin{array}{c} p^\infty \\ q^\infty \end{array} \right\} + \left\langle \left\{ \begin{array}{c} \tilde{p} \\ \tilde{q} \end{array} \right\} \right\rangle \equiv \mathbf{T}^\infty + \langle \tilde{\mathbf{T}} \rangle \tag{12}$$

where $\mathbf{T}^\infty$ is the **unperturbed** local stress field due to remote loading, and $\langle \tilde{\mathbf{T}} \rangle$ is the ensemble average of the **perturbation** in local stress field due to pairwise microcrack *interactions*:

$$\langle \tilde{\mathbf{T}} \rangle(\mathbf{x}, a, \theta) = \int_{\Xi} \langle \tilde{\mathbf{T}} \rangle(\mathbf{x}, a, \theta | \mathbf{x}_1, a_1, \theta_1) f(\mathbf{x}_1, a_1, \theta_1 | \mathbf{x}, a, \theta)\, d\theta_1 da_1 d\mathbf{x}_1 \tag{13}$$

Here $\langle \tilde{\mathbf{T}} \rangle(\mathbf{x}, a, \theta | \mathbf{x}_1, a_1, \theta_1)$ is the stress perturbation of a microcrack centered at $\mathbf{x}$ with (a, θ) averaged over the subclass of realizations which have a microcrack centered at $\mathbf{x}_1$ with (a_1, θ_1). In addition, $f(\mathbf{x}_1, a_1, \theta_1 | \mathbf{x}, a, \theta)$ is the conditional probability function for finding a microcrack centered at $\mathbf{x}_1$ with (a_1, θ_1) given one microcrack centered at $\mathbf{x}$ with (a, θ). Since only the ensemble

average is considered, the integral in (13) is performed over the domain of a *probabilistic* (not physical) RVE (in the *probability space*) which is characterized by the two-point probability function $f(\mathbf{x}_1, a_1, \theta_1 | \mathbf{x}, a, \theta)$. Thus, the shape of the physical specimen plays no role here. The active (open) integration domain Ξ also depends on loading conditions and ranges of microcrack interactions.

Assuming that microcracks do **not** intersect one another and that *reasonable randomness* holds (Hinch (1977)), then $f(\mathbf{x}_1, a_1, \theta_1 | \mathbf{x}, a, \theta)$ is simplified to $f(\mathbf{x}_1, a_1, \theta_1)$. Further, by the *local homogeneity* assumption, $f(\mathbf{x}_1, a_1, \theta_1)$ becomes approximately $f(\mathbf{x}, a, \theta)$. Therefore, Eq. (13) can be approximated by the following expression:

$$\langle \tilde{\mathbf{T}} \rangle (\mathbf{x}, a, \theta) = f(\mathbf{x}, a, \theta) \int_{\Xi} \langle \tilde{\mathbf{T}} \rangle (\mathbf{x}, a, \theta | \mathbf{x}_1, a_1, \theta_1) \, d\theta_1 da_1 d\mathbf{x}_1 \tag{14}$$

The assumption that microcracks do not intersect one another certainly introduces some unknown errors. However, there is no analytical solutions available to accommodate interactions among pairs of arbitrarily *intersected* microcracks. Therefore, following usual simplification made in the literature [Kachanov (1987), Kachanov and Laures (1989)], we do not consider the cases when microcracks intersect.

I.2.3. Approximate analytical solutions of two-microcrack interaction problem

Due to enormous complexity, it is practically impossible to obtain closed-form analytical solutions of strongly interacting *many-microcrack* problems. The formulation of arbitrarily located and oriented many-microcrack interaction problems is actually quite simple; see, e.g., Kachanov (1987), and Kachanov and Laures (1989). Nevertheless, the formulation involves $2N$ (if two-dimensional) or $3N$ (if three-dimensional) linear system of equations, where N designates the number of microcracks in an RVE (say, $N = 100$). Clearly, numerical solutions of many-microcrack interaction problems are suitable for the Monte Carlo simulation approach mentioned earlier in Section 1. By contrast, the present work intends to construct closed-form explicit stress solutions ($\tilde{\mathbf{T}}$) and analytical expressions of microcrack-induced strains ($\mathbf{e}^*$) and compliances ($\mathbf{S}^*$) for interacting microcracks within the framework of the *ensemble-average* approach.

In order to construct useful explicit analytical solutions and to gain simple physical insight for interacting microcracks, multiple-microcrack stress *reflections* will be neglected as the first approximation. Namely, we will only consider local stress perturbations based on many (arbitrary) pairwise microcrack interactions. The extension to the higher-order ensemble-average formulation will be presented in Section 4 of Part II.

The *exact* analytical solutions of the boundary-value problem of two arbitrarily located and oriented microcracks embedded in an infinite linear elastic isotropic solid are not yet available (except for some special configurations such as collinear microcracks). However, approximate analytical solutions were proposed by several investigators [e.g., Horii and Nemat-Nasser (1985), Hori and Nemat-Nasser (1987), Chudnovsky and Kachanov (1983), Chudnovsky et al. (1987a,b), and Kachanov (1987)]. In the present work, the "pseudo-traction" concept is adopted to find approximate analytical solutions of the two-microcrack interaction problem. For mathematical simplicity, only the *first term* of Taylor's expansion of the local stress field will be used to represent the average stress across the microcrack line.

The local coordinate systems 1 and 2 employed in the two-microcrack interaction problem are given in Figures 3(a) and 3(b). The two microcracks have lengths $2a_1$ and $2a_2$, respectively. The $y_1'-$ and $y_2'-$directions are set to be normal to the microcrack lines C_1 and C_2. The original two-microcrack problem is decomposed into a homogeneous problem and two sub-problems 1 and 2; see Fig. 4. In the homogeneous problem, an infinite solid without any microcrack is subjected to applied stresses at infinity. In the sub-problem j ($j = 1, 2$), an infinitely extended solid under zero remote stress at infinity has only one microcrack j, on which the boundary conditions are

$$-p_j + p_j^{\infty} + \tilde{p}_j = 0 \ ; \ \ -q_j + q_j^{\infty} + \tilde{q}_j = 0 \quad \text{on } C_j \ , \ j = 1, 2 \tag{15}$$

The quantities $\tilde{p}_j$ and $\tilde{q}_j$ are to be determined in such a way that all boundary conditions of the original problem are satisfied. In the subproblem j, the "exact" stresses are given by [Sneddon and Lowengrub (1969)]

$$\begin{aligned} \sigma_{11}^j &= p_j(-1 + E_j - F_j) + q_j(2G_j - H_j) \\ \sigma_{22}^j &= p_j(-1 + E_j + F_j) + q_j H_j \\ \sigma_{21}^j &= p_j H_j + q_j(-1 + E_j - F_j) \end{aligned} \tag{16}$$

where

$$\begin{aligned} E_j &\equiv \frac{r}{\sqrt{r_{j1} r_{j2}}} \cos\left(\theta_{j0} - \frac{\theta_{j1} + \theta_{j2}}{2}\right) \\ F_j &\equiv \frac{r a_j^2}{(r_{j1} r_{j2})^{3/2}} \sin\theta_{j0} \sin\frac{3}{2}(\theta_{j1} + \theta_{j2}) \\ G_j &\equiv \frac{r}{\sqrt{r_{j1} r_{j2}}} \sin\left(\theta_{j0} - \frac{\theta_{j1} + \theta_{j2}}{2}\right) \\ H_j &\equiv \frac{r a_j^2}{(r_{j1} r_{j2})^{3/2}} \sin\theta_{j0} \cos\frac{3}{2}(\theta_{j1} + \theta_{j2}) \end{aligned} \tag{17}$$

See Figure 3 for the definitions of r_{j1}, r_{j2}, θ_{j1} and θ_{j2}.

In order to satisfy the original boundary conditions (15), it follows that

$$\begin{aligned} \tilde{p}_j &= \mathbf{e}^j_{2(i)} \cdot \boldsymbol{\sigma}^i \cdot \mathbf{e}^j_{2(i)} \\ \tilde{q}_j &= \mathbf{e}^j_{2(i)} \cdot \boldsymbol{\sigma}^i \cdot \mathbf{e}^j_{1(i)} \end{aligned} \qquad i \neq j \ ; \ \ i,j = 1,2 \ \text{(no sum)} \tag{18}$$

where $\mathbf{e}^j_{1(i)}$ and $\mathbf{e}^j_{2(i)}$ are the two unit base vectors for the jth local coordinate system but are expressed in terms of the ith local coordinate components. The subscript i signifies that a quantity is referred to the (x'_i, y'_i) coordinate system. Substitution of Eq. (16) into Eq. (18) yields the local stresses for two microcracks:

$$\begin{Bmatrix} p_1 \\ q_1 \\ p_2 \\ q_2 \end{Bmatrix} = \begin{bmatrix} 0 & 0 & \alpha_1 & \alpha_2 \\ 0 & 0 & \alpha_3 & \alpha_4 \\ \alpha_5 & \alpha_6 & 0 & 0 \\ \alpha_7 & \alpha_8 & 0 & 0 \end{bmatrix} \begin{Bmatrix} p_1 \\ q_1 \\ p_2 \\ q_2 \end{Bmatrix} + \begin{Bmatrix} p_1^\infty \\ q_1^\infty \\ p_2^\infty \\ q_2^\infty \end{Bmatrix} \equiv \boldsymbol{\alpha} \cdot \mathbf{T}_{1-2} + \mathbf{T}^\infty_{1-2} \tag{19}$$

where

$$\begin{aligned} &\alpha_1 = -1 + E_2 + F_2 \cos 2\phi + H_2 \sin 2\phi \ ; \ \ \alpha_2 = 2G_2 \sin^2\phi + H_2 \cos 2\phi - (1 - E_2 + F_2) \sin 2\phi \\ &\alpha_3 = H_2 \cos 2\phi - F_2 \sin 2\phi \ ; \ \ \alpha_4 = (G_2 - H_2) \sin 2\phi - (1 - E_2 + F_2) \cos 2\phi \\ &\alpha_5 = -1 + E_1 + F_1 \cos 2\phi - H_1 \sin 2\phi \ ; \ \ \alpha_6 = 2G_1 \sin^2\phi + H_1 \cos 2\phi + (1 - E_1 + F_1) \sin 2\phi \\ &\alpha_7 = H_1 \cos 2\phi + F_1 \sin 2\phi \ ; \ \ \alpha_8 = -(G_1 - H_1) \sin 2\phi - (1 - E_1 + F_1) \cos 2\phi \end{aligned} \tag{20}$$

and $\phi \equiv \theta_{10} - \theta_{20}$. It is noteworthy that the "microcrack interaction matrix" $\boldsymbol{\alpha}$ in Eq. (19) actually corresponds to the "transmission factor" matrix $\boldsymbol{\Lambda}$ in Kachanov (1987). In addition, it is convenient to define $\mathbf{T}_{1-2} \equiv (p_1, q_1, p_2, q_2)^T$, $\mathbf{T}^\infty_{1-2} \equiv (p_1^\infty, q_1^\infty, p_2^\infty, q_2^\infty)^T$ and $\tilde{\mathbf{T}}_{1-2} \equiv (\tilde{p}_1, \tilde{q}_1, \tilde{p}_2, \tilde{q}_2)^T$. Since $\mathbf{T}_{1-2} = \mathbf{T}^\infty_{1-2} + \tilde{\mathbf{T}}_{1-2}$, one can solve $\tilde{\mathbf{T}}_{1-2}$ from Eq. (19):

$$\tilde{\mathbf{T}}_{1-2} = \boldsymbol{\alpha} \cdot (\mathbf{I} - \boldsymbol{\alpha})^{-1} \cdot \mathbf{T}^\infty_{1-2} \tag{21}$$

The comparison of the stress *transmission factors* obtained by using the simple "first term" approximation (Λ) and the exact solutions (Λ_{ex}) for two collinear microcracks is given in **Appendix I** for various *normalized* microcrack-tip distance ratios. When $d = 0.25$, it means that the *ratio* of the two microcrack-tip *spacing* to the microcrack *size* ($2a$) is 0.25. It is noted that $\Lambda \equiv 1$ when microcrack interaction is totally neglected. From **Table 2** in **Appendix I**, it is observed that the simple "first term" approximation is quite acceptable in general except when two microcrack tips are really close to each other (i.e., when $d < 0.1$). It is emphasized that the spatial location of the

second microcrack given the first microcrack is random. Therefore, the errors (in **Table 2**) associated with the proposed approximate analysis should be statistically *averaged* over all possible realizations.

Let us recall that $\tilde{\mathbf{T}} \equiv (\tilde{p}_1, \tilde{q}_1)^T$ and define $\mathbf{K}_1$ as the first two *rows* of the matrix $[\alpha \cdot (\mathbf{I} - \alpha)^{-1}]$. Therefore, from Eq. (21), we have

$$\tilde{\mathbf{T}} = \mathbf{K}_1 \cdot \mathbf{T}^{\infty}_{1-2} \tag{22}$$

We can now substitute Eq. (22) into (14) and (12) to find the ensemble-average stress of a primary microcrack located at $\mathbf{x}$ over all possible positions and orientations ($\mathbf{x}_1$ and θ_1) of the second neighboring microcrack. In addition, the local and global remote stresses $\mathbf{T}^{\infty}_{1-2}$ and τ^{∞} are related by the following transformation matrix $\mathbf{K}_2$:

$$\begin{Bmatrix} p_1^{\infty} \\ q_1^{\infty} \\ p_2^{\infty} \\ q_2^{\infty} \end{Bmatrix} = \begin{bmatrix} \sin^2\theta & \cos^2\theta & -\sin 2\theta \\ -\frac{1}{2}\sin 2\theta & \frac{1}{2}\sin 2\theta & \cos 2\theta \\ \sin^2(\theta+\phi) & \cos^2(\theta+\phi) & -\sin 2(\theta+\phi) \\ -\frac{1}{2}\sin 2(\theta+\phi) & \frac{1}{2}\sin 2(\theta+\phi) & \cos 2(\theta+\phi) \end{bmatrix} \begin{Bmatrix} \sigma_{11}^{\infty} \\ \sigma_{22}^{\infty} \\ \sigma_{21}^{\infty} \end{Bmatrix} \equiv \mathbf{K}_2 \cdot \tau^{\infty} \tag{23}$$

Therefore, Eq. (22) can be rephrased as

$$\tilde{\mathbf{T}} = \mathbf{K}_1 \cdot \mathbf{K}_2 \cdot \tau^{\infty} \equiv \mathbf{K} \cdot \tau^{\infty} \tag{24}$$

where $\mathbf{K} \equiv \mathbf{K}_1 \cdot \mathbf{K}_2$. The detailed *explicit* components of matrix $\mathbf{K}$ are given in **Appendix II.**

Remark 2.1. It appears that there are some typo-errors in Sneddon and Lowengrub's (1969) solutions. Eqs. (16) and (17) are the correct formulas after the problem is resolved. ∎

I.2.4. Overall moduli of brittle solids with interacting microcracks

By substituting Eqs. (24) and (22) into Eq. (12) and assuming that $\mathbf{x}$ and (a, θ) are statistically independent, one obtains the following expression for the ensemble-average stresses:

$$\langle \mathbf{T} \rangle = \langle \mathbf{T}^{\infty} + \tilde{\mathbf{T}} \rangle = \left(\mathbf{K}_0 + f(\mathbf{x}) f(a, \theta) \langle \mathbf{K} \rangle \right) \cdot \tau^{\infty} \tag{25}$$

where $\mathbf{T}^{\infty} \equiv \mathbf{K}_0 \cdot \tau^{\infty}$, and

$$\mathbf{K}_0 = \begin{bmatrix} \sin^2\theta & \cos^2\theta & -\sin 2\theta \\ -\frac{1}{2}\sin 2\theta & \frac{1}{2}\sin 2\theta & \cos 2\theta \end{bmatrix} \tag{26}$$

$$\langle \mathbf{K} \rangle \equiv \int_{\Xi} \mathbf{K}\, r dr\, d\theta_{10}\, d\theta_{20}\, da_2 \tag{27}$$

Substitution of (25) into (10) then yields the ensemble-average damage-induced strain vector:

$$\langle \mathbf{e}^* \rangle(\mathbf{x}) = \left\{ \langle \mathbf{S}^{*1} \rangle + \langle \mathbf{S}^{*2} \rangle \right\} \cdot \boldsymbol{\tau}^\infty \equiv \langle \mathbf{S}^* \rangle \cdot \boldsymbol{\tau}^\infty \tag{28}$$

where

$$\langle \mathbf{S}^{*1} \rangle \equiv \frac{\pi(1-\nu^2)}{E} f(\mathbf{x}) \int_{\mathcal{A}} a^2 \int_\Theta \mathbf{g} \cdot \mathbf{K}_0 f(a,\theta)\, d\theta\, da \tag{29}$$

$$\langle \mathbf{S}^{*2} \rangle \equiv \frac{\pi(1-\nu^2)}{E} f^2(\mathbf{x}) \int_{\mathcal{A}} a^2 \int_\Theta \mathbf{g} \cdot \langle \mathbf{K} \rangle f^2(a,\theta)\, d\theta\, da \tag{30}$$

Clearly, $\langle \mathbf{S}^* \rangle$ is the ensemble-average damage-induced compliance matrix. $f(\mathbf{x})$ and $f(a,\theta)$ depend on material microstructures and loading conditions, and should be specified by experimental observations (e.g., by scanning electron microscopy or computerized tomography).

In what follows, as an illustration for deriving an *explicit* form of overall moduli of microcracked solids, we consider the special case in which: (1) $f(a,\theta) = f(a)f(\theta)$, (2) microcrack orientation is perfectly random (i.e., $f(\theta) = 1/\pi$), (3) the initial microcrack radius a is a constant, and (4) $f(\mathbf{x})$ satisfies

$$\int_A f^2(\mathbf{x})\, dA \approx \left\{ \int_A f(\mathbf{x})\, dA \right\}^2 / A \tag{31}$$

Moreover, it is realized that

$$\int_A f(\mathbf{x})\, dA = N \tag{32}$$

where N is the total number of microcracks within an RVE (with area A). Since statistical homogeneity (in the probability space) is assumed, the volume-average coincides with the ensemble-average. The volume-average (denoted by an overline) of (28) over an RVE thus takes the form

$$\overline{\langle \mathbf{e}^* \rangle} = \frac{(1-\nu^2)}{E} \left\{ \omega \int_\Theta \mathbf{g} \cdot \mathbf{K}_0\, d\theta + \frac{\omega^2}{\pi} \int_\Theta \mathbf{g} \cdot \langle \hat{\mathbf{K}} \rangle\, d\theta \right\} \cdot \boldsymbol{\tau}^\infty \tag{33}$$

where

$$\langle \hat{\mathbf{K}} \rangle \equiv \int_{\hat{\Xi}} \mathbf{K}\, r dr d\theta_{10} d\theta_{20} \tag{34}$$

and $\hat{\Xi}$ is the active (open) probabilistic integration domain for variables r, θ_{10}, and θ_{20}. The effective radius r has been normalized with respect to the microcrack radius a. Further, $\omega \equiv \frac{Na^2}{A} \equiv na^2 \equiv \hat{\omega}/\pi$ is a measure of microcrack concentrations. It is emphasized that our definition of microcrack concentration ω differs from the commonly used definition ($\hat{\omega}$) by a multiplier π [see Budiansky and O'Connell (1976)]. The integration domains Θ and $\hat{\Xi}$ also depend on loading conditions and range of microcrack interactions.

By substituting Eq. (33) into the volume-average of Eq. (4), we finally obtain the following ensemble-volume averaged macroscopic constitutive relation (in Voigt's notation):

$$\overline{\langle \mathbf{e} \rangle} = \overline{\langle \mathbf{S} \rangle} \cdot \boldsymbol{\tau}^{\infty} \tag{35}$$

where

$$\overline{\langle \mathbf{S} \rangle} \equiv \mathbf{S}^{\circ} + \overline{\langle \mathbf{S}^{*1} \rangle} + \overline{\langle \mathbf{S}^{*2} \rangle} \tag{36}$$

That is, $\overline{\langle \mathbf{S} \rangle}$ is the ensemble-volume averaged overall effective compliance matrix of a microcracked brittle solid. Specifically, under the *plane strain* assumption, we write

$$\mathbf{S}^{\circ} = \frac{(1+\nu)}{E} \begin{bmatrix} 1-\nu & -\nu & 0 \\ -\nu & 1-\nu & 0 \\ 0 & 0 & 2 \end{bmatrix} \tag{37}$$

$$\overline{\langle \mathbf{S}^{*1} \rangle} \equiv \frac{(1-\nu^2)}{E} \omega \int_{\Theta} \mathbf{g} \cdot \mathbf{K}_0 \, d\theta \tag{38}$$

$$\overline{\langle \mathbf{S}^{*2} \rangle} \equiv \frac{(1-\nu^2)}{\pi E} \omega^2 \int_{\Theta} \mathbf{g} \cdot \langle \hat{\mathbf{K}} \rangle \, d\theta \tag{39}$$

It is noted that $\mathbf{S}^{\circ}$ denotes the elastic compliance, $\overline{\langle \mathbf{S}^{*1} \rangle}$ defines the first-order microcrack effects without interaction, and $\overline{\langle \mathbf{S}^{*2} \rangle}$ defines the second-order (in ω^2) microcrack interaction effects.

Remark 2.2. It is interesting to notice that Eq. (28) reveals that physical *nonlocal effects* are brought into constitutive equations through the process of microcrack interaction and *ensemble averaging* (not volume averaging). That is, in Eq. (28), the stress-strain law at a material point within a RVE depends *not only* on the constitutive behavior at the point, but *also* on the constitutive behavior of *neighboring* points. ∎

I.3. Some special stationary examples

In this section, we apply the proposed ensemble-volume average approach to solve three special examples. These examples are all classified as *stationary* micromechanical models. In particular, the first example shows that the proposed method recovers the well-known Taylor's model when microcrack interaction is entirely neglected in Eq. (36). In the second example, we examine the randomly located aligned (parallel) microcracks problem — for transverse cracking phenomenon in laminated composites, for instance. The last example shows that the overall compliance matrix becomes *isotropic* when all microcracks are open. Microcrack locations and orientations are assumed to be perfectly random. In what follows, for simplicity, we further assume that closed microcrack contributions are neglected.

I.3.1. Dilute microcracks — Taylor's model

The *open* microcrack angle domain $\Theta \equiv [\theta_1, \theta_2]$ can be found by solving

$$\sin^2\theta\sigma_{11}^{\infty} + \cos^2\theta\sigma_{22}^{\infty} - \sin 2\theta\sigma_{21}^{\infty} \geq 0 \tag{40}$$

where tensile normal stress is taken as positive. After dropping the interaction term in (36), the overall compliance becomes

$$\overline{\langle \mathbf{S} \rangle} = \mathbf{S}^{\circ} + \overline{\langle \mathbf{S}^{*1} \rangle} \tag{41}$$

where [by integrating Eq. (38)]

$$\overline{\langle \mathbf{S}^{*1} \rangle} = \frac{(1-\nu^2)}{E}\omega \begin{bmatrix} S_{11}^{*1} & 0 & S_{16}^{*1} \\ 0 & S_{22}^{*1} & S_{26}^{*1} \\ S_{61}^{*1} & S_{62}^{*1} & S_{66}^{*1} \end{bmatrix} \tag{42}$$

Specifically, we have

$$\begin{aligned} &S_{11}^{*1} = \theta_2 - \theta_1 - \frac{1}{2}(\sin 2\theta_2 - \sin 2\theta_1) \;\; ; \;\; S_{22}^{*1} = \theta_2 - \theta_1 + \frac{1}{2}(\sin 2\theta_2 - \sin 2\theta_1) \\ &S_{66}^{*1} = 2(\theta_2 - \theta_1) \;\; ; \;\; S_{16}^{*1} = \sin^2\theta_1 - \sin^2\theta_2 = S_{61}^{*1} = S_{26}^{*1} = S_{62}^{*1} \end{aligned} \tag{43}$$

For various biaxial loading conditions, we obtain the following results:

(1) **Uniaxial or biaxial tension.** All microcracks are open ($\theta_1 = 0, \theta_2 = \pi$) and isotropic damage is recovered. The orientation domain is $\Theta \equiv [0, \pi]$. The *non-zero* components in (43) are

$$S_{11}^{*1} = S_{22}^{*1} = \pi \; ; \quad S_{66}^{*1} = 2\pi \tag{44}$$

(2) **Biaxial tension/compression.** We have the axial stress $\sigma_{22}^{\infty} > 0$, the lateral stress $\sigma_{11}^{\infty} < 0$, and shear stress $\sigma_{21}^{\infty} = 0$. The open microcrack angle domain is defined by $\Theta \equiv [0, \theta^*] \cup [\pi - \theta^*, \pi]$, where

$$\theta^* = \tan^{-1} \sqrt{\frac{-\sigma_{22}^{\infty}}{\sigma_{11}^{\infty}}} \tag{45}$$

The *non-zero* anisotropic components in (43) are

$$S_{11}^{*1} = 2\theta^* - \sin 2\theta^* \ ; \ S_{22}^{*1} = 2\theta^* + \sin 2\theta^* \ ; \ S_{66}^{*1} = 4\theta^* \tag{46}$$

(3) **Biaxial tension and shear.** We have $\sigma_{11}^{\infty} = \sigma_{22}^{\infty} > 0$ and $\sigma_{21}^{\infty} \geq \sigma_{22}^{\infty}$. The open domain is defined by $\Theta \equiv [\frac{\pi}{2}, \pi] \cup [0, \theta^*] \cup [\frac{\pi}{2} - \theta^*, \frac{\pi}{2}]$, where

$$\theta^* = \frac{1}{2} \sin^{-1} \left(\frac{\sigma_{22}^{\infty}}{\sigma_{21}^{\infty}} \right) \tag{47}$$

The *non-zero* components in (43) are

$$\begin{aligned} S_{11}^{*1} &= \frac{\pi}{2} + 2\theta^* = S_{22}^{*1} \ ; \ S_{66}^{*1} = \pi + 4\theta^* \\ S_{16}^{*1} &= \cos 2\theta^* = S_{61}^{*1} = S_{26}^{*1} = S_{62}^{*1} \end{aligned} \tag{48}$$

I.3.2. Aligned microcracks

Attention is now focused on an array of randomly located aligned (parallel) open microcracks. This class of problems is relevant to the transverse matrix cracking problem in laminated composites; see, for example, Laws, Dvorak and Hejazi (1983), and Laws and Dvorak (1987). Since all microcracks have same orientation, Eq. (17) can be simplified as follows:

$$\begin{aligned} E_1 = E_2 &= \frac{r}{\sqrt{r_1 r_2}} \cos(\theta_{10} - \frac{\theta_{11} + \theta_{12}}{2}) \ ; \ F_1 = F_2 = \frac{ra^2}{(r_1 r_2)^{3/2}} \sin\theta_{10} \sin\frac{3}{2}(\theta_{11} + \theta_{12}) \\ G_1 = G_2 &= \frac{r}{\sqrt{r_1 r_2}} \sin(\theta_{10} - \frac{\theta_{11} + \theta_{12}}{2}) \ ; \ H_1 = H_2 = \frac{ra^2}{(r_1 r_2)^{3/2}} \sin\theta_{10} \cos\frac{3}{2}(\theta_{11} + \theta_{12}) \end{aligned} \tag{49}$$

where

$$\begin{aligned} r_1 &= (r^2 - 2ar\cos\theta_{10} + a^2)^{1/2} \ ; \ r_2 = (r^2 + 2ar\cos\theta_{10} + a^2)^{1/2} \\ \theta_{11} &= \cos^{-1}\left(\frac{r\cos\theta_{10} - a}{r_1}\right) \ ; \ \theta_{12} = \cos^{-1}\left(\frac{r\cos\theta_{10} + a}{r_1}\right) \end{aligned} \tag{50}$$

and $\theta = 0 = \phi \equiv \theta_{10} - \theta_{20}$, $\theta_{10} = \theta_{20}$.

The numerical integration of Eq. (34) will be addressed in Section 3 of Part II of this series. The minimum radius of integration in r (center distance between microcracks) is taken as $2a$. The

Table 1. Convergence behavior of $\langle \hat{K}_{ij} \rangle$ vs. r_{max}

r_{max}	$\langle \hat{K}_{12} \rangle$	$\langle \hat{K}_{23} \rangle$
4a	0.429843+00	0.173965+00
8a	0.550972+00	0.225418+00
16a	0.582654+00	0.238972+00
20a	0.586498+00	0.240618+00
40a	0.591638+00	0.242820+00
400a	0.591894+00	0.243244+00

convergence behavior for the integration in (34) (i.e., $\langle \hat{K}_{ij} \rangle$) with respect to the choice of the maximum integration radius r_{max} is given in **Table 1**. It is observed that use of $r_{max} = 20a$ is quite acceptable. After numerical Gauss integration of (34) (by using 40 Gauss points), we obtain

$$\langle \hat{\mathbf{K}} \rangle = \begin{bmatrix} 0 & 0.5865 & 0 \\ 0 & 0 & 0.2406 \end{bmatrix} \tag{51}$$

Accordingly, the transversely isotropic compliance becomes

$$\overline{\langle \mathbf{S} \rangle} = \frac{(1-\nu^2)}{E} \left\{ \begin{bmatrix} 1 & \frac{-\nu}{1-\nu} & 0 \\ \frac{-\nu}{1-\nu} & 1 & 0 \\ 0 & 0 & \frac{2}{1-\nu} \end{bmatrix} + \pi \begin{bmatrix} 0 & 0 & 0 \\ 0 & 2\omega + 1.173\omega^2 & 0 \\ 0 & 0 & 2\omega + 0.481\omega^2 \end{bmatrix} \right\} \tag{52}$$

Clearly, the first-order terms ω in Eq. (52) come from Taylor's model, and the second-order corrections ω^2 in (52) come from the pairwise microcrack interactions.

I.3.3. Isotropic damage

Under uniaxial or biaxial tension, all microcracks are typically assumed open. It is also assumed that microcracks are randomly located, randomly oriented, and of uniform size. As a result, the overall behavior is isotropic. The compliance contribution due to microcrack interaction can be evaluated by performing numerical Gauss integration of Eq. (39). The results are:

$$\overline{\langle \mathbf{S}^{*2} \rangle} = \frac{(1-\nu^2)}{E} \pi \omega^2 \begin{bmatrix} 0.373 & 0.041 & 0 \\ 0.041 & 0.373 & 0 \\ 0 & 0 & 0.664 \end{bmatrix} \tag{53}$$

Therefore, the (piane strain) overall compliance becomes

$$\overline{\langle \mathbf{S} \rangle} = \frac{(1-\nu^2)}{E} \left\{ \begin{bmatrix} 1 & \frac{-\nu}{1-\nu} & 0 \\ \frac{-\nu}{1-\nu} & 1 & 0 \\ 0 & 0 & \frac{2}{1-\nu} \end{bmatrix} + \pi \begin{bmatrix} \omega + 0.373\omega^2 & 0.041\omega^2 & 0 \\ 0.041\omega^2 & \omega + 0.373\omega^2 & 0 \\ 0 & 0 & 2\omega + 0.664\omega^2 \end{bmatrix} \right\} \tag{54}$$

It is noted that the shear moduli (in 1–2 and 2–1 directions) are changed (non-zero) due to microcrack interaction.

It is very interesting to compare the foregoing overall compliance matrix with that derived by the self-consistent model [e.g., Horii and Nemat-Nasser (1983)]. The overall compliance given by the self-consistent method in this isotropic damage case is:

$$\tilde{\mathbf{S}}^{sc} = \frac{(1-\nu^2)}{E}\begin{bmatrix} \frac{1}{1-\pi\omega} & \frac{-\nu}{1-\nu} & 0 \\ \frac{-\nu}{1-\nu} & \frac{1}{1-\pi\omega} & 0 \\ 0 & 0 & \frac{2}{1-\nu}\frac{1-\pi\nu\omega}{1-\pi\omega} \end{bmatrix} \tag{55}$$

Obviously, the overall compliance given by the self-consistent method goes to infinity at $\omega = 1/\pi$. It should be noted that any effective medium theory is inherently only applicable for low microcrack concentrations since it does **not** depend on microcrack locations.

For low values of $\omega << 1/\pi$, the Taylor's expansion of Eq. (55) renders

$$\tilde{\mathbf{S}}^{sc} = \frac{(1-\nu^2)}{E}\left\{\begin{bmatrix} 1 & \frac{-\nu}{1-\nu} & 0 \\ \frac{-\nu}{1-\nu} & 1 & 0 \\ 0 & 0 & \frac{2}{1-\nu} \end{bmatrix} + \pi\begin{bmatrix} \omega+\pi\omega^2 & 0 & 0 \\ 0 & \omega+\pi\omega^2 & 0 \\ 0 & 0 & 2(\omega+\pi\omega^2) \end{bmatrix}\right\} \tag{56}$$

Apparently, the compliance calculated by the self-consistent method is *higher* than that of the present model. In addition, the self-consistent method predicts *no change* in shear moduli in the 1–2 and 2–1 directions. Finally, it is emphasized that there is no singularity in the present method irrespective of the ω value.

From Eq. (54), it is clear that the relative weight of the second-order terms (in ω^2, due to microcrack interaction) to the first-order terms (in ω) depends on the values of ω. For example, the relative weight is 0.373ω for the 11 and 22 terms in the compliance matrix. If the microcrack density is very small (dilute), the second-order terms are negligible. On the other hand, if the microcrack density is high [e.g., $\omega = 0.5$ – corresponding to $\hat{\omega} = 0.5\pi$ defined by Budiansky and O'Connell (1976)], then contributions from the second-order terms are quite significant. It is noted that, however, when microcrack densities are extremely high, the proposed second-order method may not be accurate enough since higher-order terms should be included; see Sec. 4 of Part II for extension to the higher-order formulation.

The proposed statistical micromechanical framework is **not** restricted to widely spaced microcrack arrays. From **Table 2** in **Appendix I**, it is seen that the proposed two-microcrack interaction solutions are quite acceptable even when the ratio d is only 0.1 (i.e., when the "microcrack-tip spacing" is only one-tenth of the "microcrack size").

I.4. Conclusions

A two-dimensional statistical micromechanical theory for microcrack-weakened brittle solids is presented based on the concepts of ensemble-average and pairwise microcrack interaction. The overall compliances are derived by performing ensemble-volume averaged integration over the domain of a statistically representative volume element (in the probability space). Unlike the self-consistent method which introduces a singularity at $\omega = 1/\pi$, our method predicts a smooth increase of effective compliance as ω increases. Further, the proposed microcrack interaction framework does **not** require the use of Monte Carlo simulations. It is emphasized that the proposed second-order terms are second-order in ω^2, not second-order in geometric quantities [such as $(a/r)^2$]. In addition, pairwise interaction effects do not vanish in the event of perfectly randomly distributed microcracks; see Eq. (53). In fact, effects of pairwise microcrack interactions are equally distributed in all directions and therefore the overall behavior is isotropic.

In Part II of this series, we will further investigate issues pertaining to computational aspects of the proposed approach, extension to "evolutionary" micromechanical damage models (with "cleavage 1" microcrack growth), and a higher-order microcrack interaction model. Extension to a three-dimensional statistical micromechanical theory of brittle solids with randomly located, interacting *penny-shaped* microcracks is presented in a separate paper [Ju and Tseng (1992)]. Numerical comparisons with the Taylor's model, the self-consistent model, and the differential scheme will also be presented in Ju and Tseng (1992).

I.5. References

1. BATCHELOR, G. K., (1970), "The stress system in a suspension of force-free particles", *J. Fluid Mech.*, **41**, 545–570.

2. BATCHELOR, G. K. AND GREEN, J. T., (1972), "The determination of the bulk stress in a suspension of spherical particles to order c^2", *J. Fluid Mech.*, **56 (3)**, 401–427.

3. BENVENISTE, Y., (1986), "On the Mori-Tanaka's method in cracked bodies", *Mech. Res. Comm.*, **13**, 193–201.

4. BUDIANSKY, B. AND O'CONNELL, R. J., (1976), "Elastic moduli of a cracked solid", *Int. J. Solids & Struct.*, **12**, 81–97.

5. CHEN, H. S. AND ACRIVOS, A., (1978a), "The solution of the equations of linear elasticity for an infinite region containing two spherical inclusions", *Int. J. Solids & Struct.*, **14**, 331–348.

6. CHEN, H. S. AND ACRIVOS, A., (1978b), "The effective elastic moduli of composite materials containing spherical inclusions at non-dilute concentrations", *Int. J. Solids & Struct.*, **14**, 349–364.

7. CHRISTENSEN, R. M., (1990), "A critical evaluation for a class of micromechanics models", *J. Mech. Phys. Solids*, **38 (3)**, 379–404.

8. CHRISTENSEN, R. M. AND LO, K. H., (1979), "Solutions for effective shear properties in three phase sphere and cylinder models", *J. Mech. Phys. Solids*, **27**, 315–330.

9. CHUDNOVSKY, A. AND KACHANOV, M., (1983), "Interaction of a crack with a field of microcracks", *Int. J. Eng. Sci.*, **21**, 1009–1018.

10. CHUDNOVSKY, A., DOLGOPOLSKY, A. AND KACHANOV, M., (1987a), "Elastic interaction of a crack with a microcrack array–I. Formulation of the problem and general form of the solution", *Int. J. Solids & Struct.*, **23 (1)**, 1–10.

11. CHUDNOVSKY, A., DOLGOPOLSKY, A. AND KACHANOV, M., (1987b), "Elastic interaction of a crack with a microcrack array–II. elastic solution for two crack configurations", *Int. J. Solids & Struct.*, **23 (1)**, 11–21.

12. FANELLA, D. AND KRAJCINOVIC, D., (1988), "A micromechanical model for concrete in compression", *Eng. Fract. Mech.*, **29 (1)**, 49–66.

13. GROSS, D., (1982), "Spannungsintensitatsfaktoren von ribsystemen (Stress intensity factors of systems of cracks)", *Ing.-Arch.*, **51**, 301–310 (in German).

14. HASHIN, Z., (1988), "The differential scheme and its application to cracked materials", *J. Mech. Phys. Solids*, **36**, 719–734.

15. HILL, R., (1965), "A self-consistent mechanics of composite materials", *J. Mech. Phys. Solids*, **13**, 213–222.

16. HINCH. E. J., (1977), "An averaged-equation approach to particle interactions in a fluid suspension", *J. Fluid Mech.*, **83**, 695–720.

17. HORI, M. AND NEMAT-NASSER, S., (1987), "Interacting micro-cracks near the tip in the process zone of a macro-crack", *J. Mech. Phys. Solids*, **35**, 601–629.

18. HORII, H. AND NEMAT-NASSER, S., (1983), "Overall moduli of solids with microcracks: load-induced anisotropy", *J. Mech. Phys. Solids*, **331**, 155–171.

19. HORII, H. AND NEMAT-NASSER, S., (1985), "Elastic fields of interacting inhomogeneities", *Int. J. Solids & Struct.*, **21**, 731–745.

20. HORII, H. AND SAHASAKMONTRI, K., (1990), "Mechanical properties of cracked solids: validity of the self-consistent method", in *Micromechanics and Inhomogeneity*, ed. by G. J. Weng, M. Taya and H. Abe, pp. 137–159, Springer-Verlag, New York.

21. HUDSON, J. A., (1980), "Overall properties of a cracked solid", *Math. Proc. Camb. Phil. Soc.*, **88**, 371–384.

22. HUDSON, J. A., (1981), "Wave speeds and attenuation of elastic waves in material containing cracks", *Geophys. J. R. astr. Soc.*, **64**, 133–150.

23. HUDSON, J. A., (1986), "A higher order approximation to the wave propagation constants for a cracked solid", *Geophys. J. R. astr. Soc.*, **87**, 265–274.

24. JU, J. W., (1991a), "On two-dimensional self-consistent micromechanical damage models for brittle solids", *Int. J. Solids & Struct.*, **27 (2)**, 227–258.

25. JU, J. W., (1991b), "A micromechanical damage model for uniaxially reinforced composites weakened by interfacial arc microcracks", *J. Appl. Mech.*, **58 (4)**, 923-930.

26. JU, J. W. AND LEE, X., (1991), "On three-dimensional self-consistent micromechanical damage models for brittle solids. Part I: Tensile loadings", *J. Eng. Mech.*, ASCE, **117 (7)**, 1495–1515.

27. JU, J. W. AND TSENG, K. W., (1992), "A three-dimensional statistical micromechanical theory for brittle solids with interacting microcracks", *Int. J. Damage Mechanics*, **1 (1)**, 102–131.

28. KACHANOV, M., (1987), "Elastic solids with many cracks: a simple method of analysis", *Int J. Solids & Struct.*, **23**, 23–43.

29. KACHANOV, M. AND MONTAGUT, E., (1986), "Interaction of a crack with certain micro-crack arrays", *Eng. Fracture Mech.*, **25**, 625–636.

30. KACHANOV, M. AND LAURES, J.-P., (1989), "Three-dimensional problems of strongly interacting arbitrarily located penny-shaped cracks", *Int J. of Fract.*, **41**, 289–313.

31. KRAJCINOVIC, D., (1989), "Damage mechanics", *Mech. Mater.*, **8 (2-3)**, 117–197.

32. KRAJCINOVIC, D. AND FANELLA, D., (1986), "A micromechanical damage model for concrete", *Eng. Fract. Mech.*, **25**, 585–596.

33. KRAJCINOVIC, D. AND SUMARAC, D., (1989), "A mesomechanical model for brittle deformation processes: part I", *J. Appl. Mech.*, **56**, 51–62.

34. LAWS, N. AND DVORAK, G. J., (1987), "The effect of fiber breaks and aligned penny-shaped cracks on the stiffness and energy release rates in unidirectional composites", *Int. J. Solids & Struct.*, **23 (9)**, 1269–1283.

35. LAWS, N., DVORAK, G. J. AND HEJAZI, M., (1983), "Stiffness changes in unidirectional composites caused by crack systems", *Mech. of Mater.*, **2**, 123–137.

36. LEE, X. AND JU, J. W., (1991), "On three-dimensional self-consistent micromechanical damage models for brittle solids. Part II: Compressive loadings", *J. Eng. Mech.*, ASCE, **117 (7)**, 1516–1537.

37. MCLAUGHLIN, R., (1977), "A study of the differential scheme for composite materials", *Int. J. Engng. Sci.*, **15**, 237–244.

38. MORI, T. AND TANAKA, K., (1973), "Average stress in matrix and average elastic energy of materials with misfitting inclusions", *Acta Metallurgica*, **21**, 571–574.

39. NEMAT-NASSER, S. AND HORI, M., (1990), "Elastic solids with microdefects", in *Micromechanics and Inhomogeneity*, pp. 297–320, ed. by G. J. Weng, M. Taya and H. Abe, Springer-Verlag, New York.

40. ROSCOE, R. A., (1952), "The viscosity of suspensions of rigid spheres", *Brit. J. Appl. Phys.*, **3**, 267–269.

41. ROSCOE, R. A., (1973), "Isotropic composites with elastic or viscoelastic phases: general bounds for the moduli and solutions for special geometries", *Rheol. Acta*, **12**, 404–411.

42. SAYERS, C. M. AND KACHANOV, M., (1991), "A simple technique for finding effective elastic constants of cracked solids for arbitrary crack orientation statistics", *Int. J. Solids & Struct.*, **27 (6)**, 671–680.

43. SNEDDON, I. N. AND LOWENGRUB, M., (1969), *Crack problems in the classical theory of elasticity*, John Wiley & Sons, Inc., New York.

44. SUMARAC, D. AND KRAJCINOVIC, D., (1987), "A self-consistent model for microcrack-weakened solids", *Mech. Mater.*, **6**, 39–52.

45. SUMARAC, D. AND KRAJCINOVIC, D., (1989), "A mesomechanical model for brittle deformation processes: part II", *J. Appl. Mech.*, **56**, 57–62.

46. WILLIS, J. R. AND ACTON, J. R., (1976), "The overall elastic moduli of a dilute suspension of spheres", *Quart. J. Mech. Appl. Math.*, **29 (2)**, 163–177.

47. ZHAO, Y. H., TANDON, G. P. AND WENG, G. J., (1989), "Elastic moduli for a class of porous materials", *Acta Mechanica*, **76**, 105–130.

I.6. Appendix I. Average stress field of two collinear microcracks

The problem of two interacting collinear microcracks of equal length in an infinite plate subjected to uniform traction p^{∞} at infinity has an exact analytical solution [Sneddon and Lowengrub (1969)]. The normalized (nondimensional) distance between the two microcrack tips is denoted by $2k$ (with $k < 1$), and the normalized length for each microcrack is designated as $1 - k$. For this special configuration, we have

$$\theta_{10} = \theta_{20} = \theta_{ij} = 0\,; \quad i,j = 1,2 \tag{57}$$

and $\phi = \theta_{10} - \theta_{20} = 0$

$$r = 1 + k \;\; ; \;\; r_1 = \frac{1+3k}{2} = r_{11} = r_{21} \;\; ; \;\; r_2 = \frac{3+k}{2} = r_{12} = r_{22} \tag{58}$$

Therefore, the only non-zero components in (17) are

$$\Lambda \equiv E_1 = E_2 = \frac{2(1+k)}{\sqrt{(1+3k)(3+k)}} \tag{59}$$

Substitution of Eq. (59) into (20) and solution of Eq. (19) then render the approximate *average* normal stress p as follows

$$p = \frac{p^{\infty}}{2 - \Lambda} \tag{60}$$

The exact solution for this average normal stress takes the same format as in (60), with Λ replaced by Λ_{ex} [exact; see, e.g., Kachanov (1987)]

$$\Lambda_{ex} = \frac{\sqrt{2+2k}}{1+\sqrt{k}} \tag{61}$$

Table 2 shows the comparison between Λ and Λ_{ex} for different values of d which is defined as $d \equiv 2k/(1-k)$. It is clear that the error associated with the approximate solution increases as d decreases. This is due to the stress field singularity at microcrack tips.

Table 2. Comparison between Λ and Λ_{ex}

d	exact	approx	error(%)
10	1.001037	1.001035	0.0002
5	1.00352	1.00349	0.0025
1	1.03528	1.03280	0.2396
0.5	1.07047	1.06066	0.9161
0.25	1.118034	1.091089	2.41
0.1	1.18821	1.122683	5.51
0.05	1.23801	1.13721	8.1419
0.005	1.34863	1.15280	14.52
0.0005	1.39238	1.15451	17.08

I.7. Appendix II. Components of matrix K in Eq. (24)

$$K_{11} = k_1 \sin 2\theta + k_2 \sin^2\theta + k_3 \;;\; K_{12} = -k_1 \sin 2\theta + k_2 \cos^2\theta + k_3$$
$$K_{13} = -k_2 \sin 2\theta - 2k_1 \cos 2\theta \;;\; K_{21} = k_4 \sin 2\theta + k_5 \sin^2\theta + k_6 \qquad (62)$$
$$K_{22} = -k_4 \sin 2\theta + k_5 \cos^2\theta + k_6 \;;\; K_{23} = -k_5 \sin 2\theta - 2k_4 \cos 2\theta$$

where

$$k_1 = \frac{1}{2\Delta}(f_2 \sin 2\phi - f_1 \cos 2\phi - f_3) \;;\; k_2 = \frac{1}{\Delta}(f_2 \cos 2\phi + f_1 \sin 2\phi + f_4)$$
$$k_3 = \frac{1}{\Delta}(f_2 \sin^2\phi - \frac{1}{2} f_1 \sin 2\phi) \;;\; k_4 = \frac{1}{2\Delta}(f_6 \sin 2\phi - f_5 \cos 2\phi - f_7) \qquad (63)$$
$$k_5 = \frac{1}{\Delta}(f_6 \cos 2\phi + f_5 \sin 2\phi + f_8) \;;\; k_6 = \frac{1}{\Delta}(f_6 \sin^2\phi - \frac{1}{2} f_5 \sin 2\phi)$$

and

$$f_1 = (\alpha_1\alpha_4 - \alpha_2\alpha_3)\alpha_6 + \alpha_2 \;;\; f_2 = -(\alpha_1\alpha_4 - \alpha_2\alpha_3)\alpha_8 + \alpha_1$$
$$f_3 = \alpha_1\alpha_6 + \alpha_2\alpha_8 \;;\; f_4 = \alpha_5 f_2 + \alpha_7 f_1 \qquad (64)$$
$$f_5 = -(\alpha_1\alpha_4 - \alpha_2\alpha_3)\alpha_5 + \alpha_4 \;;\; f_6 = (\alpha_1\alpha_4 - \alpha_2\alpha_3)\alpha_7 + \alpha_3$$
$$f_7 = \alpha_8 f_5 + \alpha_6 f_6 \;;\; f_8 = \alpha_3\alpha_5 + \alpha_4\alpha_7 \;;\; \Delta = det(\mathbf{I} - \boldsymbol{\alpha})$$

I.8. Figure captions

Figure 1. Superposition of microcrack problem.

Figure 2. The local and global coordinates systems.

Figure 3(a)(b). Definitions of geometric quantities for two neighboring microcracks.

Figure 4. Decomposition of two-microcrack interaction problem.

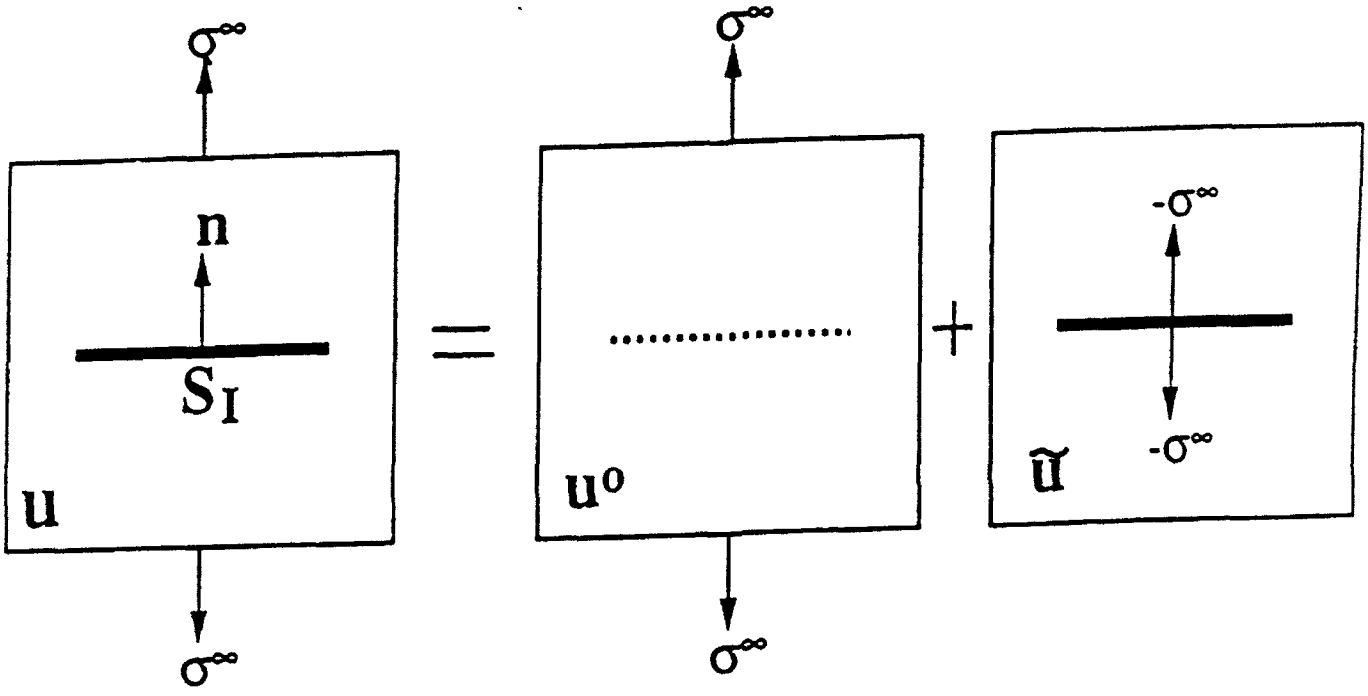

Figure 1. Superposition of microcrack problem.

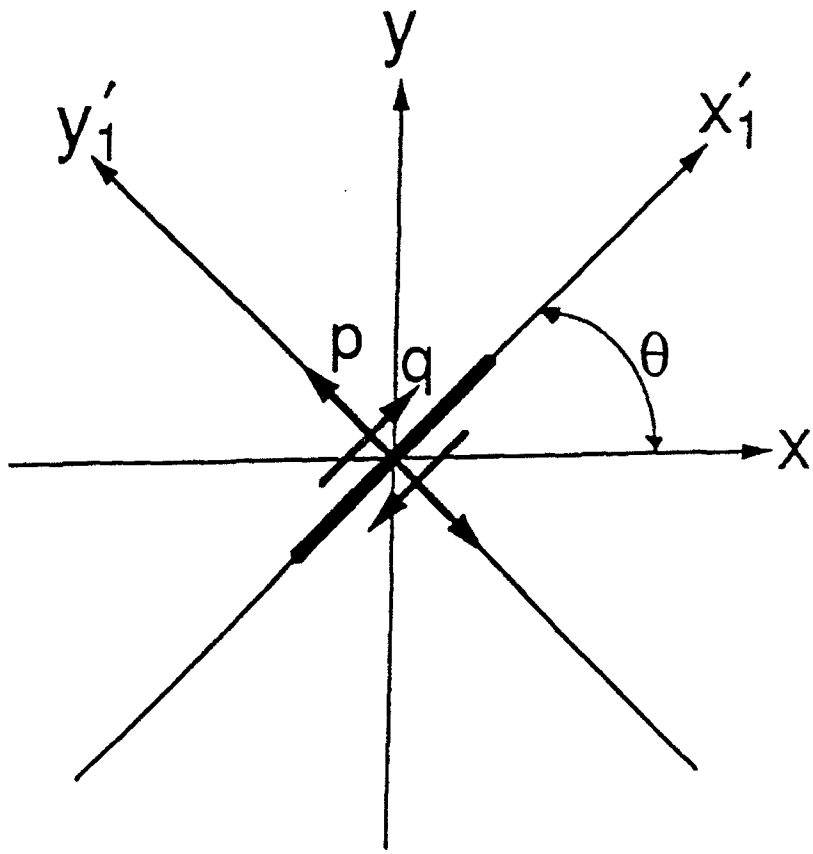

Figure 2. The local and global coordinates systems.

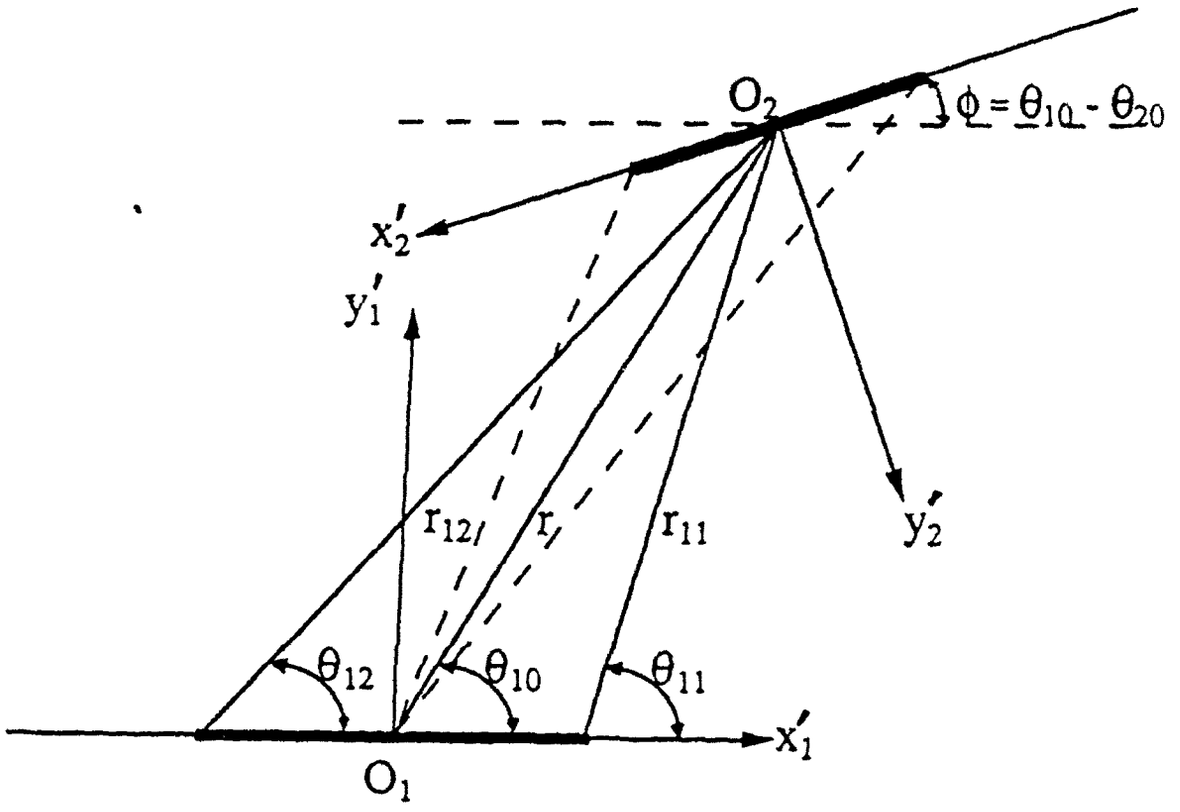

(a)

Figure 3(a)(b). Definitions of geometric quantities for two neighboring microcracks.

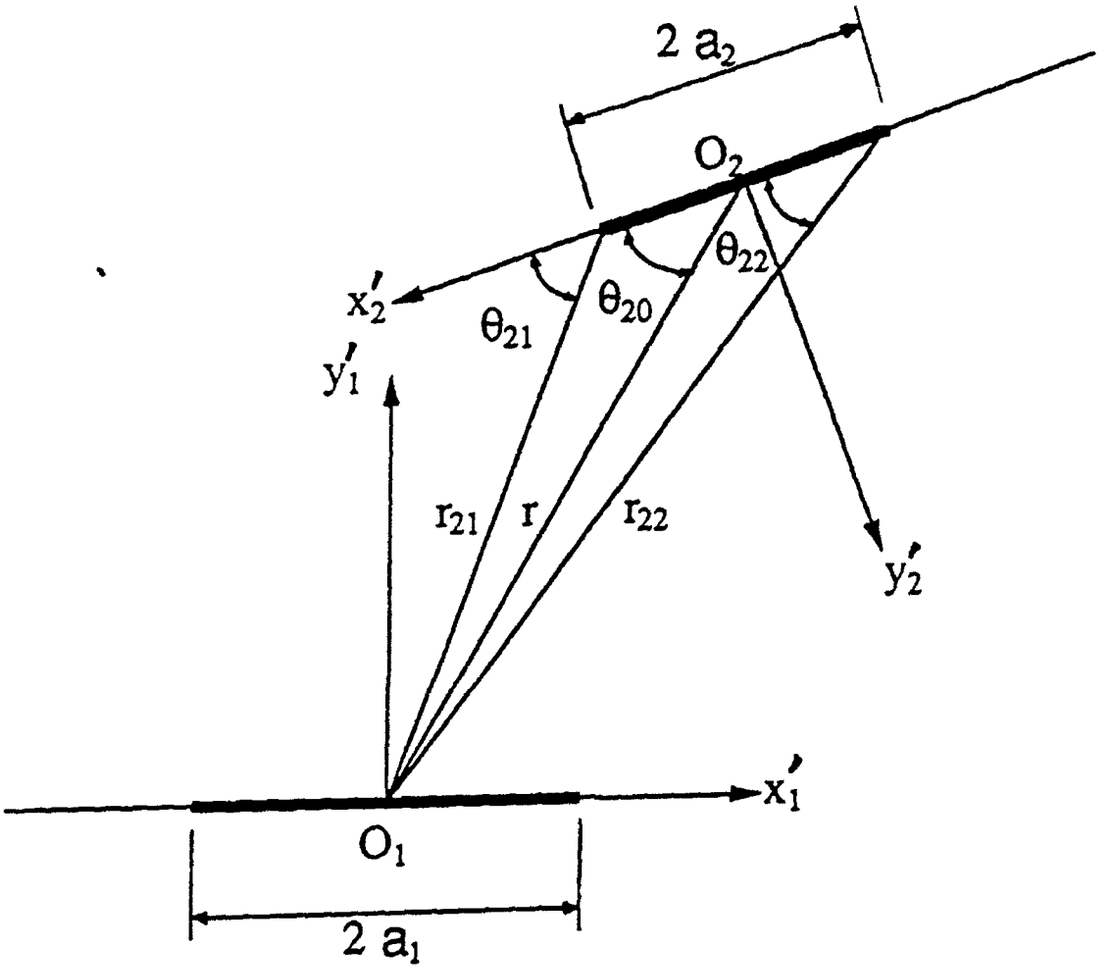

(b)

Figure 3(a)(b). Definitions of geometric quantities for two neighboring microcracks.

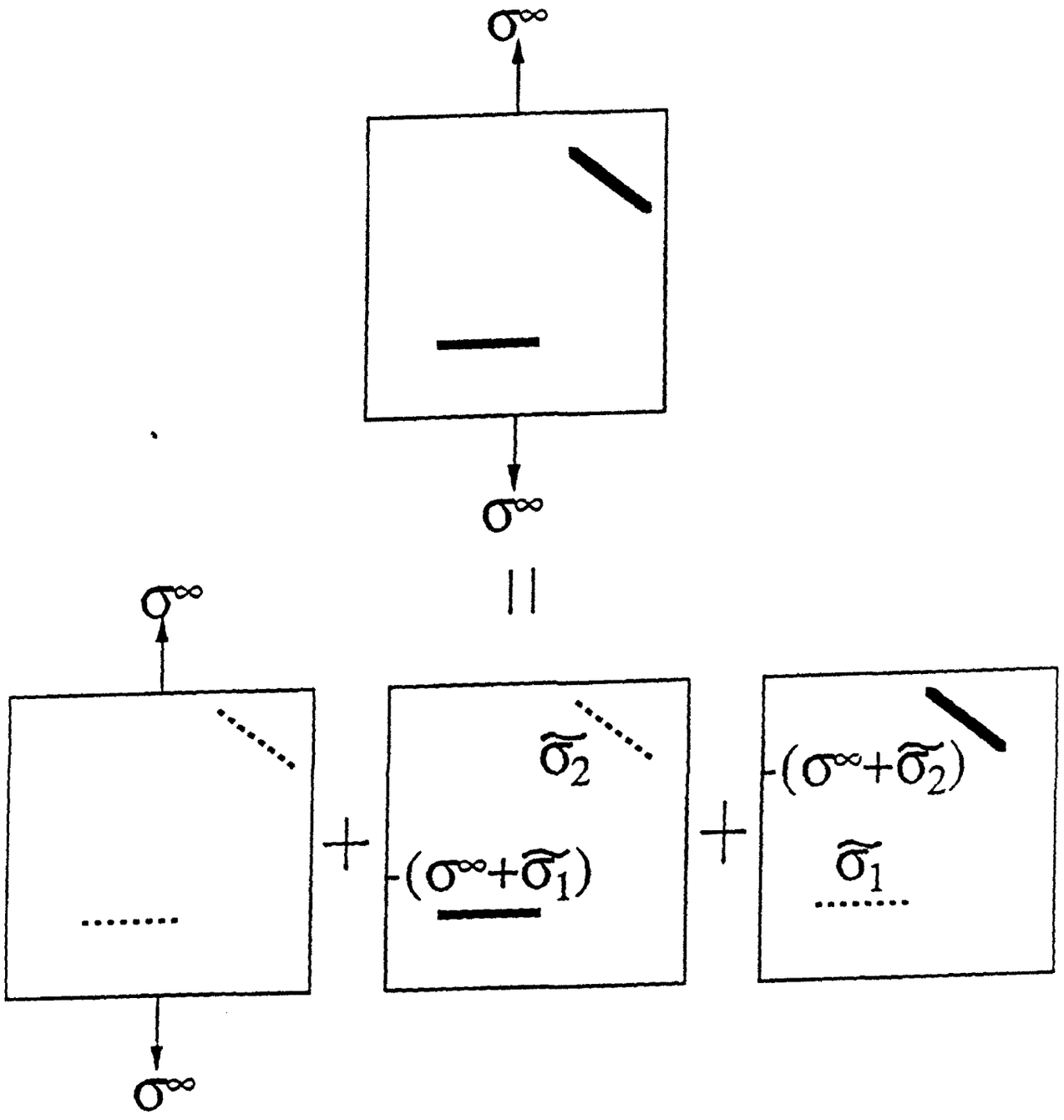

Figure 4. Decomposition of two-microcrack interaction problem.

PART II

Effective Elastic Moduli of Two-Dimensional Brittle Solids with Interacting Microcracks. II : Evolutionary Damage Models

II.0. Abstract

In Part I of this series, basic formulations of *stationary* micromechanical theory and overall responses are presented for two-dimensional brittle solids with randomly dispersed microcracks. The basic formulations hinge on an *ensemble average* approach which includes pairwise microcrack interactions. In this paper, statistical micromechanical *evolutionary models* are proposed to account for "cleavage 1" growth of randomly oriented and located microcracks under microcrack interaction effects. Biaxial tension/compression loadings are also considered to take into account mixed microcrack opening and closure effects. Efficient numerical integration algorithms for the proposed ensemble averaged constitutive equations are subsequently given. Further, uniaxial and biaxial tests are presented to illustrate the proposed models and procedures. Finally, a higher-order microcrack interaction model within the proposed micromechanical framework is discussed.

II.1. Introduction

A statistical micromechanical ensemble-volume average approach to explicitly derive overall constitutive equations for microcrack-weakened brittle solids has been presented in Part I of this series. The proposed explicit micromechanical approach takes into account interactions among microcracks, random microcrack orientations, locations and densities, and microcrack opening displacements. Damage-induced overall anisotropy can be predicted by the proposed framework. The proposed micromechanical approach is at variance with existing "effective medium theories" such as the self-consistent method [Hill (1965), Budiansky and O'Connell (1976), Horii and Nemat-Nasser (1983)], the generalized self-consistent method [Christensen and Lo (1979)], the differential scheme [Roscoe (1952, 1973), McLaughlin (1977)], and the Mori-Tanaka method [Mori and Tanaka (1973), Benveniste (1986)], etc.. In addition, the proposed framework is different from those micromechanical interaction analyses based on Monte Carlo simulations and numerical computations of stress "transmission factors" [Kachanov (1987), Kachanov and Laures (1989)]. The simple approximate analytical solutions for the two-microcrack interaction problem render *closed-form explicit* expressions for the evaluation of ensemble-average integrals.

Nevertheless, during loading histories of brittle solids, pre-existing microcracks may become unstable and *grow* along certain preferred orientations, depending on loading levels, microcrack configurations and interactions, etc.. Therefore, it is important to formulate micromechanical "cleavage 1" [Ashby (1979)] evolutionary damage models to account for both microcrack kinetics and microcrack interactions under specified loads. Some micromechanical "evolutionary" damage models were proposed in the literature for "effective medium theories"; see, e.g., Krajcinovic and Fanella (1986), Fanella and Krajcinovic (1988), Sumarac and Krajcinovic (1987), Ju (1991), Ju and Lee (1991), and Lee and Ju (1991), etc.. However, these micromechanical evolutionary damage models are only valid for weak microcrack interactions under low or at most moderate microcrack concentrations. On the other hand, microcrack interaction models due to Kachanov (1987), Kachanov and Laures (1989) do not consider microcrack growth or nucleation kinetics.

The primary objective of this paper is to extend the framework proposed in Part I to accommodate "cleavage 1" microcrack growth process under microcrack interactions. "Cleavage 1" process implies that only the growth of *pre-existing* microcracks is considered. Therefore, microcrack number remains constant during loading histories. Of course, one may also consider "cleavage 2" process [Ashby (1979)] to accommodate *nucleation* of new microcracks. However, that is beyond the scope of the present paper. In Section 2, micromechanical kinetic equations characterizing the "process domains" of active (open) microcracks are introduced. These "process domains"

together with "open microcrack domains" completely define the integration domains of the ensemble averaged constitutive equations relating macro-strain and macro-stress. Moreover, various tension/compression loadings are presented in Section 2 to illustrate the proposed approach. Efficient numerical integration algorithms are presented in Section 3 to implement the proposed damage models. A number of uniaxial and biaxial tests are also performed. Finally, discussions on a higher-order microcrack interaction model within the proposed framework is given in Section 4.

II.2. Evolutionary models with microcrack interaction

Let us consider an ensemble of randomly oriented and located microcracks within a statistically representative volume element. The microcrack number density is denoted by n and the microcrack length is denoted by $2a$. The representative element is subjected to two-dimensional external loading $\boldsymbol{\tau}^{\infty} = (\sigma_{11}^{\infty}, \sigma_{22}^{\infty}, \sigma_{21}^{\infty})^T$. In accord with Part I of this work, the overall compliance matrix $\overline{\langle \mathbf{S} \rangle}$ can be written as (plane strain with linear elastic matrix)

$$\overline{\langle \mathbf{S} \rangle} = \mathbf{S}^{\circ} + \overline{\langle \mathbf{S}^{*1} \rangle} + \overline{\langle \mathbf{S}^{*2} \rangle} \tag{1}$$

where [see Eqs. (37)–(39) in Part I]

$$\mathbf{S}^{\circ} = \frac{(1+\nu)}{E} \begin{bmatrix} 1-\nu & -\nu & 0 \\ -\nu & 1-\nu & 0 \\ 0 & 0 & 2 \end{bmatrix} \tag{2}$$

$$\overline{\langle \mathbf{S}^{*1} \rangle} \equiv \frac{(1-\nu^2)}{E} n \int_{\Theta} a_1^2 \, \mathbf{g} \cdot \mathbf{K}_0 \, d\theta \tag{3}$$

$$\overline{\langle \mathbf{S}^{*2} \rangle} \equiv \frac{(1-\nu^2)}{\pi E} n^2 \int_{\Theta} a_1^4 \, \mathbf{g} \cdot \langle \hat{\mathbf{K}} \rangle \, d\theta \tag{4}$$

and [see Eq. (34) in Part I]

$$\langle \hat{\mathbf{K}} \rangle \equiv \int_{\hat{\Xi}} \mathbf{K} \, r dr d\theta_{10} d\theta_{20} \tag{5}$$

Note that a_1 is the half-length of a primary microcrack and definitions of $\mathbf{g}$, $\mathbf{K}$ and $\mathbf{K}_0$ are given in Eqs. (11), (24) and (26) of Part I, respectively. The effective radius r has been normalized with respect to the microcrack radius a_1. Further, $\hat{\Xi}$ is the current active integration domain, including contributions from open *stationary* or *unstable* microcracks. Contributions due to closed microcracks are not considered in this paper.

For biaxial loadings, the *open* microcrack domain can be approximately defined by finding the domain of tensile (positive) normal stresses on microcrack planes as follows

$$\sigma_{11}^{\infty} \sin^2\theta + \sigma_{22}^{\infty} \cos^2\theta - \sigma_{21}^{\infty} \sin 2\theta \geq 0 \tag{6}$$

It is noted that Eq. (6) only considers the far-field stresses $\boldsymbol{\sigma}^{\infty}$. In some cases, however, the open microcrack domain can be affected by microcrack interaction. That is, some originally *open* microcracks may become closed due to strong microcrack interaction. When this occurs, the *local* stresses $\boldsymbol{\sigma}$ should be used in (6); i.e., one should check the following "local (normal) opening condition" to ensure that a microcrack is indeed open: $\langle p \rangle \geq 0$.

II.2.1. Kinetic equations for microcrack growth

In continuum damage mechanics, kinetic equations characterizing damage processes are typically postulated on the basis of hypothetical phenomenological arguments and macroscopic observations. However, as shown by Krajcinovic and Fanella (1986), microcrack kinetic equations can be actually derived based on micromechanics, probabilistic configurations of microcracks along certain microstructural weak planes, and fracture energy barriers on the mesoscale. When the *local* stress intensity factor (or strain energy release rate) reaches a certain critical value for the weak plane, a pre-existing microcrack is assumed to become unstable and grows along the weak plane in an unstable manner until reaching a certain characteristic size such as a grain or facet size [Krajcinovic and Fanella (1986), Sumarac and Krajcinovic (1987)]. This idealization is reasonable for *pre-existing* intergranular microcracks or interfacial microcracks (between the matrix and inclusions) in certain brittle materials such as concrete, ceramics, rocks, ice, and some brittle composites, etc.. For simplicity, we do not consider microcrack kinking (into the matrix or neighboring weak planes) nor nucleation of new microcracks; see Fanella and Krajcinovic (1988), Ju and Lee (1991), and Lee and Ju (1991) for some recent treatments. In other words, it is assumed that there exists a higher energy barrier serving as a microcrack trapping mechanism; e.g., a higher fracture toughness due to the matrix or due to intergranular kinking. Therefore, the proposed evolutionary damage models are only suitable for pre-peak (not post-peak) behavior of a class of brittle materials aforementioned. "Run-away instability" or localized macrocrack growth is **not** considered.

Within the context of microcrack interaction, the *local* stresses σ (not σ^{∞}) should be employed to compute the stress intensity factors (or strain energy release rates) on pre-existing microcrack tips. This treatment is completely different from existing ("effective medium") micromechanical evolutionary models which employ far field stresses σ^{∞}. Following Krajcinovic and Fanella (1986), we make the following two-stage simplification. It is assumed that the length of a pre-existing microcrack can either be $2a_0$ if the microcrack is stationary, or $2a_f$ if the microcrack is activated. Note that $2a_0$ denotes the average length of an initial microcrack and $2a_f$ signifies the average length of a propagated microcrack (e.g., the grain or facet size). The relation between the initial and final microcrack lengths is assumed to be

$$a_0 = \rho_0 \, a_f \tag{7}$$

where ρ_0 is a scalar between 0 and 1. The microcrack growth from $2a_0$ to $2a_f$ is assumed to be *instantaneous* once the local fracture energy is reached.

The actual fracture criterion of a material depends on its underlying physics of fracture. This paper does not intend to investigate fracture criteria of all materials. Instead, we attempt to demonstrate possible procedures involved in a micromechanical statistical evolutionary damage formulation. For illustration purpose, the following mixed mode fracture criterion is employed [see Kanninen and Popelar (1985, p. 50–51)]:

$$\left(\frac{K_I}{K_{Ic}}\right)^2 + \left(\frac{K_{II}}{K_{IIc}}\right)^2 = 1 \tag{8}$$

where K_I and K_{II} are the Mode I and Mode II stress intensity factors of an initial microcrack, respectively. Similarly, K_{Ic} and K_{IIc}, respectively, are the Mode I and Mode II critical stress intensity factors of the weak plane where a pre-existing microcrack is located. The foregoing fracture criterion may be suitable for some materials but modifications are necessary when application to a specific material is sought. In the spirit of statistical ensemble-average stresses, it is reasonable to write the following simple approximations (under *plane strain*):

$$K_I = \langle p \rangle \sqrt{\pi a_0} \quad ; \quad K_{II} = \langle q \rangle \sqrt{\pi a_0} \tag{9}$$

where $\langle p \rangle$ and $\langle q \rangle$ = the ensemble-averaged *local* normal and shear stresses projected on microcrack surfaces in local coordinates. Substitution of (9) into (8) leads to

$$\langle p \rangle^2 + k^2 \langle q \rangle^2 = F_c^2 \tag{10}$$

where

$$k \equiv \frac{K_{Ic}}{K_{IIc}} \quad ; \quad Fc \equiv \frac{K_{Ic}}{\sqrt{\pi a_0}} \tag{11}$$

For uniformly distributed and oriented microcracks, one has $f(\theta) = 1/\pi$ and $f(\mathbf{x}) = n$. From Eqs. (25)–(27) of Part I, one can write

$$\begin{Bmatrix} \langle p \rangle \\ \langle q \rangle \end{Bmatrix} = \left(\mathbf{K}_0 + \frac{n}{\pi}\langle \mathbf{K} \rangle\right) \cdot \begin{Bmatrix} \sigma_{11}^{\infty} \\ \sigma_{22}^{\infty} \\ \sigma_{12}^{\infty} \end{Bmatrix} \tag{12}$$

For convenience, let us define

$$\mathbf{M} \equiv \mathbf{K}_0 + \frac{n}{\pi}\langle \mathbf{K} \rangle \tag{13}$$

It is emphasized that $\langle \mathbf{K} \rangle$ (and thus $\mathbf{M}$) includes microcrack interaction effects. With (12) and (13) at hand, Eq. (10) can be rephrased as follows

$$\gamma_0 \hat{\sigma}_{11}^{\infty 2} + \gamma_2 \hat{\sigma}_{22}^{\infty 2} + \gamma_3 \hat{\sigma}_{12}^{\infty 2} + 2(\gamma_1 \hat{\sigma}_{11}^{\infty} \hat{\sigma}_{22}^{\infty} + \gamma_4 \hat{\sigma}_{11}^{\infty} \hat{\sigma}_{12}^{\infty} + \gamma_5 \hat{\sigma}_{22}^{\infty} \hat{\sigma}_{12}^{\infty}) = 1 \tag{14}$$

where $\hat{\boldsymbol{\sigma}}^{\infty} \equiv \boldsymbol{\sigma}^{\infty}/F_c$ and

$$\begin{aligned} &\gamma_0 = M_{11}^2 + k^2 M_{21}^2 \;;\; \gamma_1 = M_{11}M_{12} + k^2 M_{21}M_{22} \;;\; \gamma_2 = M_{12}^2 + k^2 M_{22}^2 \\ &\gamma_3 = M_{13}^2 + k^2 M_{23}^2 \;;\; \gamma_4 = M_{11}M_{13} + k^2 M_{21}M_{23} \;;\; \gamma_5 = M_{12}M_{13} + k^2 M_{22}M_{23} \end{aligned} \tag{15}$$

Eq. (14) can be used to solve for the "unstable angle domains" (θ^p) defining the "cleavage 1" unstable microcrack growth domains under a specified far field loading $\boldsymbol{\sigma}^{\infty}$. Conversely, for a specified "unstable growth angle domain", Eq. (14) can be used to obtain the external loading.

II.2.2. Dilute case — Taylor's model

In this case, the overall compliance of a microcrack-weakened solid takes the form

$$\overline{\langle \mathbf{S} \rangle} = \mathbf{S}^o + \overline{\langle \mathbf{S}^{*1i} \rangle} + \overline{\langle \mathbf{S}^{*1p} \rangle} \tag{16}$$

where $\overline{\langle \mathbf{S}^{*1i} \rangle}$ and $\overline{\langle \mathbf{S}^{*1p} \rangle}$ denote the compliance contributions from *initial* microcracks and microcrack *growth*, respectively. $\overline{\langle \mathbf{S}^{*1p} \rangle}$ can be expressed as [cf. (42)–(43) of Part I]:

$$\overline{\langle \mathbf{S}^{*1p} \rangle} = \frac{(1-\nu^2)}{E}\omega_0(\rho_0^{-2} - 1)\begin{bmatrix} S_{11}^{*1p} & 0 & S_{16}^{*1p} \\ 0 & S_{22}^{*1p} & S_{26}^{*1p} \\ S_{61}^{*1p} & S_{62}^{*1p} & S_{66}^{*1p} \end{bmatrix} \tag{17}$$

where $\omega_0 \equiv n a_0^2$ and

$$\begin{aligned} &S_{11}^{*1p} = \theta_2^p - \theta_1^p - \tfrac{1}{2}(\sin 2\theta_2^p - \sin 2\theta_1^p) \;;\; S_{22}^{*1p} = \theta_2^p - \theta_1^p + \tfrac{1}{2}(\sin 2\theta_2^p - \sin 2\theta_1^p) \\ &S_{66}^{*1p} = 2(\theta_2^p - \theta_1^p) \;;\; S_{16}^{*1p} = \sin^2\theta_1^p - \sin^2\theta_2^p = S_{61}^{*1p} = S_{26}^{*1p} = S_{62}^{*1p} \end{aligned} \tag{18}$$

In Eq. (18), $\Theta^p \equiv [\theta_1^p, \theta_2^p]$ is the evolutionary angle domain defined by Eq. (14).

(1) **Uniaxial tension**: $\hat{\sigma}_{22}^{\infty} > 0$, $\hat{\sigma}_{11}^{\infty} = \hat{\sigma}_{21}^{\infty} = 0$. All microcracks are open but overall responses are *anisotropic* due to preferred orientations of microcrack growth. Specifically, the process domain is $\Theta^p = [0, \theta^p] \cup [\pi - \theta^p, \pi]$ (see Fig. 1), where θ^p can be solved from (14) for given $\hat{\sigma}_{22}^{\infty}$ (or vice versa):

$$\gamma_2 = \cos^4\theta^p + k^2\cos^2\theta^p \sin^2\theta^p = \hat{\sigma}_{22}^{\infty 2} \tag{19}$$

From (18), we have

$$S_{11}^{*1p} = 2\theta^p - \sin 2\theta^p \;;\; S_{22}^{*1p} = 2\theta^p + \sin 2\theta^p \;;\; S_{66}^{*1p} = 4\theta^p \;;\quad \text{others} = 0 \tag{20}$$

(2) **Biaxial tension/compression**: $\hat{\sigma}_{22}^{\infty} > 0$, $\hat{\sigma}_{11}^{\infty} < 0$, $\hat{\sigma}_{21}^{\infty} = 0$. The bound of unstable growth angle domain, θ^p, can be computed from Eq. (14). The process domain is therefore $\Theta^p =$

$[0, \theta^p] \cup [\pi - \theta^p, \pi]$. Conversely, one can obtain the axial external tensile stress $\hat{\sigma}_{22}^{\infty}$ for given lateral external stress $\hat{\sigma}_{11}^{\infty}$ and prescribed angle bound θ^p:

$$\hat{\sigma}_{22}^{\infty} = \left(\frac{-\hat{\sigma}_{11}^{\infty}\gamma_1 + \sqrt{(\gamma_1^2 - \gamma_2\gamma_0)\hat{\sigma}_{11}^{\infty 2} + \gamma_2}}{\gamma_2} \right) \tag{21}$$

The non-zero components of $\overline{\langle \mathbf{S}^{*1p} \rangle}$ are

$$S_{11}^{*1p} = 2\theta^p - \sin 2\theta^p \;\; ; \;\; S_{22}^{*1p} = 2\theta^p + \sin 2\theta^p \;\; ; \;\; S_{33}^{*1p} = 4\theta^p \tag{22}$$

Since $\hat{\sigma}_{11}^{\infty} < 0$, it follows that ϵ_{11}^{*} is *negative* and proportional to the density ω_0. This is due to the fact that Mode II contribution to (contractive) lateral strain is *greater* than Mode I contribution for biaxial tension/compression loads. To wit, let us consider an arbitrary stationary microcrack and compare the contributions of Mode I and Mode II to ϵ_{11}^{*}:

$$\epsilon_{11}^{*I} = 2\frac{(1-\nu^2)\pi a_0^2}{E} \sin^2\theta(\cos^2\theta\sigma_{22}^{\infty} + \sin^2\theta\sigma_{11}^{\infty}) \quad \text{(Mode I)} \tag{23}$$

$$\epsilon_{11}^{*II} = -\tfrac{1}{2}\frac{(1-\nu^2)\pi a_0^2}{E} \sin^2 2\theta(\sigma_{22}^{\infty} - \sigma_{11}^{\infty}) \quad \text{(Mode II)} \tag{24}$$

The sum of Mode I and Mode II contributions is

$$\epsilon_{11}^{*} = 2\frac{(1-\nu^2)\pi a_0^2}{E} \sin^2\theta\sigma_{11}^{\infty} \leq 0 \tag{25}$$

II.2.3. Uniaxial and biaxial tension loadings

Within the proposed framework, the computation of overall compliances require. nformation regarding integration domains for microcrack *opening* and *growth*. For uniaxial tension, all microcracks are initially *open* and Eq. (14) becomes (19) in which γ_2 is evaluated by (15). The length of a microcrack is either $a_1 = a_0$ if *stationary* or $a_1 = a_f$ if *unstable*. For a prescribed configuration of microcrack growth domain, $\Theta^p = [0, \theta^p] \cup [\pi - \theta^p, \pi]$, one can systematically explore the status and length (a_2) of a second neighboring random microcrack. The details (27 possible cases) are as follows; see also Figure 2.

Category I. If $0 \leq \theta \leq \theta^p$ and $a_1 = a_f$: 9 possible cases concerning the length of a_2.

$0 \leq \theta + \theta_{10} \leq \theta^p$	a_2	$\theta^p < \theta + \theta_{10} \leq \alpha^p$	a_2
(1) $If\ 0 \leq \theta_{20} \leq \theta + \theta_{10} + \theta^p$, *then*	a_f	(4) $If\ 0 \leq \theta_{20} \leq \theta + \theta_{10} - \theta^p$, *then*	a_0
(2) $If\ \theta + \theta_{10} + \theta^p < \theta_{20} \leq \theta + \theta_{10} + \alpha^p$	a_0	(5) $If\ \theta + \theta_{10} - \theta^p < \theta_{20} \leq \theta + \theta_{10} + \theta^p$	a_f
(3) $If\ \theta + \theta_{10} + \alpha^p < \theta_{20} \leq \pi$	a_f	(6) $If\ \theta + \theta_{10} + \theta^p < \theta_{20} \leq \pi$	a_0

$\alpha^p < \theta + \theta_{10} \leq 2\pi$	a_2
(7) $If\ 0 \leq \theta_{20} \leq \theta + \theta_{10} - \alpha^p$, *then*	a_f
(8) $If\ \theta + \theta_{10} - \alpha^p < \theta_{20} \leq \theta + \theta_{10} - \theta^p$	a_0
(9) $If\ \theta + \theta_{10} - \theta^p < \theta_{20} \leq \pi$	a_f

Category II. If $\theta^p < \theta \leq \alpha^p$ and $a_1 = a_0$: 9 possible cases concerning the length of a_2.

$\theta^p \leq \theta + \theta_{10} \leq \alpha^p$	a_2	$\alpha^p < \theta + \theta_{10} \leq \beta^p$	a_2
(1) $If\ 0 \leq \theta_{20} \leq \theta + \theta_{10} - \theta^p$, *then*	a_0	(4) $If\ 0 \leq \theta_{20} \leq \theta + \theta_{10} - \alpha^p$, *then*	a_f
(2) $If\ \theta + \theta_{10} - \theta^p < \theta_{20} \leq \theta + \theta_{10} + \theta^p$	a_f	(5) $If\ \theta + \theta_{10} - \alpha^p < \theta_{20} \leq \theta + \theta_{10} - \theta^p$	a_0
(3) $If\ \theta + \theta_{10} + \theta^p < \theta_{20} \leq \pi$	a_0	(6) $If\ \theta + \theta_{10} - \theta^p < \theta_{20} \leq \pi$	a_f

$\beta^p < \theta + \theta_{10} \leq 2\pi$	a_2
(7) $If\ 0 \leq \theta_{20} \leq \theta + \theta_{10} - \beta^p$, *then*	a_0
(8) $If\ \theta + \theta_{10} - \beta^p < \theta_{20} \leq \theta + \theta_{10} - \alpha^p$	a_f
(9) $If\ \theta + \theta_{10} - \alpha^p < \theta_{20} \leq \pi$	a_0

Category III. If $\alpha^p \leq \theta \leq \pi$ and $a_1 = a_f$: 9 possible cases concerning the length of a_2.

$\alpha^p < \theta + \theta_{10} \leq \beta^p$	a_2	$\beta^p < \theta + \theta_{10} \leq \pi + \alpha^p$	a_2
(1) $If\ 0 \leq \theta_{20} \leq \theta + \theta_{10} - \alpha^p$, *then*	a_f	(4) $If\ 0 \leq \theta_{20} \leq \theta + \theta_{10} - \beta^p$, *then*	a_0
(2) $If\ \theta + \theta_{10} - \alpha^p < \theta_{20} \leq \theta + \theta_{10} - \theta^p$	a_0	(5) $If\ \theta + \theta_{10} - \beta^p < \theta_{20} \leq \theta + \theta_{10} - \alpha^p$	a_f
(3) $If\ \theta + \theta_{10} - \theta^p < \theta_{20} \leq \pi$	a_f	(6) $If\ \theta + \theta_{10} - \alpha^p < \theta_{20} \leq \pi$	a_0

$\pi + \alpha^p < \theta + \theta_{10} \leq 2\pi$	a_2
(7) $If\ 0 \leq \theta_{20} \leq \theta + \theta_{10} - \alpha^p - \pi,\ then$	a_f
(8) $If\ \theta + \theta_{10} - \alpha^p - \pi < \theta_{20} \leq \theta + \theta_{10} - \beta^p$	a_0
(9) $If\ \theta + \theta_{10} - \beta^p < \theta_{20} \leq \pi$	a_f

We have employed the definitions $\alpha^p \equiv \pi - \theta^p$ and $\beta^p \equiv \pi + \theta^p$. With the foregoing analysis at hand, one can evaluate the integrals in Eqs. (4)–(5) and the external stress $\hat{\sigma}_{22}^{\infty}$ from (19). For biaxial tension, the foregoing integration domains remain the same and the only difference is the evaluation of θ^p in Eq. (14).

II.2.4. Biaxial tension/compression loadings

In the case of biaxial tension/compression loadings, some microcracks are open while others are closed. Microcrack *process* and *open* domains are coupled and affect each other. For prescribed lateral stress $\hat{\sigma}_{11}^{\infty}$ and "process angle" θ^p, one has to compute the corresponding normal stress $\hat{\sigma}_{22}^{\infty}$ (evaluated at $\theta = \theta^p$) and the open/closed microcrack angle boundary θ^* by Eqs. (14) and (6) in order to predict progressive *stress-strain* responses. In particular, Eqs. (14) and (6) can be recast as

$$\hat{\sigma}_{22}^{\infty} = \left(\frac{-\hat{\sigma}_{11}^{\infty}\gamma_1 + \sqrt{(\gamma_1^2 - \gamma_2\gamma_0)\hat{\sigma}_{11}^{\infty 2} + \gamma_2}}{\gamma_2} \right)_{(\theta^*, \theta^p, \hat{\sigma}_{11}^{\infty})} \quad ; \quad \theta^* = \cos^{-1}\left(\sqrt{\frac{\hat{\sigma}_{11}^{\infty}}{-\hat{\sigma}_{22}^{\infty} + \hat{\sigma}_{11}^{\infty}}} \right)_{(\theta^p, \hat{\sigma}_{11}^{\infty})} \tag{26}$$

As mentioned earlier in Section 2, Eq. (6) [and therefore $(26)_2$] is based on far-field stresses and is therefore an approximation of the local stress formula (in biaxial tension/compression):

$$\langle p \rangle = M_{11}\hat{\sigma}_{11}^{\infty} + M_{12}\hat{\sigma}_{22}^{\infty} \geq 0 \tag{27}$$

From a mathematical viewpoint, use of (26) corresponds to a second-order (in ω^2) accurate interactive microcrack theory. On the other hand, use of $(26)_1$ and (27) produces third- and higher-order terms (in ω^3). Since our aim is to develop a second-order theory (in ω^2), Eqs. (26) can be regarded as a good approximation. Nevertheless, Eq. (27) should always be checked against any possible microcrack orientation to ensure that a microcrack is indeed *open*.

The microstructural integration domains can be systematically summarized as follows. Note that there are 76 possible cases in total and $\alpha^* \equiv \pi - \theta^*$ and $\beta^* \equiv \pi + \theta^*$.

Category I If $0 \le \theta \le \theta^p$ and $a_1 = a_f$: 19 possible cases concerning the length of a_2.

$0 \le \theta + \theta_{10} \le \theta^p$	a_2	$\theta^p < \theta + \theta_{10} \le \theta^*$	a_2
(1) $If\ 0 \le \theta_{20} \le \theta + \theta_{10} + \theta^p$, *then*	a_f	(5) $If\ 0 \le \theta_{20} \le \theta + \theta_{10} - \theta^p$, *then*	a_0
(2) $If\ \theta + \theta_{10} + \theta^p < \theta_{20} \le \theta + \theta_{10} + \theta^*$	a_0	(6) $If\ \theta + \theta_{10} - \theta^p < \theta_{20} \le \theta + \theta_{10} + \theta^p$	a_f
(3) $If\ \theta + \theta_{10} - \alpha^* < \theta_{20} \le \theta + \theta_{10} - \alpha^p$	a_0	(7) $If\ \theta + \theta_{10} + \theta^p < \theta_{20} \le \theta + \theta_{10} + \theta^*$	a_0
(4) $If\ \theta + \theta_{10} - \alpha^p < \theta_{20} \le \pi$	a_f	(8) $If\ \theta + \theta_{10} + \alpha^* < \theta_{20} \le \pi$	a_0

$\alpha^* < \theta + \theta_{10} \le \alpha^p$	a_2	$\alpha^p \le \theta + \theta_{10} \le 2\pi$	a_2
(9) $If\ 0 \le \theta_{20} \le \theta + \theta_{10} - \alpha^*$, *then*	a_0	(13) $If\ 0 \le \theta_{20} \le \theta + \theta_{10} - \alpha^p$, *then*	a_f
(10) $If\ \theta + \theta_{10} - \theta^* < \theta_{20} \le \theta + \theta_{10} - \theta^p$	a_0	(14) $If\ \theta + \theta_{10} - \alpha^p < \theta_{20} \le \theta + \theta_{10} - \alpha^*$	a_0
(11) $If\ \theta + \theta_{10} - \theta^p < \theta_{20} \le \theta + \theta_{10} + \theta^p$	a_f	(15) $If\ \theta + \theta_{10} - \theta^* < \theta_{20} \le \theta + \theta_{10} - \theta^p$	a_0
(12) $If\ \theta + \theta_{10} + \theta^p < \theta_{20} \le \pi$	a_0	(16) $If\ \theta + \theta_{10} - \theta^p < \theta_{20} \le \pi$	a_f

$\theta^* < \theta + \theta_{10} \le \alpha^*$	a_2
(17) $If\ \theta + \theta_{10} - \theta^* \le \theta_{20} \le \theta + \theta_{10} - \theta^p$	a_0
(18) $If\ \theta + \theta_{10} - \theta^p < \theta_{20} \le \theta + \theta_{10} + \theta^p$	a_f
(19) $If\ \theta + \theta_{10} + \theta^p < \theta_{20} \le \theta + \theta_{10} + \theta^*$	a_0

Category II. If $\theta^p < \theta \leq \theta^*$ and $a_1 = a_0$: 19 possible cases concerning the length of a_2.

$\theta^p \leq \theta + \theta_{10} \leq \theta^*$	a_2	$\alpha^* < \theta + \theta_{10} \leq \alpha^p$	a_2
(1) $If\ 0 \leq \theta_{20} \leq \theta + \theta_{10} - \theta^p$, *then*	a_0	(5) $If\ 0 \leq \theta_{20} \leq \theta + \theta_{10} - \alpha^*$, *then*	a_0
(2) $If\ \theta + \theta_{10} - \theta^p < \theta_{20} \leq \theta + \theta_{10} + \theta^p$	a_f	(6) $If\ \theta + \theta_{10} - \theta^* < \theta_{20} \leq \theta + \theta_{10} - \theta^p$	a_0
(3) $If\ \theta + \theta_{10} + \theta^p < \theta_{20} \leq \theta + \theta_{10} + \theta^*$	a_0	(7) $If\ \theta + \theta_{10} - \theta^p < \theta_{20} \leq \theta + \theta_{10} + \theta^p$	a_f
(4) $If\ \theta + \theta_{10} + \alpha^* < \theta_{20} \leq \pi$	a_0	(8) $If\ \theta + \theta_{10} + \theta^p < \theta_{20} \leq \pi$	a_0

$\alpha^p < \theta + \theta_{10} \leq \beta^p$	a_2	$\beta^p \leq \theta + \theta_{10} \leq 2\pi$	a_2
(9) $If\ 0 \leq \theta_{20} \leq \theta + \theta_{10} - \alpha^p$, *then*	a_f	(13) $If\ 0 \leq \theta_{20} \leq \theta + \theta_{10} - \beta^p$, *then*	a_0
(10) $If\ \theta + \theta_{10} - \alpha^p < \theta_{20} \leq \theta + \theta_{10} - \alpha^*$	a_0	(14) $If\ \theta + \theta_{10} - \beta^p < \theta_{20} \leq \theta + \theta_{10} - \alpha^p$	a_f
(11) $If\ \theta + \theta_{10} - \theta^* < \theta_{20} \leq \theta + \theta_{10} - \theta^p$	a_0	(15) $If\ \theta + \theta_{10} - \alpha^p < \theta_{20} \leq \theta + \theta_{10} - \alpha^*$	a_0
(12) $If\ \theta + \theta_{10} - \theta^p < \theta_{20} \leq \pi$	a_f	(16) $If\ \theta + \theta_{10} - \alpha^* < \theta_{20} \leq \pi$	a_0

$\theta^* < \theta + \theta_{10} \leq \alpha^*$	a_2
(17) $If\ \theta + \theta_{10} - \theta^* \leq \theta_{20} \leq \theta + \theta_{10} - \theta^p$	a_0
(18) $If\ \theta + \theta_{10} - \theta^p < \theta_{20} \leq \theta + \theta_{10} + \theta^p$	a_f
(19) $If\ \theta + \theta_{10} + \theta^p < \theta_{20} \leq \theta + \theta_{10} + \theta^*$	a_0

Category III. If $\alpha^* < \theta \leq \alpha^p$ and $a_1 = a_0$: 19 possible cases concerning the length of a_2.

$\alpha^* \leq \theta + \theta_{10} \leq \alpha^p$	a_2	$\alpha^p < \theta + \theta_{10} \leq \beta^p$	a_2
(1) *If* $0 \leq \theta_{20} \leq \theta + \theta_{10} - \alpha^*$, *then*	a_0	(5) *If* $0 \leq \theta_{20} \leq \theta + \theta_{10} - \alpha^p$, *then*	a_f
(2) *If* $\theta + \theta_{10} - \theta^* < \theta_{20} \leq \theta + \theta_{10} - \theta^p$	a_0	(6) *If* $\theta + \theta_{10} - \alpha^p < \theta_{20} \leq \theta + \theta_{10} - \alpha^*$	a_0
(3) *If* $\theta + \theta_{10} - \theta^p < \theta_{20} \leq \theta + \theta_{10} + \theta^p$	a_f	(7) *If* $\theta + \theta_{10} - \theta^* < \theta_{20} \leq \theta + \theta_{10} - \theta^p$	a_0
(4) *If* $\theta + \theta_{10} + \theta^p < \theta_{20} \leq \pi$	a_0	(8) *If* $\theta + \theta_{10} - \theta^p < \theta_{20} \leq \pi$	a_f

$\beta^p < \theta + \theta_{10} \leq \beta^*$	a_2	$\pi + \alpha^* < \theta + \theta_{10} \leq 2\pi$	a_2
(9) *If* $0 \leq \theta_{20} \leq \theta + \theta_{10} - \beta^p$, *then*	a_0	(13) *If* $0 \leq \theta_{20} \leq \theta + \theta_{10} - \alpha^* - \pi$, *then*	a_0
(10) *If* $\theta + \theta_{10} - \beta^p < \theta_{20} \leq \theta + \theta_{10} - \alpha^p$	a_f	(14) *If* $\theta + \theta_{10} - \beta^* < \theta_{20} \leq \theta + \theta_{10} - \beta^p$	a_0
(11) *If* $\theta + \theta_{10} - \alpha^p < \theta_{20} \leq \theta + \theta_{10} - \alpha^*$	a_0	(15) *If* $\theta + \theta_{10} - \beta^p < \theta_{20} \leq \theta + \theta_{10} - \alpha^p$	a_f
(12) *If* $\theta + \theta_{10} - \theta^* < \theta_{20} \leq \pi$	a_0	(16) *If* $\theta + \theta_{10} - \alpha^p < \theta_{20} \leq \pi$	a_0

$\beta^* < \theta + \theta_{10} \leq \pi + \alpha^*$	a_2
(17) *If* $\theta + \theta_{10} - \beta^* \leq \theta_{20} \leq \theta + \theta_{10} - \beta^p$	a_0
(18) *If* $\theta + \theta_{10} - \beta^p < \theta_{20} \leq \theta + \theta_{10} - \alpha^p$	a_f
(19) *If* $\theta + \theta_{10} - \alpha^p < \theta_{20} \leq \theta + \theta_{10} - \alpha^*$	a_0

Category IV. If $\alpha^p < \theta \leq \pi$ and $a_1 = a_f$: 19 possible cases concerning the length of a_2.

$\alpha^p \leq \theta + \theta_{10} \leq \beta^p$	a_2	$\beta^p < \theta + \theta_{10} \leq \beta^*$	a_2
(1) $If\ 0 \leq \theta_{20} \leq \theta + \theta_{10} - \alpha^p$, *then*	a_f	(5) $If\ 0 \leq \theta_{20} \leq \theta + \theta_{10} - \beta^p$, *then*	a_0
(2) $If\ \theta + \theta_{10} - \alpha^p < \theta_{20} \leq \theta + \theta_{10} - \alpha^*$	a_0	(6) $If\ \theta + \theta_{10} - \beta^p < \theta_{20} \leq \theta + \theta_{10} - \alpha^p$	a_f
(3) $If\ \theta + \theta_{10} - \theta^* < \theta_{20} \leq \theta + \theta_{10} - \theta^p$	a_0	(7) $If\ \theta + \theta_{10} - \alpha^p < \theta_{20} \leq \theta + \theta_{10} - \alpha^*$	a_0
(4) $If\ \theta + \theta_{10} - \theta^p < \theta_{20} \leq \pi$	a_f	(8) $If\ \theta + \theta_{10} - \theta^* < \theta_{20} \leq \pi$	a_0

$\pi + \alpha^* < \theta + \theta_{10} \leq \pi + \alpha^p$	a_2	$\pi + \alpha^p < \theta + \theta_{10} \leq 2\pi$	a_2
(9) $If\ 0 \leq \theta_{20} \leq \theta + \theta_{10} - \alpha^* - \pi$, *then*	a_0	(13) $If\ 0 \leq \theta_{20} \leq \theta + \theta_{10} - \alpha^p - \pi$, *then*	a_f
(10) $If\ \theta + \theta_{10} - \beta^* < \theta_{20} \leq \theta + \theta_{10} - \beta^p$	a_0	(14) $If\ \theta + \theta_{10} - \alpha^p - \pi < \theta_{20} \leq \theta + \theta_{10} - \alpha^* - \pi$	a_0
(11) $If\ \theta + \theta_{10} - \beta^p < \theta_{20} \leq \theta + \theta_{10} - \alpha^p$	a_f	(15) $If\ \theta + \theta_{10} - \beta^* < \theta_{20} \leq \theta + \theta_{10} - \beta^p$	a_0
(12) $If\ \theta + \theta_{10} - \alpha^p < \theta_{20} \leq \pi$	a_0	(16) $If\ \theta + \theta_{10} - \beta^p < \theta_{20} \leq \pi$	a_f

$\beta^* < \theta + \theta_{10} \leq \pi + \alpha^*$	a_2
(17) $If\ \theta + \theta_{10} - \beta^* \leq \theta_{20} \leq \theta + \theta_{10} - \beta^p$	a_0
(18) $If\ \theta + \theta_{10} - \beta^p < \theta_{20} \leq \theta + \theta_{10} - \alpha^p$	a_f
(19) $If\ \theta + \theta_{10} - \alpha^p < \theta_{20} \leq \theta + \theta_{10} - \alpha^*$	a_0

The foregoing integration domains completely define the integrals in Eqs. (3)–(5), and therefore effective compliances can be computed. In a *strain-driven* algorithm, the axial tensile stress $\hat{\sigma}_{22}^{\infty}$ can also be computed accordingly. It is emphasized that microcrack interactions affect the values of γ_i and thus $\hat{\sigma}_{22}^{\infty}$; see $(26)_1$. In turn, $\hat{\sigma}_{22}^{\infty}$ affects the "opening angle" θ^*; see $(26)_2$.

II.3. Numerical algorithms and applications

II.3.1. Numerical integration algorithms

As previously mentioned, one needs to numerically evaluate the integrals involved in Eqs. (3)–(5). Furthermore, one needs to develop efficient numerical algorithm to solve Eq. (26) involving both process and opening domains. First, the numerical integrations of (3)–(5) can be efficiently achieved by using the "Gauss quadrature" scheme. In carrying out the Gauss quadrature numerical scheme, we have chosen the following integration ranges: $[2a, 20a]$ for the distance r, and $[0, \pi]$ for the angle θ_{10}. The integration bounds for θ_{20} and θ are subsequently determined from the systematic analyses presented in Sections 2.3 and 2.4.

Another issue is the number of Gauss points needed for each integration zone aforementioned in Sections 2.3 and 2.4. **Table 1** gives the convergence behavior of Gauss quadrature with respect

to the number of Gauss points used for each integration zone for the "aligned microcracks" problem previously considered in Section 3.2 of Part I. Clearly, use of 20 Gauss points in each integration zone is sufficiently accurate. An efficient, iterative numerical integration algorithm to solve Eq. (26) is summarized in **Box 1**.

Remark 3.1. For uniaxial and biaxial tensile loadings, Eq. (6) is automatically satisfied unless the axial stress goes to infinity; i.e., $\theta^* = \pi/2$. Therefore, the iterative process for finding the opening angle bound θ^* in Step (5) of **Box 1** is unnecessary. ∎

II.3.2. Uniaxial tension loading tests

In this section, we consider two (plane strain) uniaxial tension tests with different initial microcrack concentrations: $\omega_0 \equiv na_0^2 = 0.1$ (moderate density) and 0.4 (high density). It should be realized that these two concentrations are equal to 0.1π and 0.4π in terms of the commonly used definition ($\hat{\omega} \equiv n\pi a_0^2$). Moreover, the k value in Eq. (11) is taken as 0.5, initial Poisson's ratio $\nu = 0.2$, and $\rho_0 = 0.6$ in (7). For convenience, all strains are normalized (dimensionless) as follows:

$$\hat{\epsilon} \equiv \frac{\epsilon}{F_c\left(\frac{1-\nu^2}{E}\right)} \tag{28}$$

The *normalized* stress-strain curves are displayed in Figure 3. All compliances have also been normalized by dividing the common factor $(1 - \nu^2)/E$. We observe that microcrack interactions effectively *lower* the onset (threshold stress) of microcrack propagation. The existence of "corner points" on the axial stress-strain curves in Fig. 3 is a consequence of the *deterministic* fracture criterion (14) and the uniform initial microcrack size a_0. If we employ a *probabilistic* fracture criterion or *nonuniform* initial microcrack sizes, the "corner points" will disappear and be replaced by smooth transitions [c.f. Ju and Lee (1991), and Lee and Ju (1991)]. It is noted that the axial stress/lateral strain curves are the same for $\omega_0 = 0.1$ and 0.4 for Taylor's model due to the fact that microcracks have no contribution to $\hat{\epsilon}_{11}$. In the case of the proposed microcrack interaction theory, a significant *reduction* in the magnitude of lateral strains is observed. That is, microcrack interactions enhance Mode I displacements and reduce Mode II displacements, and therefore *reduce* the magnitude of lateral contraction.

Figures 4 and 5 show the *normalized* overall compliance components predicted by both Taylor's and the proposed models. It is noted that Taylor's model does not change either $\overline{\langle S_{12}\rangle}$ or $\overline{\langle S_{21}\rangle}$ components despite damage. By contrast, the proposed interaction model shows that the shear components $\overline{\langle S_{12}\rangle}$ and $\overline{\langle S_{21}\rangle}$ change. It is also observed that $\overline{\langle S_{12}\rangle}$ and $\overline{\langle S_{21}\rangle}$ become slightly different

as the microcrack concentration increases. As the normalized axial stress $\hat{\sigma}_{22}^{\infty}$ goes to infinity, one may expect that the overall compliance matrix asymptotically becomes isotropic because all pre-existing random microcracks grow to same length a_f. This is indeed the case for Taylor's model and the self-consistent model. However, this may not be always true if microcrack interactions are considered. The reason is that some initially *open* stationary microcracks (a_0) in the very close neighborhood of $\theta = \pi/2$ may become *closed* due to interactions with neighboring propagated microcracks (a_f). Biaxial tension loadings can be treated in a similar fashion and therefore are not repeated here.

II.3.3. Biaxial tension/compression loading tests

One has to determine the open domain (θ^*) and the corresponding axial tensile stress $\hat{\sigma}_{22}^{\infty}$ by solving the system of equations (26) for specified values of θ^p and $\hat{\sigma}_{11}^{\infty}$ in order to compute overall compliances. A good initial guess for θ^* can be obtained from Taylor's model by solving Eqs. (6) and (19). With this initial guess $\theta^{*(0)}$, one can obtain the trial value $\hat{\sigma}_{22}^{\infty(1)}$ by using Eq. $(26)_1$. Subsequently, an improved trial value $\theta^{*(1)}$ can be rendered by using $(26)_2$, and so on. In what follows, we adopt the following properties: $\nu = 0.2$, $\rho_0 = 0.6$ and $k = 0.5$.

To illustrate the performance of the proposed numerical algorithm summarized in **Box 1**, let us consider the *onset* point of the "cleavage 1" microcrack growth. **Table 2** shows the convergence behavior of this case for $\omega_0 = 0.1$ and $\hat{\sigma}_{11}^{\infty} = -0.1$. It is observed that remarkable convergence is reached within only two to three iterations.

The *normalized* axial stress-strain curves for four different biaxial tension/compression tests with $\omega_0 = 0.1, 0.4$ and lateral compression $\hat{\sigma}_{11}^{\infty} = -0.1, -0.4$, respectively, are similar to those of the uniaxial tension tests in Figure 3. However, the behavior of axial stress/ lateral strain curves depends on $\hat{\sigma}_{11}^{\infty}$ (or the ratio $|\hat{\sigma}_{22}^{\infty}/\hat{\sigma}_{11}^{\infty}|$) and ω_0; see Figures 6 and 7. The magnitude of lateral (contractive) strains are higher for higher lateral compression $\hat{\sigma}_{11}^{\infty} = -0.4$; compare Figures 6 and 7. On the other hand, the loading ratio $|\hat{\sigma}_{22}^{\infty}/\hat{\sigma}_{11}^{\infty}|$ affects the size of the open and process domains. The *sizes* and *orientations* of these open and process domains, in turn, affect the effects of microcrack interaction on lateral strains. In particular, for *higher* loading ratio $|\hat{\sigma}_{22}^{\infty}/\hat{\sigma}_{11}^{\infty}|$, the net effects of microcrack interaction *enhance* the Mode I (dilatational) contributions and *reduce* the Mode II (contractive) contributions. By contrast, when the loading ratio $|\hat{\sigma}_{22}^{\infty}/\hat{\sigma}_{11}^{\infty}|$ is relatively *small*, the net effects of microcrack interaction *enhance* the Mode II (contractive) contributions; see Fig. 7. It is worth mentioning that if $\hat{\sigma}_{22}^{\infty}$ continues to increase in Fig. 7, then the two solid lines in Fig. 7 will also intersect each other just as they do in Fig. 6.

Finally, Figure 8 displays the normalized $\overline{\langle S_{22} \rangle}$ and $\overline{\langle S_{11} \rangle}$ compliances vs. axial stresses for $\omega_0 = 0.4$ and $\hat{\sigma}_{11}^{\infty} = -0.1$. Due to closure of some microcracks, overall compliances are always *anisotropic*. It is also noted that due to microcrack interactions, the overall compliance matrix becomes *non-symmetric* (i.e., $S_{12} \neq S_{21}$).

II.4. A higher-order microcrack interaction model

The statistical micromechanical damage models presented so far are based on the concept of *pairwise* microcrack interaction. This pairwise microcrack interaction mechanism essentially corresponds to a *second-order* damage theory (in ω^2). Within the context of the ensemble-volume average approach, one can systematically incorporate many-microcrack interaction mechanisms into the proposed framework. In essence, one needs to re-derive the ensemble-average of the **perturbation** in local stress field due to n-microcrack *interactions* ($n \geq 3$).

To illustrate the foregoing statements, let us consider a three-microcrack (third-order in ω^3) interaction mechanism. Following the definitions and assumptions described in Part I of this study, one can recast the local ensemble stress perturbation in Eq. (12) of Part I as follows:

$$\langle \tilde{\mathbf{T}} \rangle + \langle \tilde{\tilde{\mathbf{T}}} \rangle \equiv \langle \left\{ \begin{matrix} \tilde{p} \\ \tilde{q} \end{matrix} \right\} \rangle + \langle \left\{ \begin{matrix} \tilde{\tilde{p}} \\ \tilde{\tilde{q}} \end{matrix} \right\} \rangle \tag{29}$$

where $\langle \tilde{\mathbf{T}} \rangle$ is the first-order local ensemble stress perturbation due to pairwise microcrack interactions, and $\langle \tilde{\tilde{\mathbf{T}}} \rangle$ is the second-order local ensemble stress perturbation due to the third order microcrack interactions. In particular, $\langle \tilde{\tilde{\mathbf{T}}} \rangle$ can be expressed as [cf. Eq. (13) of Part I]

$$\langle \tilde{\tilde{\mathbf{T}}} \rangle = \int_{\Xi} \langle \tilde{\tilde{\mathbf{T}}} \rangle (\mathbf{x}, a, \theta; \mathbf{x}_1, a_1, \theta_1 | \mathbf{x}_2, a_2, \theta_2) f(\mathbf{x}_2, a_2, \theta_2 | \mathbf{x}, a, \theta; \mathbf{x}_1, a_1, \theta_1) \, d\theta_2 da_2 d\mathbf{x}_2 \tag{30}$$

Here, $\langle \tilde{\tilde{\mathbf{T}}} \rangle (\mathbf{x}, a, \theta; \mathbf{x}_1, a_1, \theta_1 | \mathbf{x}_2, a_2, \theta_2)$ is the second-order *stress perturbation* of a microcrack centered at $\mathbf{x}$ with (a, θ), given a microcrack centered at $\mathbf{x}_1$ with (a_1, θ_1), averaged over the subclass of realizations having a microcrack centered at $\mathbf{x}_2$ with (a_2, θ_2). Further, $f(\mathbf{x}_2, a_2, \theta_2 | \mathbf{x}, a, \theta; \mathbf{x}_1, a_1, \theta_1)$ is the conditional probability function for finding a microcrack centered at $\mathbf{x}_2$ with (a_2, θ_2) given two microcracks fixed at $\mathbf{x}$ with (a, θ) and at $\mathbf{x}_1$ with (a_1, θ_1). $f(\mathbf{x}_2, a_2, \theta_2 | \mathbf{x}, a, \theta; \mathbf{x}_1, a_1, \theta_1)$ can be simplified to $f(\mathbf{x}, a, \theta)$ by the assumptions of local homogeneity and reasonable randomness.

The solutions of $\tilde{\tilde{\mathbf{T}}}$ for a system of three (or many) arbitrarily located and oriented microcracks were previously investigated by Horii and Nemat-Nasser (1985), and Kachanov (1987). In particular, Kachanov (1987) pursued extensive numerical computations in order to obtain the "transmission factors" for local stresses. Alternatively, one can derive approximate analytical solutions for $\tilde{\tilde{\mathbf{T}}}$ by following the procedures presented in Sec. 2.3 of Part I.

For clarity, let us express $\mathbf{T}$ and $\langle \boldsymbol{\varepsilon}^* \rangle (\mathbf{x})$ as follows [cf. Eqs. (25) and (28) of Part I]:

$$\langle \mathbf{T} \rangle = \langle \mathbf{T}^{\infty} + \tilde{\mathbf{T}} + \tilde{\tilde{\mathbf{T}}} \rangle = \left(\mathbf{K}_0 + f(\mathbf{x}) f(a, \theta) \langle \mathbf{K} \rangle + f^2(\mathbf{x}) f^2(a, \theta) \langle \mathbf{K}' \rangle \right) \cdot \boldsymbol{\tau}^{\infty} \tag{31}$$

$$\langle \mathbf{e}^* \rangle(\mathbf{x}) = \left\{ \langle \mathbf{S}^{*1} \rangle + \langle \mathbf{S}^{*2} \rangle + \langle \mathbf{S}^{*3} \rangle \right\} \cdot \boldsymbol{\tau}^\infty \equiv \langle \mathbf{S}^* \rangle \cdot \boldsymbol{\tau}^\infty \tag{32}$$

where $\tilde{\tilde{\mathbf{T}}} \equiv \mathbf{K}' \cdot \boldsymbol{\tau}^\infty$ and [see Eqs. (29)–(30) of Part I]

$$\langle \mathbf{S}^{*1} \rangle \equiv \frac{\pi(1-\nu^2)}{E} f(\mathbf{x}) \int_{\mathcal{A}} a^2 \int_{\Theta} \mathbf{g} \cdot \mathbf{K}_0 f(a,\theta)\, d\theta da \tag{33}$$

$$\langle \mathbf{S}^{*2} \rangle \equiv \frac{\pi(1-\nu^2)}{E} f^2(\mathbf{x}) \int_{\mathcal{A}} a^2 \int_{\Theta} \mathbf{g} \cdot \langle \mathbf{K} \rangle f^2(a,\theta)\, d\theta da \tag{34}$$

$$\langle \mathbf{S}^{*3} \rangle \equiv \frac{\pi(1-\nu^2)}{E} f^3(\mathbf{x}) \int_{\mathcal{A}} a^2 \int_{\Theta} \mathbf{g} \cdot \langle \mathbf{K}' \rangle f^3(a,\theta)\, d\theta da \tag{35}$$

In the above equations, $\mathbf{K}$, $\mathbf{K}_0$ and $\langle \mathbf{K} \rangle$ have been previously defined in Eqs. (24), (26) and (27) of Part I, respectively. Similarly, $\mathbf{K}'$ (or $\tilde{\tilde{\mathbf{T}}}$) can also be constructed as follows. One starts by expanding Eq. (15) of Part I into six linear equations with $j = 1, 2, 3$. Then, one obtains Eqs. (16)–(17) of Part I with the understanding that $j = 1, 2, 3$ and the permutations 1–2, 2–3, 3–1 are involved in Eq. (17). Eq. (18) of Part I is modified to include the kth ($k \neq j$ and $k \neq i$) microcrack's contribution to stress perturbations. Subsequently, Eq. (19) of Part I is expanded to a six-equation system with α denoting a six by six coefficient matrix. The components of α are identical to those in Eq. (20) of Part I with the understanding that the 1–2–3 permutations are involved. Therefore, we arrive at explicit formulas similar to Eqs. (21)–(24) in Part I. Finally, it is noted that the computation of $\langle \mathbf{K}' \rangle$ involves integration over the probabilistic domain of all possible positions and orientations of two active neighboring microcracks. Following the standard procedures presented in Sec. 2.4 of Part I, it can be shown that $\langle \mathbf{S}^{*3} \rangle$ in Eq. (35) introduces third-order terms (in ω^3) to overall compliance. Therefore, a third-order statistical micromechanical model can be constructed. By repeating the foregoing procedures, we can formulate a complete hierarchical family of statistical micromechanical theories of arbitrary order.

II.5. Conclusions

In this paper, basic two-dimensional formulations presented in Part I of this investigation are further extended to account for "cleavage 1" microcrack growth processes with microcrack interactions. Stemming from a micromechanical viewpoint, a mixed fracture criterion is used to derive microcrack kinetic equations for interacting, randomly located and oriented microcracks. As a result, the proposed approach is capable of predicting the *progressive* stress-strain curves for biaxial loadings. This constitutive predictive capability is not found in the current literature on stationary microcrack interaction models. Both tensile and mixed tensile/compressive loadings are considered in Sec. 2, including systematic analyses regarding detailed integration domains. Further, efficient numerical integration algorithms are presented for biaxial loadings in Sec. 3. A number of model predictions and comparisons are also performed. It is shown that load-induced anisotropy and non-symmetry of overall compliances can be predicted by the proposed micromechanical models. It is emphasized that the proposed models do **not** employ any fitted "material parameters" and do **not** require the use of Monte Carlo simulations.

The proposed pairwise interaction framework is subsequently generalized to a higher-order damage model to account for higher (third and above) order microcrack interaction effects in Sec. 4. However, a higher-order micromechanical damage model requires much more complicated analyses. Experimental validation of the proposed micromechanical evolutionary damage models is needed to further assess their validity for practical engineering problems.

II.6. References

1. ASHBY, M. F., (1979), "Micromechanisms of fracture in static and cyclic failure," in: R. A. Smith, ed., *Fracture Mechanics, Current Status, Future Prospects*, Pergamon Press, Oxford, **1**, 1–27.

2. BENVENISTE, Y., (1986), "On the Mori-Tanaka's method in cracked bodies", *Mech. Res. Comm.*, **13**, 193–201.

3. BUDIANSKY, B. AND O'CONNELL, R. J., (1976), "Elastic moduli of a cracked solid", *Int. J. Solids & Struct.*, **12**, 81–97.

4. CHRISTENSEN, R. M. AND LO, K. H., (1979), "Solutions for effective shear properties in three phase sphere and cylinder models", *J. Mech. Phys. Solids*, **27**, 315–330.

5. FANELLA, D. AND KRAJCINOVIC, D., (1988), "A micromechanical model for concrete in compression", *Eng. Fract. Mech.*, **29 (1)**, 49–66.

6. HILL, R., (1965), "A self-consistent mechanics of composite materials", *J. Mech Phys. Solids*, **13**, 213–222.

7. HORII, H. AND NEMAT-NASSER, S., (1983), "Overall moduli of solids with microcracks: load-induced anisotropy", *J. Mech. Phys. Solids*, **331**, 155–171.

8. HORII, H. AND NEMAT-NASSER, S., (1985), "Elastic fields of interacting inhomogeneities", *Int. J. Solids Structures*, **21**, 731–745.

9. JU, J. W., (1991), "On two-dimensional self-consistent micromechanical damage models for brittle solids", *Int. J. Solids & Struct.*, **27 (2)**, 227–258.

10. JU, J. W. AND LEE, X., (1991), "On three-dimensional self-consistent micromechanical damage models for brittle solids. Part I: Tensile loadings", *J. Eng. Mech.*, ASCE, **117 (7)**, 1495–1515.

11. KACHANOV, M., (1987), "Elastic solids with many cracks: a simple method of analysis", *Int J. Solids & Struct.*, **23**, 23–43.

12. KACHANOV, M. AND LAURES, J.-P., (1989), "Three-dimensional problems of strongly interacting arbitrarily located penny-shaped cracks", *Int J. of Fract.*, **41**, 289–313.

13. KANNINEN, M. F. AND POPELAR, C. H., (1985), *Advanced Fracture Mechanics*, Oxford University Press, New York, and Clarendon Press, Oxford.

14. KRAJCINOVIC, D. AND FANELLA, D., (1986), "A micromechanical model for concrete", *Eng. Fract. Mech.*, **25**, 585–596.

15. LEE, X. AND JU, J. W., (1991), "On three-dimensional self-consistent micromechanical damage models for brittle solids. Part II: Compressive loadings", *J. Eng. Mech.*, ASCE, **117** (7), 1516–1537.

16. MCLAUGHLIN, R., (1977), "A study of the differential scheme for composite materials", *Int. J. Engng. Sci.*, **15**, 237–244.

17. MORI, T. AND TANAKA, K., (1973), "Average stress in matrix and average elastic energy of materials with misfitting inclusions", *Acta Metallurgica*, **21**, 571–574.

18. ROSCOE, R. A., (1952), "The viscosity of suspensions of rigid spheres", *Brit. J. Appl. Phys.*, **3**, 267–269.

19. ROSCOE, R. A., (1973), "Isotropic composites with elastic or viscoelastic phases: general bounds for the moduli and solutions for special geometries", *Rheol. Acta*, **12**, 404–411.

20. SUMARAC, D. AND KRAJCINOVIC, D., (1987), "A self-consistent model for microcrack weakened solids", *Mech. Mater.*, **6**, 39–52.

Box 1. Numerical integration algorithm

(1) Specify θ^p and $\hat{\sigma}_{11}^{\infty}$, and guess an initial bound of opening domain θ^* (e.g., from Taylor's model analysis).

(2) Integrate (3)–(5) over θ and θ_{10}. Note that

$$a_1 = \begin{cases} a_f, & \text{if } \theta \text{ in process domains;} \\ a_0, & \text{otherwise.} \end{cases}$$

(3) Integrate (3)–(5) over θ_{20} for each value of $\theta + \theta_{10}$. Note that

$$a_2 = \begin{cases} a_f, & \text{if } \theta_{20} \text{ in process domains;} \\ a_0, & \text{otherwise.} \end{cases}$$

(4) Integrate Eqs. (4)–(5) from $r = (a_1 + a_2)$ to $max(20a_1, 20a_2)$.

(5) For a given fracture criterion, find the corresponding threshold stress $\hat{\sigma}_{22}^{\infty}$ by $(26)_1$. Calculate the updated opening angle bound θ^* by $(26)_2$ or (27). If the difference between the initial guess and the updated θ^*-value is not acceptable, then go back to Step (2) and re-iterate until proper convergence is reached.

(6) Go to Step (1) and specify new θ^p and $\hat{\sigma}_{11}^{\infty}$ values.

Table 1. Convergence behavior ($r_{max} = 20a$)

No. Gauss points	$\langle \hat{K}_{12} \rangle$	$\langle \hat{K}_{23} \rangle$
10	0.5862290322	0.2405392992
20	0.5864980549	0.2406183532
30	0.5864981079	0.2406183630
40	0.5864981080	0.2406183630
80	0.5864981080	0.2406183630

Table 2. Convergence behavior

No. of iteration (i)	$\theta^{*(i)}$	$\lvert\theta^{*(i+1)} - \theta^{*(i)}\rvert$
0	1.2645189576	–
1	1.2592833120	5.2356456171E−03
2	1.2592966258	1.3313781921E−05
3	1.2592965919	3.3915545705E−08
4	1.2592965920	8.6395779419E−11
5	1.2592965920	2.1960211427E−13

II.7. Figure captions

Figure 1. Schematic sketch for the definitions of process domains (θ^p) and opening domains (θ^*).

Figure 2. Schematic sketch for various integration domains, with x denoting the global reference axis, (x_1', y_1') denoting the first set of local coordinates, and (x_2', y_2') denoting the second set of local coordinates.

Figure 3. The normalized axial stress-strain curves for uniaxial tension tests. The dotted lines and solid lines are predictions from Taylor's and the proposed models, respectively.

Figure 4. The normalized $\overline{\langle S_{22} \rangle}$ and $\overline{\langle S_{11} \rangle}$ compliances vs. axial stress curves for uniaxial tension tests with $\omega_0 = 0.1$. The compliances have been normalized by the factor $(1 - \nu^2)/E$. The dotted lines and solid lines are predictions from Taylor's and the proposed models, respectively.

Figure 5. The normalized $\overline{\langle S_{12} \rangle}$ and $\overline{\langle S_{21} \rangle}$ compliances vs. axial stress curves for uniaxial tension tests with $\omega_0 = 0.1$ and $\omega_0 = 0.4$. The dotted line is the prediction from Taylor's model for both $\omega_0 = 0.1$ and $\omega_0 = 0.4$. The dash-dot lines and solid lines are $\overline{\langle S_{12} \rangle}$ and $\overline{\langle S_{21} \rangle}$ predictions, respectively, from the proposed model.

Figure 6. The normalized axial stress vs. lateral strain curves for biaxial tension/compression tests with $\hat{\sigma}_{11}^{\infty} = -0.1$. The dotted lines and solid lines are predictions from Taylor's and the proposed models, respectively.

Figure 7. The normalized axial stress vs. lateral strain curves for biaxial tension/compression tests with $\hat{\sigma}_{11}^{\infty} = -0.4$. The dotted lines and solid lines are predictions from Taylor's and the proposed models, respectively.

Figure 8. The normalized $\overline{\langle S_{22} \rangle}$ and $\overline{\langle S_{11} \rangle}$ compliances vs. axial stress curves for biaxial tension/compression tests with $\omega_0 = 0.4$ and $\hat{\sigma}_{11}^{\infty} = -0.1$. The dotted lines and solid lines are predictions from Taylor's and the proposed models, respectively.

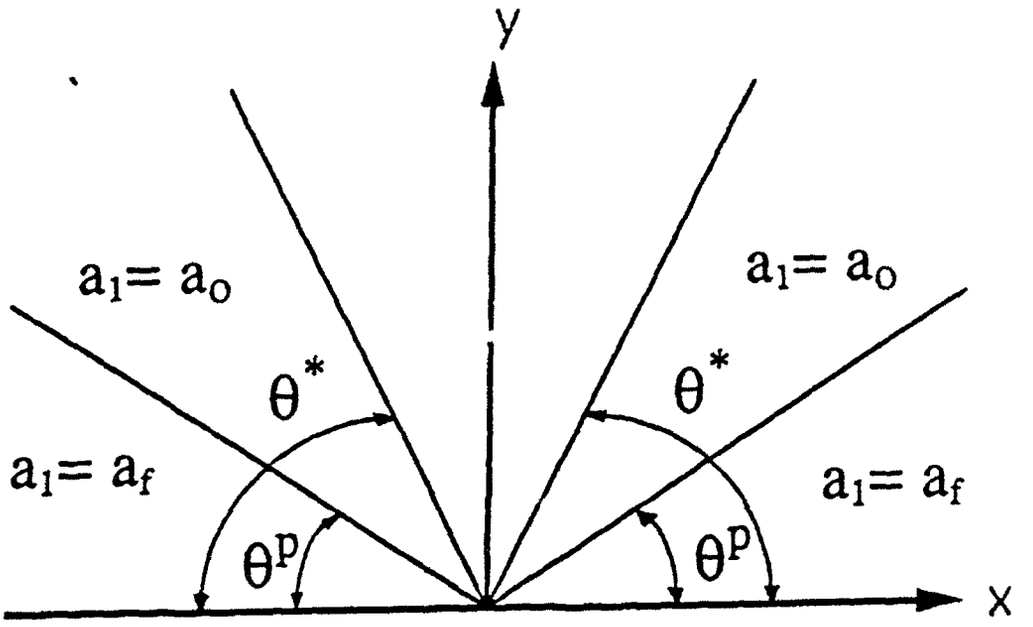

Figure 1. Schematic sketch for the definitions of process domains (θ^p) and opening domains (θ^*).

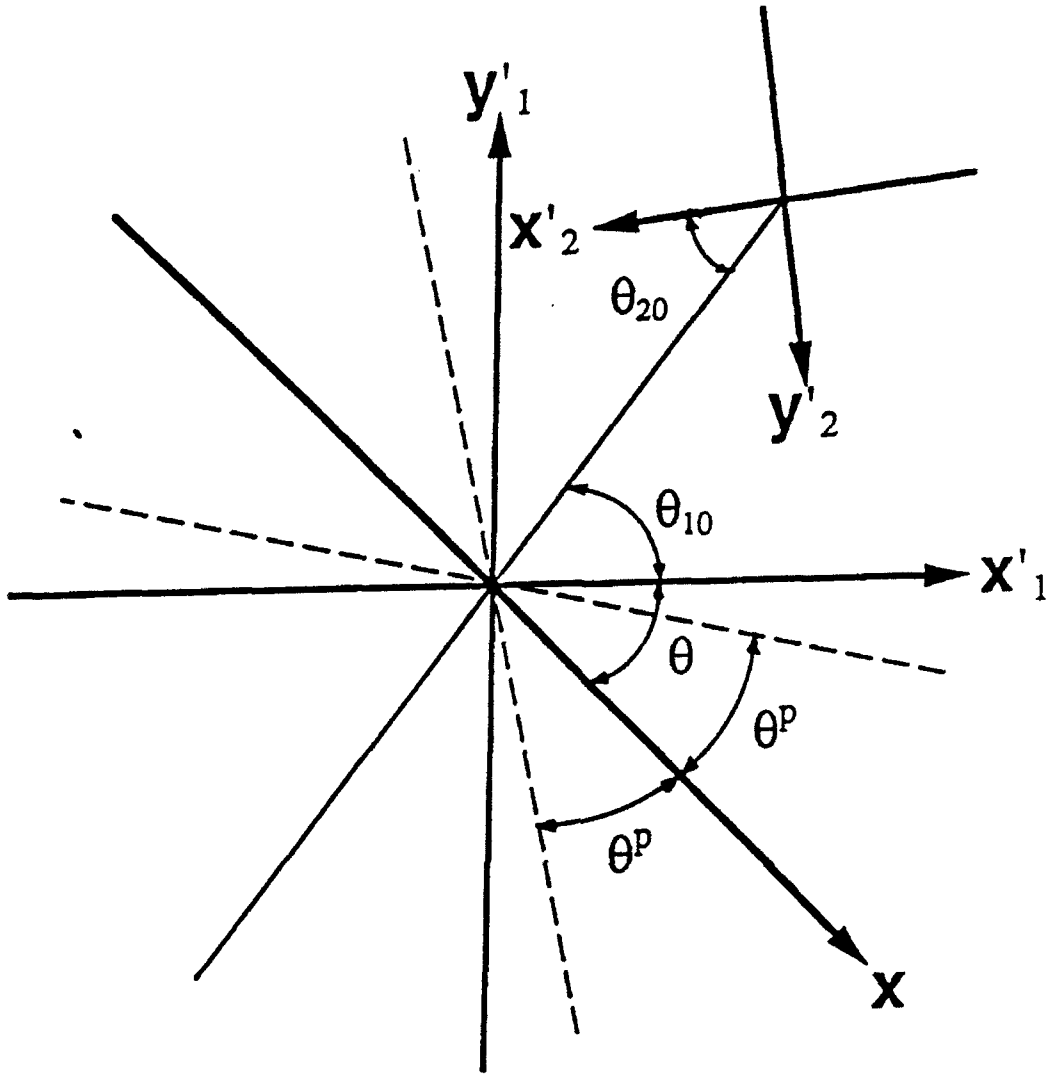

Figure 2. Schematic sketch for various integration domains, with x denoting the global reference axis, (x_1', y_1') denoting the first set of local coordinates, and (x_2', y_2') denoting the second set of local coordinates.

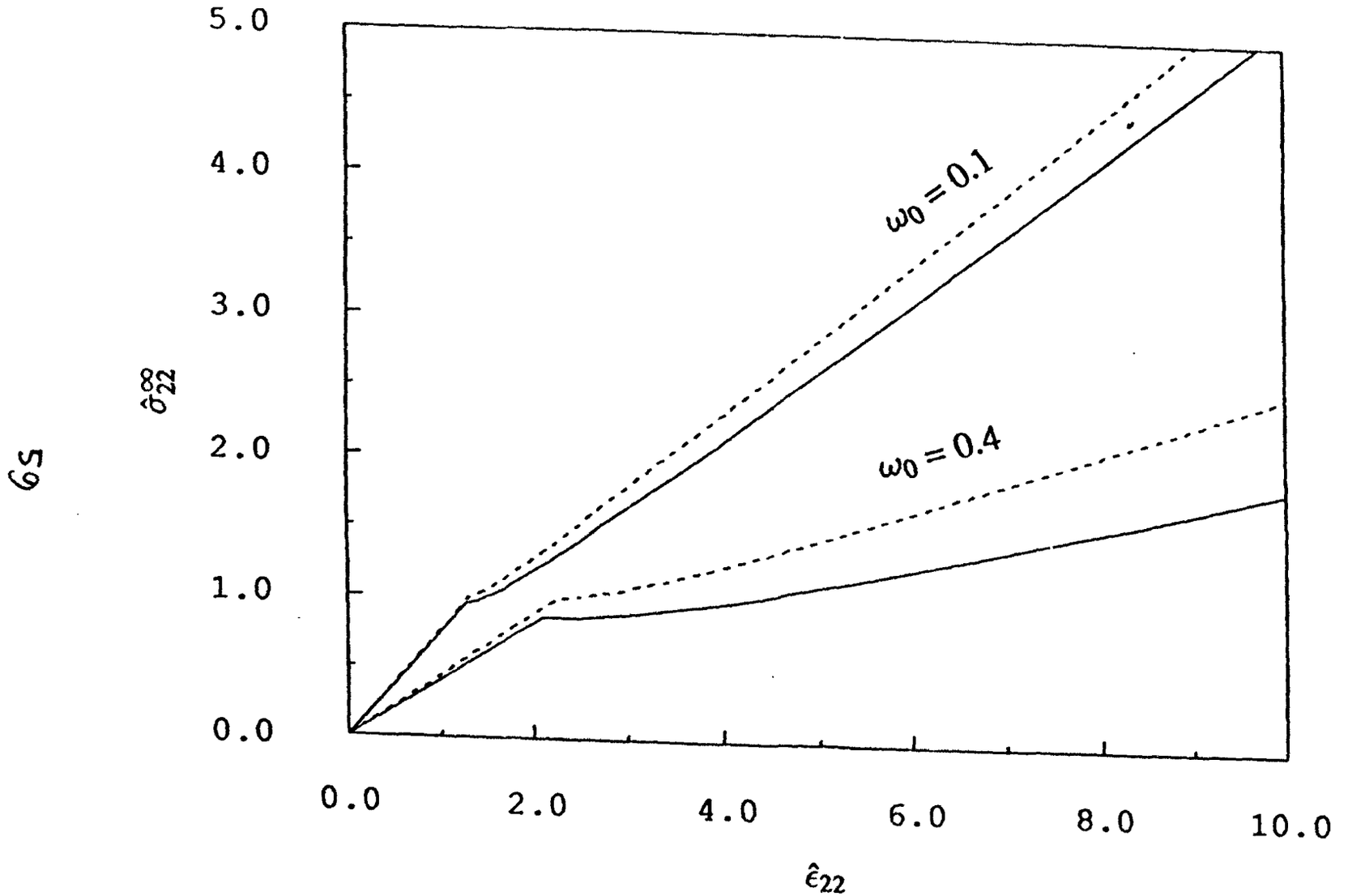

Figure 3. The normalized axial stress-strain curves for uniaxial tension tests. The dotted lines and solid lines are predictions from Taylor's and the proposed models, respectively.

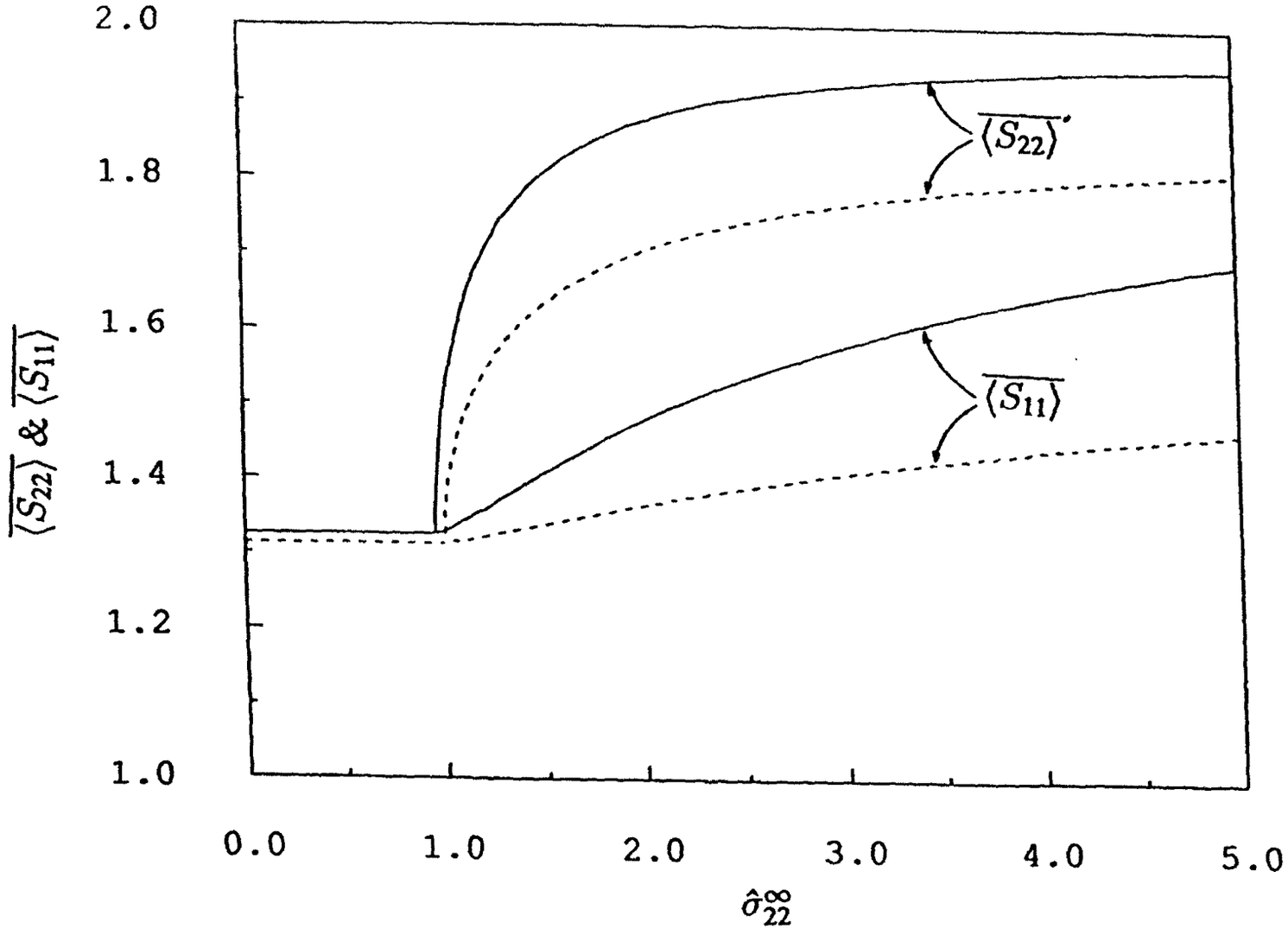

Figure 4. The normalized $\overline{\langle S_{22}\rangle}$ and $\overline{\langle S_{11}\rangle}$ compliances vs. axial stress curves for uniaxial tension tests with $\omega_0 = 0.1$. The compliances have been normalized by the factor $(1 - \nu^2)/E$. The dotted lines and solid lines are predictions from Taylor's and the proposed models, respectively.

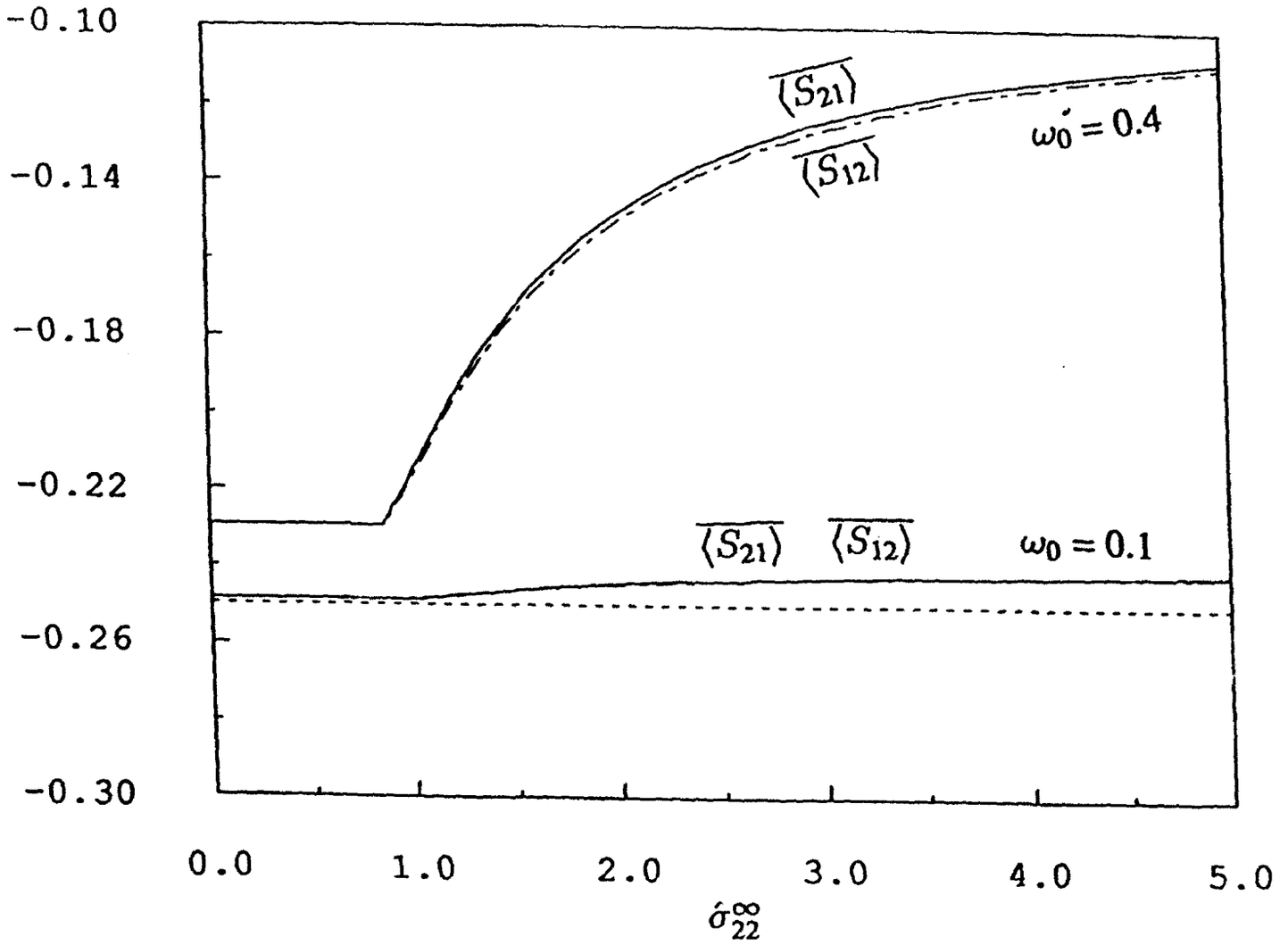

Figure 5. The normalized $\overline{\langle S_{12}\rangle}$ and $\overline{\langle S_{21}\rangle}$ compliances vs. axial stress curves for uniaxial tension tests with $\omega_0 = 0.1$ and $\omega_0 = 0.4$. The dotted line is the prediction from Taylor's model for both $\omega_0 = 0.1$ and $\omega_0 = 0.4$. The dash-dot lines and solid lines are $\overline{\langle S_{12}\rangle}$ and $\overline{\langle S_{21}\rangle}$ predictions, respectively, from the proposed model.

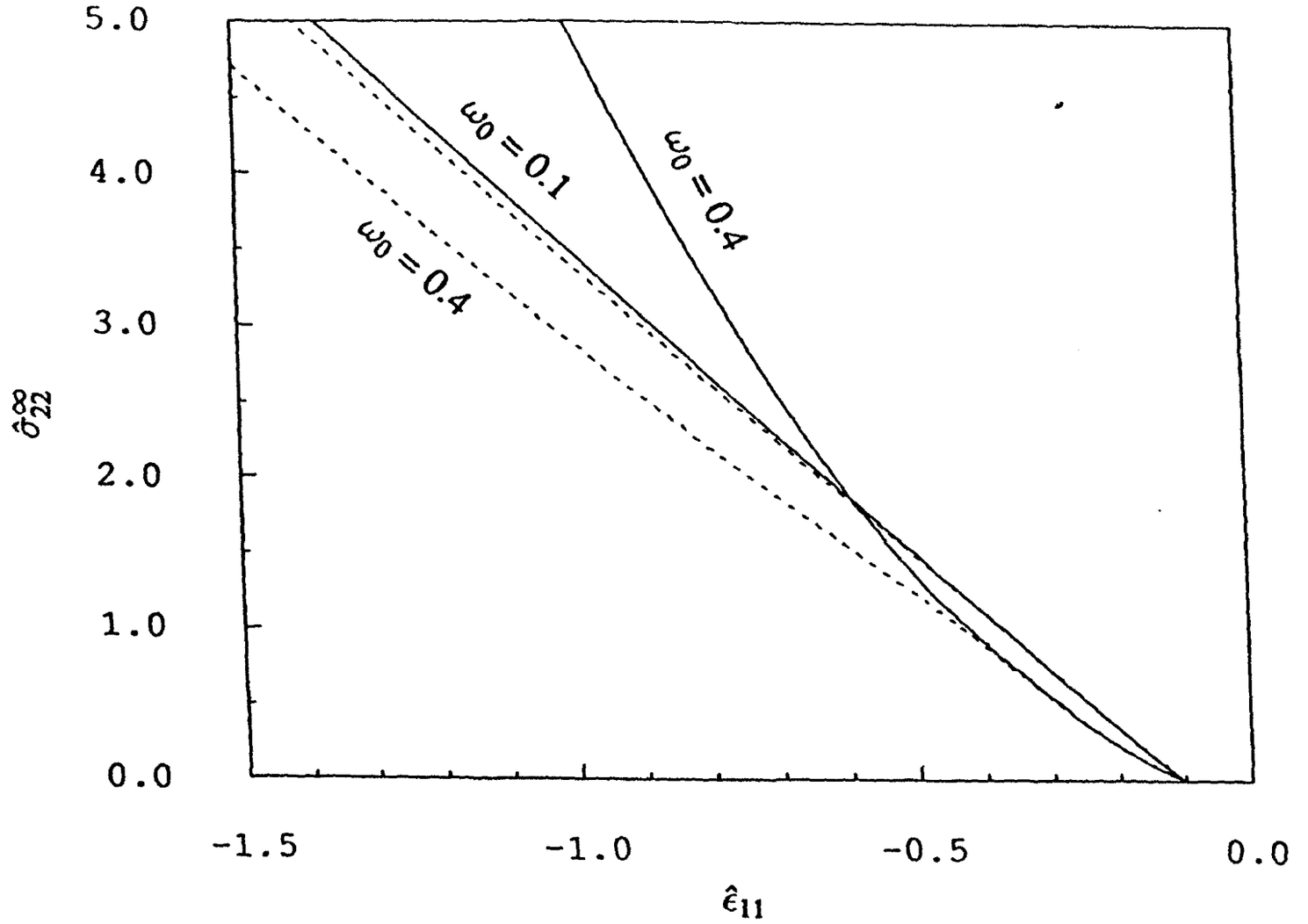

Figure 6. The normalized axial stress vs. lateral strain curves for biaxial tension/compression tests with $\hat{\sigma}_{11}^{\infty} = -0.1$. The dotted lines and solid lines are predictions from Taylor's and the proposed models, respectively.

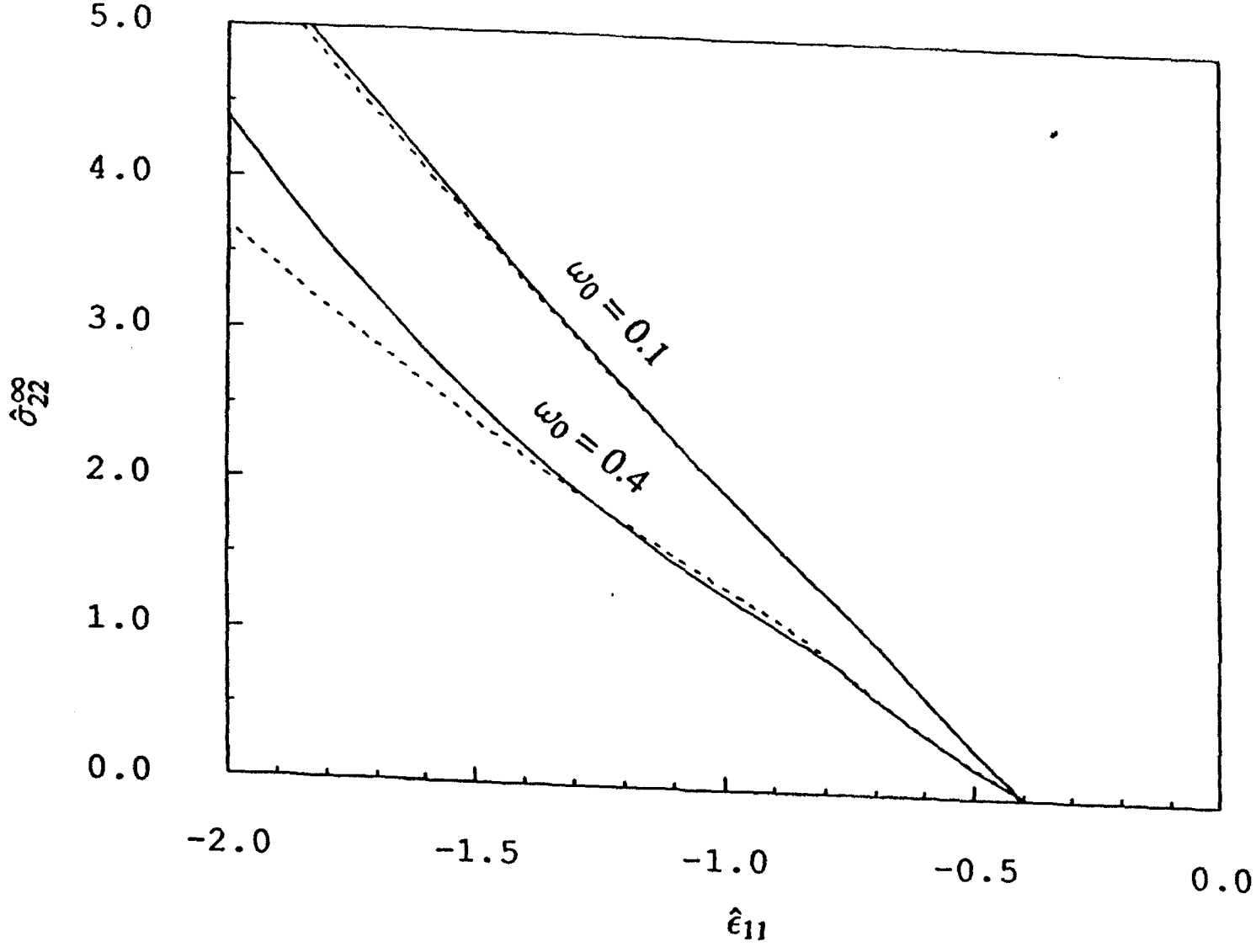

Figure 7. The normalized axial stress vs. lateral strain curves for biaxial tension/compression tests with $\hat{\sigma}_{11}^{\infty} = -0.4$. The dotted lines and solid lines are predictions from Taylor's and the proposed models, respectively.

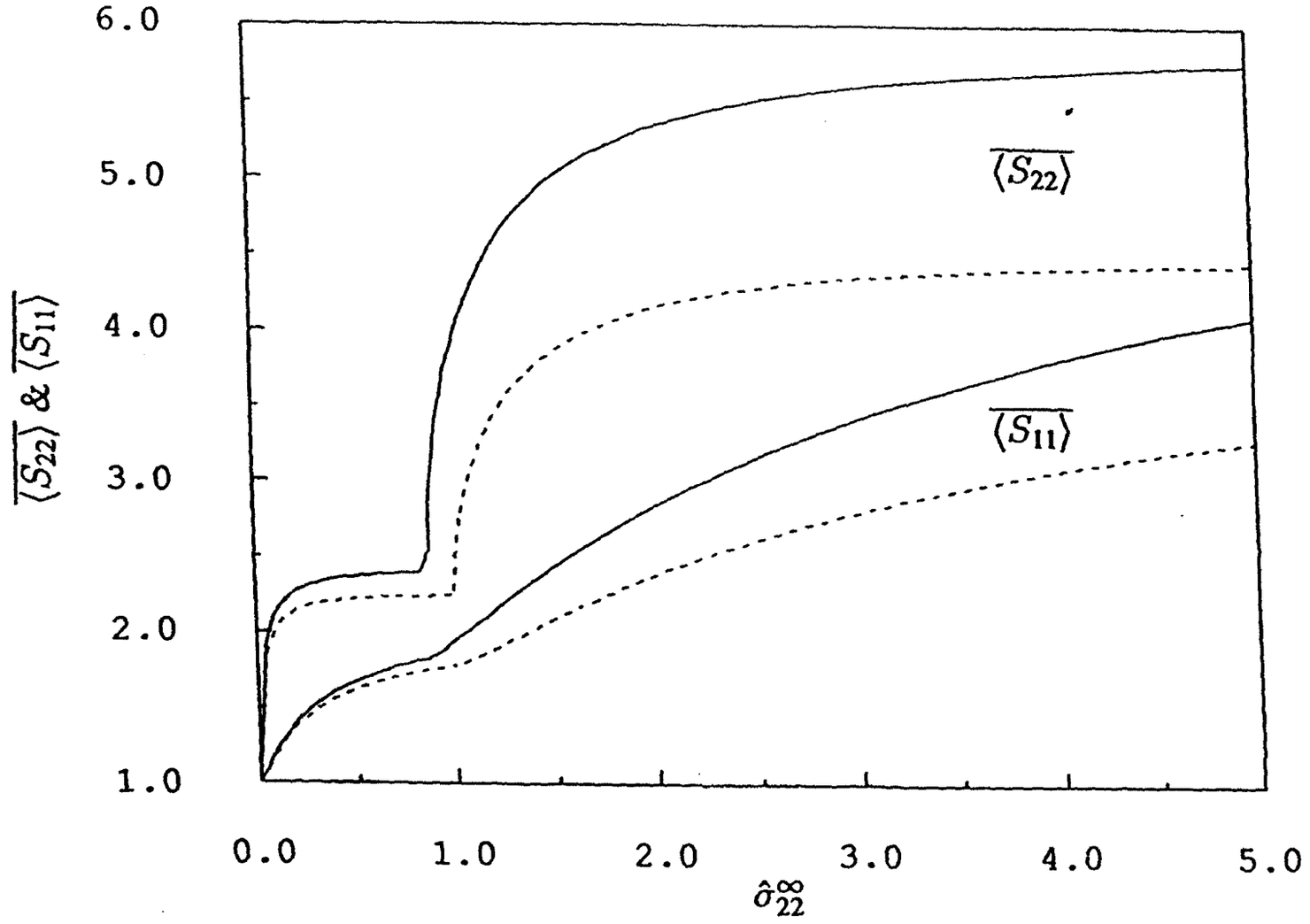

Figure 8. The normalized $\overline{\langle S_{22}\rangle}$ and $\overline{\langle S_{11}\rangle}$ compliances vs. axial stress curves for biaxial tension/compression tests with $\omega_0 = 0.4$ and $\hat{\sigma}_{11}^{\infty} = -0.1$. The dotted lines and solid lines are predictions from Taylor's and the proposed models, respectively.

PART III

A Three-Dimensional Statistical Micromechanical Theory for Brittle Solids with Interacting Microcracks

III.0. Abstract

A three-dimensional statistical micromechanical theory is presented to investigate effective elastic moduli of brittle solids with many randomly located, penny-shaped microcracks. The macroscopic constitutive relations are statistically and micromechanically derived by taking the *ensemble average* over all possible realizations which feature the same statistical distribution of microcracks. Approximate analytical solutions of a two-microcrack interaction model are presented to account for *pairwise* microcrack interaction among many randomly located, aligned microcracks. Therefore, the ensemble-averaged stress perturbations due to microcrack interaction can be constructed in closed-form. The overall effective compliances of microcrack-weakened brittle solids are derived by further taking the *volume average* of the *ensemble-averaged* stress-strain relations over the entire mesostructural domain of a representative volume element. Some numerical examples are given to illustrate the behavior of the proposed method. Comparisons with some existing methods are also appended. Finally, a higher-order ensemble-average formulation of microcrack interaction is briefly discussed. The proposed framework is fundamentally different from existing "effective medium methods" which do not depend on microcrack locations and configurations. It is emphasized that no Monte Carlo simulations are necessary in the proposed framework.

III.1. Introduction

Damage mechanics has emerged as an important branch of solid mechanics pertaining to microcrack nucleation, growth, coalescence and interaction, as well as their effects on overall mechanical responses of materials. Basically, there are two types of models: (a) phenomenological damage models (e.g., Ju (1989a,b), Chow and Wang (1987)), and (b) micromechanical damage models. We refer to Krajcinovic (1989) for an excellent comprehensive literature review on damage mechanics.

The majority of micromechanical damage theories falls into the category of "effective medium methods". When microcrack interactions are totally ignored, the resulting micromechanical models are termed "Taylor's models"; see, e.g., Krajcinovic and Fanella (1986), Fanella and Krajcinovic (1988), and Ju (1991b) for some micromechanical evolutionary models. The "self-consistent method" (Hill (1965)) was applied to damaged solids by Budiansky and O'Connell (1976) focusing on randomly distributed, *weakly* interacting microcracks. The self-consistent method was further explored by Horii and Nemat-Nasser (1983), Laws et al. (1983), Laws and Dvorak (1987), Sumarac and Krajcinovic (1987, 1989), Krajcinovic and Sumarac (1989), Horii and Sahasakmontri (1990), Nemat-Nasser and Hori (1990), Ju (1991a), Ju and Lee (1991), and Lee and Ju (1991), etc.. In addition, a three-phase "generalized self-consistent model" was proposed by Christensen and Lo (1979), and Christensen (1990). The "differential scheme" was investigated by Roscoe (1952, 1973), McLaughlin (1977), Laws and Dvorak (1987), Hashin (1988), Nemat-Nasser and Hori (1990), and so on.

On the other hand, based on variational principles, Hashin and Shtrikman (1962, 1963) proposed upper and lower bounds for elastic composites with elastic inclusions. Extension of their work to penny-shaped microcracks is possible, see, for example, Willis (1977). Moreover, the "Mori-Tanaka method" was studied by Mori and Tanaka (1973), Benveniste (1986), Zhao, Tandon and Weng (1989), and Weng (1990). The Mori-Tanaka method produces identical results to the Hashin-Shtrikman bounds (1962, 1963) under many situations; see Weng (1990) for details.

It is noted that effective medium methods are only valid for low or at most moderate microcrack concentrations since they do *not* depend on microcrack locations or configurations. When microcrack concentrations are higher and microcrack spacings are smaller, *strong* microcrack interactions become significant and microcrack locations should be accounted for. Excellent strong microcrack interaction models were proposed by Gross (1982), Horii and Nemat-Nasser (1985), and Hori and Nemat-Nasser (1987) for two-dimensional deterministic microcracks (not at the constitutive level). More comprehensive studies were investigated by Kachanov (1985), Kachanov

and Montagut (1986), Kachanov (1987), Montagut and Kachanov (1988), Kachanov and Laures (1989), and Laures and Kachanov (1991) for two- and three-dimensional *deterministic* arbitrary microcrack arrays (at the constitutive level). In particular, the valuable work due to Kachanov (1987) and Kachanov and Laures (1989) are ideally suited for deterministic microcracks. However, one needs to perform Monte Carlo simulations associated with their method in the event of *statistically* distributed microcrack arrays.

In this paper, we attempt to establish a statistical micromechanical framework to predict effective moduli of brittle solids with many interacting, randomly located penny-shaped microcracks. Random microcrack locations and relative configurations are accommodated through probability density functions and the ensemble average approach. It is noteworthy that Batchelor (1970), Batchelor and Green (1972), Willis and Acton (1976), Hinch (1977), and Chen and Acrivos (1978a,b) employed similar methods to characterize elastic particulate composites. On the other hand, the proposed method is quite different from that proposed by Hudson (1980, 1981, 1986). Hudson's method, though using the ensemble average approach, is based on a second order *stiffness* theory and therefore leads to irrational behavior for solids with moderate or high microcrack concentrations (Sayers and Kachanov, 1991). The proposed approach is free from this anomaly.

This paper is organized as follows. In Section 2, the *ensemble average* approach to derive local damaged stress-strain relations is introduced. Approximate closed-form solutions are subsequently presented for the interaction problem of two aligned but arbitrarily located penny-shaped microcracks. The overall moduli of a representative volume element are then derived by the *volume averaging* process in Section 3. In Section 4, applications are made to some special cases. In particular, in the event of dilute microcracks, the present approach recovers the well-known Taylor's model by neglecting interactions among microcracks. Comparisons with some existing methods are also presented. Finally, a higher-order microcrack interaction formulation within the proposed framework is discussed in Section 5.

III.2. An ensemble average approach to 3-D aligned microcrack interaction

In this section, we start by studying the ensemble averages of microcrack-perturbed stresses and strains. Approximate closed-form analytical solutions of two arbitrarily located, aligned microcracks are subsequently given. Finally, some test problems are examined to assess the accuracy of the proposed approximate analytical solutions.

Following the current literature, it is assumed that the volume-average stress $\bar{\sigma}$ is approximately equal to the far-field stress σ^{∞}. This common assumption can actually be removed and further improvements are possible. These and related issues will be addressed in a forthcoming paper.

III.2.1. Ensemble averages of microcrack-perturbed stresses and strains

Due to the existence and interaction of microcracks, local stresses and strains in the matrix material are perturbed. The ensemble average approach hinges on the concept that local stresses, strains and compliances (or stiffnesses) at a typical point within a representative volume element (RVE) of a microcrack-weakened solid can be obtained by averaging over the ensemble of all *statistical realizations* of randomly distributed microcracks. Batchelor (1970), Batchelor and Green (1972), and Hinch (1977) applied this approach to the study of fluid suspensions within the framework of pairwise (second order) interaction. The ensemble average approach with pairwise interaction was later applied to composite materials with interacting inclusions (inhomogeneities) by Willis and Acton (1976), as well as Chen and Acrivos (1978a,b). Recently, Chen and Ju (1991) and Ju and Chen (1991) proposed two-dimensional (second-order and higher-order) micromechanical damage theories for brittle solids with interacting *slit* microcracks by employing the ensemble average method and micromechanical fracture mechanics. It is noted that local displacements, strains and stresses vary with *positions* within a RVE.

For simplicity, we consider a two-phase composite composed of a linear elastic matrix and many randomly located *penny-shaped* microcracks. The local strain tensor at a point $\mathbf{x}$ within the RVE takes the form:

$$\epsilon(\mathbf{x}) = \mathbf{S}^0 : \sigma(\mathbf{x}) + \epsilon^*(\mathbf{x}, C) \tag{1}$$

where ϵ and σ denote the local strain and stress, respectively; ϵ^* is the *perturbed* strain due to the existence and interaction of microcracks; and C denotes the set of all possible configurations of microcracks. It is emphasized that ϵ^* is zero if $\mathbf{x}$ is a point in the matrix and non-zero if $\mathbf{x}$ is a point on the microcrack surfaces. Taking the ensemble average over Eq. (1), we arrive at

$$\langle\epsilon\rangle(\mathbf{x}) = \mathbf{S}^0 : \langle\sigma\rangle(\mathbf{x}) + \langle\epsilon^*\rangle(\mathbf{x}) \tag{2}$$

where the angle brackets $\langle\cdot\rangle$ signify the ensemble average.

Throughout the development of this paper, for simplicity, we shall assume that the solid is *locally homogeneous* (Hinch (1977)) and penny-shaped microcracks do **not** intersect one another. *Local homogeneity* implies that all probability density functions (PDF) do not vary under small translation on a macroscopic length scale. It can be shown (Chen and Ju (1991)) that, in the case of microcracks, the perturbed strain can be expressed as

$$\langle \epsilon^* \rangle(\mathbf{x}) = f(\mathbf{x}) \int_{\mathcal{G}} \int_{S_i} \frac{1}{2} \langle [\![\mathbf{u}]\!] \otimes \mathbf{n} + \mathbf{n} \otimes [\![\mathbf{u}]\!] \rangle (\mathbf{x}' | \mathbf{x}, \mathcal{G}) f(\mathcal{G})\, d\mathcal{G} dS_i \tag{3}$$

Here, $\mathcal{G} \equiv (a, \mathbf{n})$ indicates the microcrack radius a and orientation $\mathbf{n}$. Furthermore, $\mathbf{x}'$ denotes a point on the surfaces (S_i) of a microcrack centered at $\mathbf{x}$; $f(\mathbf{x})$ is the PDF for a microcrack being centered at $\mathbf{x}$; $[\![\mathbf{u}]\!]$ is the vector of microcrack opening displacements; and $f(\mathcal{G})$ is the PDF for a microcrack with a geometry $\mathcal{G}$. If all penny-shaped microcracks are aligned (parallel) and of equal size, then there is no variation in $\mathcal{G}$. This could correspond to, for example, microcracks generated by fiber breaks in unidirectional fiber composites (see, e.g., Laws and Dvorak (1987)). In this event, Eq. (3) can be simplified as follows

$$\langle \epsilon^* \rangle(\mathbf{x}) = f(\mathbf{x}) \int_{S_i} \frac{1}{2} \langle [\![\mathbf{u}]\!] \otimes \mathbf{n} + \mathbf{n} \otimes [\![\mathbf{u}]\!] \rangle (\mathbf{x}' | \mathbf{x})\, dS_i \tag{4}$$

It is well known that, for an open penny-shaped microcrack with radius a embedded in an infinite linear elastic isotropic matrix, the microcrack opening displacements at $\mathbf{x}'$ (at a distance ρ from the center of the microcrack) are:

$$\begin{Bmatrix} [\![u_x']\!] \\ [\![u_y']\!] \\ [\![u_z']\!] \end{Bmatrix} = \frac{8(1-\nu^2)}{\pi E(2-\nu)} \sqrt{a^2 - \rho^2} \begin{Bmatrix} 2s \\ 2t \\ (2-\nu)p \end{Bmatrix} \tag{5}$$

where E and ν = the Young's modulus and Poisson's ratio of the virgin matrix material, respectively. Moreover, p, s and t are the z-direction normal, the x-direction shear and the y-direction shear stresses projected on the microcrack surface in its local coordinates; see Fig. 1 for a schematic plot.

If all (open) microcracks are *aligned* (parallel), then we can define $\mathbf{n} = (0, 0, 1)^T$. By substituting Eq. (5) into (4) and carring out the integration, we obtain (assuming equal microcrack size)

$$\langle \mathbf{e}^* \rangle(\mathbf{x}) = f(\mathbf{x}) \frac{16(1-\nu^2)}{3E(2-\nu)} a^3\, \mathbf{g} \cdot (\mathbf{T}) \tag{6}$$

where (the Voigt's notation)

$$\langle \mathbf{e}^* \rangle \equiv \begin{Bmatrix} \langle e_1^* \rangle \\ \langle e_2^* \rangle \\ \langle e_3^* \rangle \\ \langle e_4^* \rangle \\ \langle e_5^* \rangle \\ \langle e_6^* \rangle \end{Bmatrix} \equiv \begin{Bmatrix} \langle \epsilon_{xx}^* \rangle \\ \langle \epsilon_{yy}^* \rangle \\ \langle \epsilon_{zz}^* \rangle \\ 2\langle \epsilon_{xy}^* \rangle \\ 2\langle \epsilon_{yz}^* \rangle \\ 2\langle \epsilon_{zx}^* \rangle \end{Bmatrix} \tag{7}$$

In addition, $\mathbf{g}$ is the transformation matrix and $\mathbf{T}$ is the *local* stress vector:

$$\mathbf{g} = \begin{bmatrix} 0 & 0 & 0 \\ 0 & 0 & 0 \\ 2-\nu & 0 & 0 \\ 0 & 0 & 0 \\ 0 & 0 & 2 \\ 0 & 2 & 0 \end{bmatrix} \quad ; \quad \mathbf{T} = \begin{Bmatrix} p \\ s \\ t \end{Bmatrix} \tag{8}$$

In the event of distributed (nonuniform) microcrack lengths and orientations, similar (though more complicated) expressions can be constructed accordingly.

On the other hand, the local stress vector $\langle \mathbf{T} \rangle$ can be shown to be (see Eq. (14) in Sec. 2.2):

$$\mathbf{T} = \mathbf{T}^\infty + \tilde{\mathbf{T}} \equiv \begin{Bmatrix} p^\infty \\ s^\infty \\ t^\infty \end{Bmatrix} + \begin{Bmatrix} \tilde{p} \\ \tilde{s} \\ \tilde{t} \end{Bmatrix} \tag{9}$$

Here, $\mathbf{T}^\infty$ denotes the unperturbed local stress vector due to remote loading, and $\tilde{\mathbf{T}}$ denotes the local stress perturbation due to three-dimensional microcrack interactions. In what follows, attention is focused on *pairwise* microcrack interactions. Higher-order microcrack interactions will be discussed in Sec. 5. By assuming that all microcracks are aligned with a chosen global coordinate system, the stress $\mathbf{T}^\infty$ due to far field loads can be expressed as

$$\mathbf{T}^\infty = \mathbf{K}_0 \cdot \boldsymbol{\tau}^\infty \tag{10}$$

where

$$\mathbf{K}_0 = \begin{bmatrix} 0 & 0 & 1 & 0 & 0 & 0 \\ 0 & 0 & 0 & 0 & 0 & 1 \\ 0 & 0 & 0 & 0 & 1 & 0 \end{bmatrix} \quad ; \quad \boldsymbol{\tau}^\infty \equiv \begin{Bmatrix} \sigma_{xx}^\infty \\ \sigma_{yy}^\infty \\ \sigma_{zz}^\infty \\ \sigma_{xy}^\infty \\ \sigma_{yz}^\infty \\ \sigma_{zx}^\infty \end{Bmatrix} \tag{11}$$

The ensemble average of local stress perturbation, on the other hand, takes the form (assuming uniform size and aligned orientation):

$$\langle \tilde{\mathbf{T}} \rangle (\mathbf{x}) = \int_\Xi \langle \tilde{\mathbf{T}} \rangle (\mathbf{x}|\mathbf{x}_1) f(\mathbf{x}_1|\mathbf{x}) \, d\mathbf{x}_1 \tag{12}$$

where $\langle\tilde{\mathbf{T}}\rangle(\mathbf{x}|\mathbf{x}_1)$ = the ensemble-average stress perturbation for a microcrack centered at $\mathbf{x}$ over the subclass of realizations having a microcrack centered at $\mathbf{x}_1$; and $f(\mathbf{x}_1|\mathbf{x})$ = the conditional PDF for finding a microcrack centered at $\mathbf{x}_1$ given a microcrack centered at $\mathbf{x}$. Further, Ξ designates the active (open) integration domain which depends on the loading conditions.

The conditional PDF $f(\mathbf{x}_1|\mathbf{x})$ can be simplified to $f(\mathbf{x}_1)$ if microcracks do *not* intersect and *reasonable randomness* holds (Hinch (1977)). The *local homogeneity* assumption enables us to further approximate $f(\mathbf{x}_1)$ by $f(\mathbf{x})$. Therefore, Eq. (12) can be recast as:

$$\langle\tilde{\mathbf{T}}\rangle(\mathbf{x}) = f(\mathbf{x}) \int_{\Xi} \langle\tilde{\mathbf{T}}\rangle(\mathbf{x}|\mathbf{x}_1)\, d\mathbf{x}_1 \tag{13}$$

The quantity $\tilde{\mathbf{T}}(\mathbf{x}|\mathbf{x}_1)$ corresponding to the pairwise microcrack interaction will be the main subject of the next section.

III.2.2. Approximate explicit solutions for pairwise interaction of aligned microcracks

The objective of this section is to construct approximate closed-form *explicit* expressions for perturbed stresses $\tilde{\mathbf{T}}$ due to the two-microcrack interaction so that the ensemble-average formalism proposed in Sec. 2.1 can be realized. It is actually possible to derive explicit expressions for $\tilde{\mathbf{T}}$ in the interaction problem involving two arbitrarily oriented and located penny-shaped microcracks. However, general solutions of the two-microcrack interaction problem are rather complicated and no reasonably compact closed-form explicit solutions can be presented within normal journal page limit. Therefore, for demonstration purpose, attention will be foucused on explicit solutions of two randomly located, aligned (parallel), equal-sized, penny-shaped microcracks embedded in an infinite, linear elastic isotropic matrix. Nonetheless, in a forthcoming paper, *arbitrary* microcrack orientations, locations and sizes will be accommodated through *numerical* "microcrack interaction matrix" and the ensemble average approach.

The "pseudo-traction" method is adopted here to derive approximate expressions for $\tilde{\mathbf{T}}$ since *exact* solutions are not yet available. For mathematical simplicity, only the *first term* of Taylor's expansion of the local stress field is used to represent the average stress across the microcrack surface. Higher-order terms in polynomial expansions may be included if desired, however, at the high cost of a much larger system of equations and much more complicated analytical expressions. Stemming from a different viewpoint, the more accurate "transmission factor"-type formulation proposed by Kachanov (1987) is well suited for *deterministic numerical* computations. Within the

framework of statistical ensemble average, nevertheless, closed-form *explicit* solutions for stress-interaction are preferred.

Figure 1 shows the local coordinate systems for microcracks 1 and 2 of radius a. The z-axis is chosen as the direction normal to the microcrack surface. In accord with the pseudo-traction concept, the problem of two interacting microcracks subjected to far field stresses can be decomposed into a homogeneous problem and two sub-problems (see also Chen and Ju (1991)). In the homogeneous problem, a microcrack-free solid is subjected to applied stresses at far field. In the sub-problem j ($j = 1, 2$), an infinitely extended solid contains only *one* penny-shaped microcrack and is subjected to zero remote stress at infinity. Since stresses vanish on microcrack surfaces (S_j), the following boundary conditions must be satisfied ($j = 1, 2$):

$$-p_j + p_j^{\infty} + \tilde{p}_j = 0 \quad ; \quad -s_j + s_j^{\infty} + \tilde{s}_j = 0 \quad ; \quad -t_j + t_j^{\infty} + \tilde{t}_1 = 0 \tag{14}$$

In the first sub-problem (containing only the 'microcrack 1'), let us define a cylindrical coordinate system with the center of the 'microcrack 1' as its origin. Accordingly, the center location of the 'microcrack 2' can be characterized by (ρ, ϕ, z); see Fig. 1. For convenience, we shall introduce the following definitions:

$$\sigma_1 \equiv \sigma_{xx} + \sigma_{yy} \quad ; \quad \sigma_2 \equiv \sigma_{xx} - \sigma_{yy} - 2i\sigma_{xy} \tag{15}$$

$$\sigma_z \equiv \sigma_{zz} \quad ; \quad \tau_z \equiv \sigma_{xz} + i\sigma_{yz} \tag{16}$$

If the surfaces of the 'microcrack 1' are subjected to applied *normal* stress $p^{(1)}$, then perturbed stresses at the 'microcrack 2' location are given by (Fabrikant (1989, p. 252–257)):

$$\begin{aligned}
\sigma_1'^{(1)} &= \frac{2p^{(1)}}{\pi}\left\{(1+2\nu)\left[\frac{a(l_2^2-a^2)^{1/2}}{l_2^2-l_1^2} - \sin^{-1}\left(\frac{a}{l_2}\right)\right] + \frac{az^2\left[l_1^4 + a^2(2a^2+2z^2-3\rho^2)\right]}{(l_2^2-l_1^2)^3(l_2^2-a^2)^{1/2}}\right\} \\
\sigma_2'^{(1)} &= \frac{2p^{(1)}}{\pi}\frac{al_1^2e^{2i\phi}(l_2^2-a^2)^{1/2}}{l_2^2(l_2^2-l_1^2)}\left\{(1-2\nu) + \frac{z^2\left[a^2(6l_2^2-2l_1^2+\rho^2) - 5l_2^4\right]}{(l_2^2-l_1^2)^2(l_2^2-a^2)}\right\} \\
\sigma_z'^{(1)} &= \frac{2p^{(1)}}{\pi}\left\{\frac{a(l_2^2-a^2)^{1/2}}{l_2^2-l_1^2} - \sin^{-1}\left(\frac{a}{l_2}\right) - \frac{az^2\left[l_1^4 + a^2(2a^2+2z^2-3\rho^2)\right]}{(l_2^2-l_1^2)^3(l^2-a^2)^{1/2}}\right\} \\
\tau_z'^{(1)} &= -\frac{2p^{(1)}}{\pi}\frac{zl_1e^{i\phi}(l_2^2-a^2)^{1/2}\left[a^2(4l_2^2-5\rho^2) + l_1^4\right]}{l_2(l_2^2-l_1^2)^3}
\end{aligned} \tag{17}$$

where

$$\begin{aligned}
l_1 &\equiv \frac{1}{2}\left\{\left[(a+\rho)^2+z^2\right]^{1/2} - \left[(a-\rho)^2+z^2\right]^{1/2}\right\} \\
l_2 &\equiv \frac{1}{2}\left\{\left[(a+\rho)^2+z^2\right]^{1/2} + \left[(a-\rho)^2+z^2\right]^{1/2}\right\}
\end{aligned} \tag{18}$$

Furthermore, when the surfaces of the 'microcrack 1' are loaded by the combined shear stresses $\tau^{(1)} = s^{(1)} + it^{(1)}$, the perturbed stresses at the 'microcrack 2' location are (Fabrikant (1989, p. 257–261)):

$$\sigma''^{(1)}_1 = \frac{2(\bar{\tau}^{(1)}e^{i\phi} + \tau^{(1)}e^{-i\phi})}{\pi(2-\nu)} \left\{ -2(1+\nu)\frac{al_1(a^2-l_1^2)^{1/2}}{l_2(l_2^2-l_1^2)} + \frac{zl_1(l_2^2-a^2)^{1/2}\left[a^2(4l_2^2-5\rho^2)+l_1^4\right]}{l_2(l_2^2-l_1^2)^3} \right\}$$

$$\sigma''^{(1)}_2 = \frac{-2e^{i\phi}}{\pi(2-\nu)} \left\{ 4(1-\nu)\frac{al_1(a^2-l_1^2)^{1/2}}{l_2(l_2^2-l_1^2)}\tau^{(1)} + \frac{zl_1(l_2^2-a^2)^{1/2}}{l_2(l_2^2-l_1^2)} \left[\frac{4a^2}{l_2^2}\bar{\tau}^{(1)}e^{2i\phi} - \frac{a^2(4l_2^2-5\rho^2)+l_1^4}{(l_2^2-l_1^2)^2}(\tau^{(1)}+\bar{\tau}^{(1)}e^{2i\phi}) \right] \right\}$$

$$\sigma''^{(1)}_z = -\frac{2(\bar{\tau}^{(1)}e^{i\phi} + \tau^{(1)}e^{-i\phi})}{\pi(2-\nu)} \frac{zl_1(l_2^2-a^2)^{1/2}\left[a^2(4l_2^2-5\rho^2)+l_1^4\right]}{l_2(l_2^2-l_1^2)^3}$$

$$\tau''^{(1)}_z = \frac{2}{\pi(2-\nu)} \left\{ \left[(2-\nu)\left(\frac{a(l_2^2-a^2)^{1/2}}{l_2^2-l_1^2} - \sin^{-1}\left(\frac{a}{l_2}\right) \right) + \frac{z(a^2-l_1^2)^{1/2}\left[l_1^4+a^2(2a^2+2z^2-3\rho^2)\right]}{(l_2^2-l_1^2)^3} \right] \tau^{(1)} \right.$$
$$\left. + \left[\nu a(l_2^2-a^2)^{1/2} + \frac{z(a^2-l_1^2)^{1/2}\left[a^2(6l_2^2-2l_1^2+\rho^2)-5l_2^4\right]}{(l_2^2-l_1^2)^2} \right] \frac{l_1^2 e^{2i\phi}}{l_2^2(l_2^2-l_1^2)}\bar{\tau}^{(1)} \right\} \tag{19}$$

where $\bar{\tau}^{(1)}$ is the complex conjugate of $\tau^{(1)}$. The total perturbed stresses due to combined normal loading $p^{(1)}$ and shear loading $\tau^{(1)}$ are therefore obtained:

$$\begin{aligned} \sigma_1^{(1)} &= \sigma'^{(1)}_1 + \sigma''^{(1)}_1 \quad ; \quad \sigma_2^{(1)} = \sigma'^{(1)}_2 + \sigma''^{(1)}_2 \\ \sigma_z^{(1)} &= \sigma'^{(1)}_z + \sigma''^{(1)}_z \quad ; \quad \tau_z^{(1)} = \tau'^{(1)}_z + \tau''^{(1)}_z \end{aligned} \tag{20}$$

It can be shown that the Cartesian stress components are

$$\begin{aligned} \sigma_{xx}^{(1)} &= \frac{1}{2}\left[\sigma_1^{(1)} + \mathrm{Re}(\sigma_2^{(1)})\right] \quad ; \quad \sigma_{yy}^{(1)} = \frac{1}{2}\left[\sigma_1^{(1)} - \mathrm{Re}(\sigma_2^{(1)})\right] \\ \sigma_{zz}^{(1)} &= \sigma_z^{(1)} \quad ; \quad \sigma_{xy}^{(1)} = \frac{1}{2}\mathrm{Im}(\sigma_2^{(1)}) \\ \sigma_{yz}^{(1)} &= \mathrm{Im}(\tau_z^{(1)}) \quad ; \quad \sigma_{zx}^{(1)} = \mathrm{Re}(\tau_z^{(1)}) \end{aligned} \tag{21}$$

where "Re" and "Im" are the real and imaginary parts, respectively, of a complex variable.

Eq. (21) can be recapitulated into the following matrix form:

$$\boldsymbol{\tau}^{(1)} \equiv \begin{Bmatrix} \sigma_{xx} \\ \sigma_{yy} \\ \sigma_{zz} \\ \sigma_{xy} \\ \sigma_{yz} \\ \sigma_{zx} \end{Bmatrix}^{(1)} = \begin{bmatrix} \frac{b_1+b_2}{2} & \frac{c_1+c_2}{2} & \frac{d_1+d_2}{2} \\ \frac{b_1-b_2}{2} & \frac{c_1-c_2}{2} & \frac{d_1-d_2}{2} \\ b_3 & c_3 & d_3 \\ \frac{b_4}{2} & \frac{c_4}{2} & \frac{d_4}{2} \\ b_5 & c_5 & d_5 \\ b_6 & c_6 & d_6 \end{bmatrix}^{(1)} \begin{Bmatrix} p \\ s \\ t \end{Bmatrix}^{(1)} \tag{22}$$

where definitions of the parameters b_i, c_i, and d_i can be found in **Appendix I**. Symbolically, we can express $\boldsymbol{\tau}^{(1)}$ as a function of coordinates and normal and shear stresses as follows:

$$\boldsymbol{\tau}^{(1)} \equiv \boldsymbol{\tau}(\rho, \phi, z; p_1, s_1, t_1) \tag{23}$$

Since microcracks 1 and 2 are aligned, the perturbed normal and shear stresses along the surfaces at the 'microcrack 2' location are

$$\begin{aligned} \tilde{p}_2 &= \mathbf{e}_z \cdot \boldsymbol{\tau}^{(1)} \cdot \mathbf{e}_z = \sigma_{zz}^{(1)} \\ \tilde{s}_2 &= \mathbf{e}_z \cdot \boldsymbol{\tau}^{(1)} \cdot \mathbf{e}_x = \sigma_{zx}^{(1)} \\ \tilde{t}_2 &= \mathbf{e}_z \cdot \boldsymbol{\tau}^{(1)} \cdot \mathbf{e}_y = \sigma_{yz}^{(1)} \end{aligned} \tag{24}$$

where $\mathbf{e}_x$, $\mathbf{e}_y$, and $\mathbf{e}_z$ are the unit base vectors in the Cartesian (x, y, and z) coordinates.

Similarly, in the sub-problem 2 (containing only the 'microcrack 2'), it can be shown that the perturbed normal and shear stresses along the surfaces at the 'microcrack 1' location are

$$\tilde{p}_1 = \sigma_{zz}^{(2)} \;\; ; \;\; \tilde{s}_1 = -\sigma_{zx}^{(2)} \;\; ; \;\; \tilde{t}_1 = \sigma_{yz}^{(2)} \tag{25}$$

where symbolic representations similar to Eq. (23) and (24) have been employed:

$$\boldsymbol{\tau}^{(2)} \equiv \boldsymbol{\tau}(\rho, \pi - \phi, z; p_2, -s_2, t_2) \tag{26}$$

Eq. (24) together with (25) then leads to

$$\begin{Bmatrix} \tilde{p}_1 \\ \tilde{s}_1 \\ \tilde{t}_1 \\ \tilde{p}_2 \\ \tilde{s}_2 \\ \tilde{t}_2 \end{Bmatrix} = \begin{bmatrix} 0 & 0 & 0 & b_4^{(2)} & -c_4^{(2)} & d_4^{(2)} \\ 0 & 0 & 0 & -b_5^{(2)} & c_5^{(2)} & -d_5^{(2)} \\ 0 & 0 & 0 & b_6^{(2)} & -c_6^{(2)} & d_6^{(2)} \\ b_4^{(1)} & c_4^{(1)} & d_4^{(1)} & 0 & 0 & 0 \\ b_5^{(1)} & c_5^{(1)} & d_5^{(1)} & 0 & 0 & 0 \\ b_6^{(1)} & c_6^{(1)} & d_6^{(1)} & 0 & 0 & 0 \end{bmatrix} \begin{Bmatrix} p_1 \\ s_1 \\ t_1 \\ p_2 \\ s_2 \\ t_2 \end{Bmatrix} \tag{27}$$

For convenience in the following derivations, let us define

$$\mathbf{T}_{1-2} \equiv \begin{Bmatrix} p_1 \\ s_1 \\ t_1 \\ p_2 \\ s_2 \\ t_2 \end{Bmatrix} \;\; ; \;\; \mathbf{T}_{1-2}^{\infty} \equiv \begin{Bmatrix} p_1^{\infty} \\ s_1^{\infty} \\ t_1^{\infty} \\ p_2^{\infty} \\ s_2^{\infty} \\ t_2^{\infty} \end{Bmatrix} \;\; ; \;\; \tilde{\mathbf{T}}_{1-2} \equiv \begin{Bmatrix} \tilde{p}_1 \\ \tilde{s}_1 \\ \tilde{t}_1 \\ \tilde{p}_2 \\ \tilde{s}_2 \\ \tilde{t}_2 \end{Bmatrix} \tag{28}$$

and $\boldsymbol{\alpha} \equiv$ the 6×6 "*microcrack interaction matrix*" in Eq. (27). It is noteworthy that our $\boldsymbol{\alpha}$ matrix, in fact, corresponds to the A matrix (the "transmission factor" or "crack interaction matrix") in Kachanov (1987) and Kachanov and Laures (1989). With these notations at hand, Eq. (27) can be rewritten as

$$\tilde{\mathbf{T}}_{1-2} = \boldsymbol{\alpha} \cdot \mathbf{T}_{1-2} \tag{29}$$

Since $\mathbf{T}_{1-2} = \mathbf{T}_{1-2}^{\infty} + \tilde{\mathbf{T}}_{1-2}$, $\tilde{\mathbf{T}}_{1-2}$ can be solved from Eq. (29):

$$\tilde{\mathbf{T}}_{1-2} = \tilde{\mathbf{K}} \cdot \mathbf{T}_{1-2}^{\infty} \;\; ; \;\; \text{where} \;\; \tilde{\mathbf{K}} \equiv \boldsymbol{\alpha} \cdot (\mathbf{I} - \boldsymbol{\alpha})^{-1} \tag{30}$$

Further, we define $\tilde{\mathbf{T}} \equiv (\tilde{p}_1, \tilde{s}_1, \tilde{t}_1)^T$ and $\mathbf{K}_1 \equiv$ the first three *rows* of $\tilde{\mathbf{K}}$. Hence, from Eq. (30), the perturbed stresses on surfaces of a microcrack due to the existence of the second microcrack are:

$$\tilde{\mathbf{T}} = \mathbf{K}_1 \cdot \mathbf{T}^{\infty}_{1-2} \tag{31}$$

Finally, since the two microcracks under consideration are aligned, it can be easily shown that

$$\mathbf{T}^{\infty}_{1-2} \equiv \begin{Bmatrix} p_1^{\infty} \\ s_1^{\infty} \\ t_1^{\infty} \\ p_2^{\infty} \\ s_2^{\infty} \\ t_2^{\infty} \end{Bmatrix} = \begin{bmatrix} 0 & 0 & 1 & 0 & 0 & 0 \\ 0 & 0 & 0 & 0 & 0 & 1 \\ 0 & 0 & 0 & 0 & 1 & 0 \\ 0 & 0 & 1 & 0 & 0 & 0 \\ 0 & 0 & 0 & 0 & 0 & 1 \\ 0 & 0 & 0 & 0 & 1 & 0 \end{bmatrix} \begin{Bmatrix} \sigma_{xx}^{\infty} \\ \sigma_{yy}^{\infty} \\ \sigma_{zz}^{\infty} \\ \sigma_{xy}^{\infty} \\ \sigma_{yz}^{\infty} \\ \sigma_{zx}^{\infty} \end{Bmatrix} \equiv \mathbf{K}_2 \cdot \boldsymbol{\tau}^{\infty} \tag{32}$$

From Eq. (32) and (31), we conclude that the *average* perturbed stress vector $\tilde{\mathbf{T}}$ over surfaces of a microcrack is simply:

$$\tilde{\mathbf{T}} = \mathbf{K} \cdot \boldsymbol{\tau}^{\infty} \quad ; \quad \text{where} \quad \mathbf{K} \equiv \mathbf{K}_1 \cdot \mathbf{K}_2 \tag{33}$$

Substitution of Eq. (33) into (13) then renders realizations for $(\tilde{\mathbf{T}})$ in the previous section. Therefore, the *ensemble average* approach is completely defined. For non-aligned penny-shaped microcracks, more complicated derivations will be involved.

III.2.3. Some test problems for two-microcrack interaction

A number of test problems are considered in this section to examine the performance of the approximate analytical solutions presented in Sec. 2.2. These include normal and shear loadings for two aligned *coplanar* or *stacked* penny-shaped microcracks. It is not our intention, however, to propose highly accurate analytical solutions to compute *local* stresses and stress intensity factors (SIFs) at all points on microcrack surfaces for a two-microcrack interaction problem. Instead, reasonably accurate *analytical average* perturbed stresses (in terms of elementary functions) over microcrack surfaces are sought in order to exploit the ensemble average approach. In fact, if one is interested in deterministic 3-D microcrack interaction, excellent *numerical* method has been proposed by Kachanov and Laures (1989). It is noted that key steps in Kachanov and Laures' (1989) method also focus on the computation of *average* pairwise stress "transmission factors" and *average* tractions. Once average tractions become known, one can certainly compute *projected* local stresses and SIFs at any point on microcrack surfaces. In general, the simple analytical solutions presented in Sec. 2.2 are not as accurate as those proposed in Kachanov and Laures (1989). Nonetheless, the latter relies on extensive numerical computations of transmission factors for all points on microcrack surfaces and is therefore not employed here.

It is emphasized that, given an existing microcrack, the location of the second microcrack is *random* within the ensemble average framework. Although stress interactions between two moderately spaced random microcracks are not very strong, their cumulative effects are important due to high spatial probabilities. On the other hand, stress interactions between two closely spaced random microcracks are strong yet their spatial probabilities are lower. Therefore, contributions from both closely and moderately spaced microcracks should be accounted for in the ensemble average approach. The ensemble-average spacing of microcrack arrays, clearly, depends on microcrack concentration.

Case I: *Two equal-sized coplanar microcracks under normal loading*. Though numerical results for SIFs are available for two coplanar microcracks under normal and shear loadings (Fabrikant (1987, 1989)), exact results for average tractions projected over microcrack surfaces are not documented. Nevertheless, Kachanov and Laures (1989) show that their results for SIFs are very close to those of Fabrikant (1987, 1989) for two equal-sized coplanar microcracks. Therefore, the average tractions computed by Kachanov and Laures (1989) should be quite accurate in the case of *coplanar* microcracks. The ratios of perturbed vs. far-field average normal stresses (p/p^{∞}) obtained by the proposed method are listed in **Table 1** for various $l/2a$ values (the Poisson ratio ν = 0.25). Here, l signifies the center-to-center distance between two microcracks and $2a$ is the microcrack size. For example, $l/2a$ = 1.00025 means that the smallest distance between microcrack tips is only $0.00025a$. The results reported in Kachanov and Laures (1989) and relative differences between the two results are also given in **Table 1** for comparison purpose. From **Table 1**, it is clear that interaction renders average stress *amplification*. The effect of microcrack interaction decays as the distance between two microcracks increases. Moreover, the differences between our simple calculations and those of Kachanov and Laures (1989) are small.

Case II: *Two equal-sized coplanar microcracks under shear loading*. The ratios of perturbed vs. far-field average shear stresses (τ/τ^{∞}) obtained by the present method are listed in **Table 2** for various $l/2a$ values (the Poisson ratio ν = 0.5). From **Table 2**, it is seen again that interaction renders average stress *amplification*. The differences between our simple calculations and those of Kachanov and Laures (1989) are small.

Case III: *Two equal-sized stacked microcracks under normal loading*. The ratios of perturbed vs. far-field average normal stresses (p/p^{∞}) are listed in **Table 3** for various $l/2a$ values (the Poisson ratio ν = 0.25). Obviously, from **Table 3**, interaction renders strong average stress *shielding*.

The degree of shielding in this case is much stronger than the degree of amplification in Cases I or II. Fabrikant (1989) did not provide numerical results for SIFs nor average stresses for two stacked microcracks under normal or shear loadings. Therefore, exact results are not available. For comparison, the differences between our simple calculations and those of Kachanov and Laures (1989) are listed in **Table 3**. It is observed that the difference is not very significant if $l/2a$ is greater than 0.5. The difference increases as the two microcracks move closer, due to sharp variations of stress fields in the close neighborhood of interacting microcracks.

Case IV: *Two equal-sized stacked microcracks under shear loading*. The ratios of perturbed vs. far-field average normal stresses (p/p^{∞}) are given in **Table 4** for various $l/2a$ values (the Poisson ratio $\nu = 0.25$). From **Table 4**, interaction renders average stress *shielding* when the distance l is small and very weak stress *amplification* when $l/2a > 0.5$. The differences between our simple calculations and those of Kachanov and Laures (1989) are small for $l/2a$ greater than 0.25.

Since pairwise microcrack interactions are random (probabilistic) within the framework of the ensemble average approach, the errors associated with the present approximate analysis should be statistically averaged over all possible realizations. Therefore, the ensemble-average error of the present method should be small as long as microcrack concentration is not extremely high.

III.3. Effective moduli of brittle solids with interacting microcracks

With the ensemble average framework and analytical pairwise interaction solutions at hand, we are now ready to construct the *ensemble-average* constitutive equations of brittle solids with many randomly located, aligned interacting microcracks. By substituting Eq. (10) and (33) into (9) and taking the ensemble average, we arrive at

$$\langle \mathbf{T} \rangle = (\mathbf{K}_0 + f(\mathbf{x})\langle \mathbf{K} \rangle) \cdot \boldsymbol{\tau}^{\infty} \tag{34}$$

where

$$\langle \mathbf{K} \rangle \equiv \int_{\Xi} \mathbf{K}\, d\mathbf{x}_1 = \int_{\Xi} \mathbf{K} r^2 \sin\psi \, dr d\psi d\theta \tag{35}$$

In the foregoing equations, it is implicitly assumed that all microcracks are of equal size and of same orientation. In addition, the spherical coordinate system (r, ψ, θ) is used to describe the random location $(\mathbf{x}_1)$ of the second microcrack relative to the first random microcrack centered at $\mathbf{x}$. Note that ψ varies from 0 to π and θ ranges from 0 to 2π. If we normalize r with respect to the microcrack radius a (i.e., $\xi \equiv r/a$), then Eq. (35) can be recast as

$$\langle \mathbf{K} \rangle \equiv a^3 \langle \hat{\mathbf{K}} \rangle = a^3 \int_{\Xi} \mathbf{K} \xi^2 \sin\psi \, d\xi d\psi d\theta \tag{36}$$

Combining Eq. (6), (34) and (36), we obtain the *local* ensemble-averaged damage-induced strain (at a typical point $\mathbf{x}$):

$$\langle \mathbf{e}^* \rangle(\mathbf{x}) = \langle \mathbf{S}^* \rangle(\mathbf{x}) \cdot \boldsymbol{\tau}^{\infty} \tag{37}$$

Here the ensemble-averaged, damage-induced *local* compliance has two components:

$$\langle \mathbf{S}^* \rangle(\mathbf{x}) = \langle \mathbf{S}^{*1} \rangle(\mathbf{x}) + \langle \mathbf{S}^{*2} \rangle(\mathbf{x}) \tag{38}$$

where

$$\begin{aligned} \langle \mathbf{S}^{*1} \rangle(\mathbf{x}) &= \frac{16(1-\nu^2)}{3E(2-\nu)} f(\mathbf{x}) a^3 \mathbf{g} \cdot \mathbf{K}_0 \\ \langle \mathbf{S}^{*2} \rangle(\mathbf{x}) &= \frac{16(1-\nu^2)}{3E(2-\nu)} f^2(\mathbf{x}) a^6 \mathbf{g} \cdot \langle \hat{\mathbf{K}} \rangle \end{aligned} \tag{39}$$

It is noteworthy that Eq. (39) actually reveals physical *nonlocal effects* in constitutive equations through microcrack interaction and the *ensemble averaging* process. That is, the stress-strain laws at a material point $\mathbf{x}$ within a RVE depend on the constitutive laws of *all neighboring* points. This is a *physical* nonlocal approach, at variance with the *postulated* nonlocal theories due to Eringen and Edelen (1972).

To obtain *volume averaged* moduli due to microcracks within a RVE, one simply applies the volume-average operator to Eq. (38)–(39). As a consequence, we have

$$\overline{\langle \mathbf{S}^* \rangle} \equiv \frac{1}{V}\int_V \langle \mathbf{S}^* \rangle(\mathbf{x})\, d\mathbf{x} = \frac{1}{V}\left[\int_V \langle \mathbf{S}^{*1} \rangle(\mathbf{x})\, d\mathbf{x} + \int_V \langle \mathbf{S}^{*2} \rangle(\mathbf{x})\, d\mathbf{x}\right] = \overline{\langle \mathbf{S}^{*1} \rangle} + \overline{\langle \mathbf{S}^{*2} \rangle} \tag{40}$$

where

$$\begin{aligned} \overline{\langle \mathbf{S}^{*1} \rangle} &= \frac{16(1-\nu^2)}{3E(2-\nu)}\mathbf{g}\cdot\mathbf{K}_0\, a^3\, \frac{\int_V f(\mathbf{x})\, d\mathbf{x}}{V} \\ \overline{\langle \mathbf{S}^{*2} \rangle} &= \frac{16(1-\nu^2)}{3E(2-\nu)}\mathbf{g}\cdot\langle \hat{\mathbf{K}} \rangle\, a^6\, \frac{\int_V f^2(\mathbf{x})\, d\mathbf{x}}{V} \end{aligned} \tag{41}$$

Let us assume that there are N microcracks in the RVE; i.e.,

$$\int_V f(\mathbf{x})\, d\mathbf{x} = N \tag{42}$$

Further, consider the case in which the variance of the PDF ($f(\mathbf{x})$) for locations of microcracks is *small* (e.g., uniform probability). We may therefore write

$$\int_V f^2(\mathbf{x})\, d\mathbf{x} \simeq \frac{\left[\int_V f(\mathbf{x})\, d\mathbf{x}\right]^2}{V} = \frac{N^2}{V} \tag{43}$$

Substitution of Eq. (42) and (43) into (41) then leads to

$$\begin{aligned} \overline{\langle \mathbf{S}^{*1} \rangle} &= \frac{16(1-\nu^2)}{3E(2-\nu)}\mathbf{g}\cdot\mathbf{K}_0\, \omega \\ \overline{\langle \mathbf{S}^{*2} \rangle} &= \frac{16(1-\nu^2)}{3E(2-\nu)}\mathbf{g}\cdot\langle \hat{\mathbf{K}} \rangle\, \omega^2 \end{aligned} \tag{44}$$

where

$$\omega \equiv \frac{Na^3}{V} \tag{45}$$

is the (volume-averaged) microcrack concentration parameter. We emphasize that our definition of ω is different from that defined by Budiansky and O'Connell (1976). The two definitions differ by a scalar factor $4\pi/3$. It is noted that $\overline{\langle \mathbf{S}^{*1} \rangle}$ actually corresponds to the first-order contribution due to non-interacting microcracks; i.e., the simple Taylor's model is recovered. Moreover, $\overline{\langle \mathbf{S}^{*2} \rangle}$ represents the second-order (in ω^2) contribution due to pairwise microcrack interaction.

Finally, the overall (volume-ensemble averaged) effective moduli for a microcrack-weakened solid is obtained by adding the elastic compliance $\mathbf{S}^0$ to $\overline{\langle \mathbf{S}^* \rangle}$:

$$\overline{\langle \mathbf{S} \rangle} \equiv \mathbf{S}^0 + \overline{\langle \mathbf{S}^{*1} \rangle} + \overline{\langle \mathbf{S}^{*2} \rangle} \tag{46}$$

In particular, in the case of 3-D linear isotropic elasticity, $\mathbf{S}^0$ reads

$$\mathbf{S}^0 = \frac{1}{E}\begin{bmatrix} 1 & -\nu & -\nu & 0 & 0 & 0 \\ -\nu & 1 & -\nu & 0 & 0 & 0 \\ -\nu & -\nu & 1 & 0 & 0 & 0 \\ 0 & 0 & 0 & 2(1+\nu) & 0 & 0 \\ 0 & 0 & 0 & 0 & 2(1+\nu) & 0 \\ 0 & 0 & 0 & 0 & 0 & 2(1+\nu) \end{bmatrix} \tag{47}$$

It is emphasized that *local* macroscopic constitutive laws for a RVE are recovered by the volume averaging process. However, if one stops at the ensemble averaging level without further performing the volume averaging process, the constitutive relations are nonlocal.

III.4. Some numerical examples

In this section, some numerical examples involving aligned microcracks are presented to illustrate the proposed ensemble-volume average approach in three-dimension. In the first example, effects of microcrack interactions are neglected and the well-known Taylor's model is recovered. Subsequently, the proposed second-order microcrack interaction model is implemented. Finally, we compare the results of the present approach with some existing methods, including the Taylor's model, the self-consistent method and the differential scheme. Closed (nonactive) microcrack contributions to compliances are neglected in this work.

III.4.1. Dilute non-interacting aligned microcracks

Let us consider the case in which effects of microcrack interactions are totally neglected. This can be done by simply dropping the term $\overline{\langle \mathbf{S}^{*2} \rangle}$ in Eq. (46):

$$\overline{\langle \mathbf{S} \rangle} = \mathbf{S}^0 + \overline{\langle \mathbf{S}^{*1} \rangle} \tag{48}$$

From Eq. (8), (11), and (44), we obtain

$$\overline{\langle \mathbf{S}^{*1} \rangle} = \frac{16(1-\nu^2)\omega}{3E(2-\nu)} \begin{bmatrix} 0 & 0 & 0 & 0 & 0 & 0 \\ 0 & 0 & 0 & 0 & 0 & 0 \\ 0 & 0 & 2-\nu & 0 & 0 & 0 \\ 0 & 0 & 0 & 0 & 0 & 0 \\ 0 & 0 & 0 & 0 & 2 & 0 \\ 0 & 0 & 0 & 0 & 0 & 2 \end{bmatrix} \tag{49}$$

Combination of Eq. (47) and (49) then yields

$$\overline{\langle \mathbf{S} \rangle} = \begin{bmatrix} S^0_{11} & S^0_{12} & S^0_{13} & 0 & 0 & 0 \\ S^0_{21} & S^0_{22} & S^0_{23} & 0 & 0 & 0 \\ S^0_{31} & S^0_{32} & \overline{S}_{33} & 0 & 0 & 0 \\ 0 & 0 & 0 & S^0_{44} & 0 & 0 \\ 0 & 0 & 0 & 0 & \overline{S}_{55} & 0 \\ 0 & 0 & 0 & 0 & 0 & \overline{S}_{66} \end{bmatrix} \tag{50}$$

where $1 = xx, 2 = yy, 3 = zz, 4 = xy, 5 = yz, 6 = zx$ (Voigt's notation); S^0_{ij} components are given in (47), and

$$\begin{aligned} \overline{S}_{33} &= S^0_{33} + \overline{S}^{*1}_{33} \\ \overline{S}_{55} &= S^0_{55} + \overline{S}^{*1}_{55} \\ \overline{S}_{66} &= S^0_{66} + \overline{S}^{*1}_{66} \end{aligned} \tag{51}$$

in which

$$\begin{aligned} \overline{S}^{*1}_{33} &\equiv \frac{16(1-\nu^2)}{3E}\,\omega \\ \overline{S}^{*1}_{55} &= \overline{S}^{*1}_{66} \equiv \frac{32(1-\nu^2)}{3E(2-\nu)}\,\omega \end{aligned} \tag{52}$$

It is observed that only the three compliance components in Eq. (51) are changed due to the presence of randomly located, aligned, penny-shaped microcracks. One notes that Eqs. (50)–(52) indeed recover the well-known Taylor's model. Further, the effective constitutive equations belong to the category of transverse isotropy. This is typical of *fiber breaks* in unidirectionally reinforced fiber composites.

III.4.2. Aligned interacting penny-shaped microcracks

We now focus on the proposed ensemble-volume averaged, pairwise interaction model. For a given microcrack concentration ω, the overall effective moduli in Eq. (46) can be evaluated by carrying out the integration in Eq. (36). That is, one needs to perform integration for the matrix $\mathbf{K}$ over the active microcrack domain (ξ, ψ, θ). It is emphasized that the values of $\mathbf{K}$ decay rapidly as the distance between a pair of randomly located microcracks increases. Therefore, compliance contributions due to remote integration region can be neglected.

The integration in Eq. (36) can be effectively computed by the Gauss quadrature scheme with three independent variables: ξ, ψ and θ; see **Table 5** for the convergence behavior. Our numerical experiments show that use of $\xi_{max} = 20$ (or $r_{max} = 20a$) is quite acceptable; i.e., contributions from the $\xi > 20$ domain can be neglected. In **Table 5**, the minimum radius of integration for r (or ξ) is assumed to be $r_{min} = 2a$ (or $\xi_{min} = 2$). The only *nonzero* components in $\langle \hat{\mathbf{K}} \rangle$ are $\langle \hat{K}_{13} \rangle$, $\langle \hat{K}_{26} \rangle$ and $\langle \hat{K}_{35} \rangle$ (the latter two are equal). It is observed that the normal component $\langle \hat{K}_{13} \rangle$ is much greater than the shear components $\langle \hat{K}_{26} \rangle$ and $\langle \hat{K}_{35} \rangle$. Furthermore, use of $r_{min} = 2a$ implies that the minimum allowable distance between any two microcrack-centers is $2a$. Therefore, according to the "face-center cubic" calculation, the maximum allowable ω is $1/4\sqrt{2} \simeq 0.1768$ for $r_{min} = 2a$. Note that the maximum allowable microcrack density would be 0.741 if ω is defined as $4\pi N a^3/3V$ (Budiansky and O'Connell, 1976).

To achieve higher maximum permissible microcrack densities, various minimum radii of integration r_{min} are used to compute $\langle \hat{\mathbf{K}} \rangle$; see **Table 6** for details. The value of ξ_{max} is chosen as 20.0 in **Table 6**. We observe significant increases in both $\langle \hat{K}_{13} \rangle$ and $\langle \hat{K}_{26} \rangle$ as ξ_{min} decreases. The maximum microcrack concentration ω corresponding to the $\xi_{min} = 1.1a$ case is found to be 1.0627 (or 4.451 if the definition of Budiansky and O'Connell (1976) is employed). It is emphasized that **Table 6** is *not* a summary of convergence behavior, but a display of $\langle \hat{\mathbf{K}} \rangle$ for different maximum allowable microcrack densities.

For convenience, let us define $\langle \hat{K}_{13} \rangle \equiv \hat{k}_1$ and $\langle \hat{K}_{26} \rangle = \langle \hat{K}_{35} \rangle \equiv \hat{k}_2$. Therefore, according to Eq. (8) and (44), we obtain

$$\overline{\langle \mathbf{S}^{*2} \rangle} = \frac{16(1-\nu^2)}{3E(2-\nu)} \omega^2 \begin{bmatrix} 0 & 0 & 0 & 0 & 0 & 0 \\ 0 & 0 & 0 & 0 & 0 & 0 \\ 0 & 0 & (2-\nu)\hat{k}_1 & 0 & 0 & \\ 0 & 0 & 0 & 0 & 0 & 0 \\ 0 & 0 & 0 & 0 & 2\hat{k}_2 & 0 \\ 0 & 0 & 0 & 0 & 0 & 2\hat{k}_2 \end{bmatrix} \tag{53}$$

Adding Eq. (53) to (50), we thus arrive at the expression for overall effective compliances with the second-order microcrack interaction. Apart from the three compliance components $\overline{\langle S_{33} \rangle}$, $\overline{\langle S_{55} \rangle}$ and $\overline{\langle S_{66} \rangle}$, it is seen that all other components are identical to the elastic components. In particular, the three compliance components which change under microcrack interaction take the following explicit forms:

$$\begin{aligned} \overline{\langle S_{33} \rangle} &= S_{33}^0 + \frac{16(1-\nu^2)}{3E} (\omega + \hat{k}_1 \omega^2) \\ \overline{\langle S_{55} \rangle} &= \overline{\langle S_{66} \rangle} = S_{55}^0 + \frac{32(1-\nu^2)}{3E(2-\nu)} (\omega + \hat{k}_2 \omega^2) \end{aligned} \tag{54}$$

Clearly, the relative weight of the second-order compliance terms (in ω^2) to the first-order terms depends on the values of microcrack densities. For dilute (very low) ω, the second-order terms are negligible. By contrast, the compliance contributions are significant for high ω values.

III.4.3. Comparison with some existing methods

The effects of fiber breaks and aligned penny-shaped microcracks on the stiffness of unidirectional fiber composites have been studied extensively in the literature. We refer to Laws and Dvorak (1987) for an excellent presentation by using the self-consistent method and the differential scheme. It is noted that, in Laws and Dvorak (1987), the microcrack density is defined as $\alpha \equiv 8Na^3/V$; i.e., their α is equal to 8ω in this paper. The maximum microcrack concentration considered in Laws and Dvorak (1987) is $\omega = \alpha/8 = 0.125$. The macroscopic (overall) material behavior is, not surprisingly, transversely isotropic. It should be realized that the Taylor's model, the self-consistent method and the differential scheme all belong to the category of "effective medium" approaches. Namely, theses methods do *not* depend on the distributions of microcrack locations at all.

In the following numerical computations, the Young's modulus E is taken as 0.5 MPa and the shear modulus G as 0.2 MPa ($\nu = 0.25$) for the virgin matrix material. The overall (ensemble-volume averaged) longitudinal normal and shear compliances, $\overline{\langle S_{33} \rangle}$ and $\overline{\langle S_{55} \rangle}$, are plotted against the microcrack concentration parameter ω in Figures 2 and 3, respectively. The values of $\hat{k}_1$ and $\hat{k}_2$

in Eq. (54) are taken as 1.049792 and 0.355988, respectively, which correspond to $\xi_{min} = 1.1$ (i.e., the maximum allowable density $\omega = 1.0627$). Note that, once more, $\omega = 1$ corresponds to $\alpha = 8$ in Laws and Dvorak (1987). For comparison, the results obtained by using the Taylor's model, the self-consistent method and the differential scheme are also displayed in Figures 2 and 3. We would like to comment that: (a) the Taylor's model is really suitable for dilute microcrack concentrations; (b) the self-consistent method and the differential scheme are suitable for low or moderate ω; and (c) the proposed statistical pairwise microcrack interaction model is suitable for moderately high (not extremely high) ω.

Figures 4 and 5 show the effects of microcrack density ω on the normalized longitudinal Young's modulus E_L/E and shear modulus G_L/G for four different models. We have employed the standard notation: $E_L \equiv 1/\overline{\langle S_{33} \rangle}$ and $G_L \equiv 1/\overline{\langle S_{55} \rangle}$. In addition, it is straightforward to express the normalized moduli in Figures 4 and 5 as follows for the Taylor's model:

$$\frac{E_L}{E} = \frac{1}{1+5\omega} \quad ; \quad \frac{G_L}{G} = \frac{1}{1+2.28571\omega} \tag{55}$$

and for the present model:

$$\frac{E_L}{E} = \frac{1}{1+5\omega(1+1.05\omega)} \quad ; \quad \frac{G_L}{G} = \frac{1}{1+2.28571\omega(1+0.356\omega)} \tag{56}$$

III.5. A higher-order ensemble-average formulation of microcrack interaction

So far, attention has been focused on the second-order statistical model based on the concept of *pairwise* microcrack interaction. In this section, extension to accommodate higher-order interaction mechanism is considered within the ensemble-volume average framework; see also Ju and Chen (1991) for two-dimensional problems. The proposed higher-order formulation hinges on the derivation of higher-order (the third or above) corrections on local stress fields $\langle \mathbf{T} \rangle$ due to n-microcrack interaction ($n \geq 3$); see Eq. (9)–(12).

As an illustration, let us consider a three-microcrack (the third-order in ω^3) interaction mechanism within the proposed framework. For simplicity, we assume that all microcracks are aligned and of equal size. Following the definitions and assumptions previously described in Section 2.1, one can rephrase the local ensemble stress perturbation as (cf. Eq. (9)):

$$\langle \tilde{\mathbf{T}} \rangle + \langle \tilde{\tilde{\mathbf{T}}} \rangle \equiv \left\langle \begin{Bmatrix} \tilde{p} \\ \tilde{s} \\ \tilde{t} \end{Bmatrix} \right\rangle + \left\langle \begin{Bmatrix} \tilde{\tilde{p}} \\ \tilde{\tilde{s}} \\ \tilde{\tilde{t}} \end{Bmatrix} \right\rangle \tag{57}$$

where $\langle \tilde{\mathbf{T}} \rangle$ is the second-order local ensemble stress perturbation due to pairwise microcrack interactions (see Eq. (9) and (12)), and $\langle \tilde{\tilde{\mathbf{T}}} \rangle$ is the third-order local ensemble stress perturbation due to 3-microcrack interactions. In particular, $\langle \tilde{\tilde{\mathbf{T}}} \rangle$ can be expressed as (cf. Eq. (12))

$$\langle \tilde{\tilde{\mathbf{T}}} \rangle = \int_{\Xi} \langle \tilde{\tilde{\mathbf{T}}} \rangle (\mathbf{x}; \mathbf{x}_1 | \mathbf{x}_2) f(\mathbf{x}_2 | \mathbf{x}; \mathbf{x}_1) \, d\mathbf{x}_2 \tag{58}$$

Here, $\langle \tilde{\tilde{\mathbf{T}}} \rangle (\mathbf{x}; \mathbf{x}_1 | \mathbf{x}_2)$ is the third-order ensemble-average *stress perturbation* of a microcrack centered at $\mathbf{x}$, given a microcrack centered at $\mathbf{x}_1$, over a subclass of realizations which have a microcrack centered at $\mathbf{x}_2$. Further, $f(\mathbf{x}_2 | \mathbf{x}; \mathbf{x}_1)$ is the conditional probability density function (PDF) for finding a microcrack centered at $\mathbf{x}_2$ given two microcracks fixed at $\mathbf{x}$ and at $\mathbf{x}_1$, respectively. The conditional PDF $f(\mathbf{x}_2 | \mathbf{x}; \mathbf{x}_1)$ can be further simplified to $f(\mathbf{x})$ by the assumptions of local homogeneity and reasonable randomness (i.e., statistical independence). The active (open) integration domain Ξ depends on loading conditions.

For clarity, let us express $\langle \mathbf{T} \rangle$ and $\langle \mathbf{e}^* \rangle (\mathbf{x})$ as follows (cf. Eq. (34), (37) and (38), assuming local homogeneity and reasonable randomness):

$$\langle \mathbf{T} \rangle = \langle \mathbf{T}^{\infty} + \tilde{\mathbf{T}} + \tilde{\tilde{\mathbf{T}}} \rangle = \left(\mathbf{K}_0 + f(\mathbf{x}) \langle \mathbf{K} \rangle + f^2(\mathbf{x}) \langle \mathbf{K}' \rangle \right) \cdot \boldsymbol{\tau}^{\infty} \tag{59}$$

$$\langle \mathbf{e}^* \rangle (\mathbf{x}) = \left\{ \langle \mathbf{S}^{*1} \rangle (\mathbf{x}) + \langle \mathbf{S}^{*2} \rangle (\mathbf{x}) + \langle \mathbf{S}^{*3} \rangle (\mathbf{x}) \right\} \cdot \boldsymbol{\tau}^{\infty} \equiv \langle \mathbf{S}^* \rangle (\mathbf{x}) \cdot \boldsymbol{\tau}^{\infty} \tag{60}$$

where $\tilde{\tilde{\mathbf{T}}} \equiv \mathbf{K}' \cdot \boldsymbol{\tau}^{\infty}$ and (cf. Eq. (39))

$$\langle \mathbf{S}^{*3} \rangle(\mathbf{x}) \equiv \frac{16(1-\nu^2)}{3E(2-\nu)} f^3(\mathbf{x}) a^9 \mathbf{g} \cdot \langle \hat{\mathbf{K}}' \rangle \tag{61}$$

In Eq. (61), we have defined $\langle \hat{\mathbf{K}}' \rangle \equiv 1/a^6 \langle \mathbf{K}' \rangle$. We recall that both $\mathbf{K}_0$ and $\hat{\mathbf{K}}$ are expressed *explicitly* in *closed-form* formulas. Similarly, $\hat{\mathbf{K}}'$ (or $\tilde{\tilde{\mathbf{T}}}$) can also be constructed in closed-form as follows. One starts by expanding Eq. (14) into nine linear equations with $j = 1, 2, 3$. Then, one obtains expressions similar to Eq. (22), with the understanding that permutations 1–2, 2–3, 3–1 are involved. Eq. (24) in Sec. 2.2 is modified to include the third microcrack's contribution to stress perturbations. Subsequently, Eq. (27) is expanded to a 9 by 9 system with α denoting a 9 by 9 coefficient matrix. Therefore, we arrive at explicit formulas similar to Eq. (30)–(33); and $\hat{\mathbf{K}}'$, $\tilde{\tilde{\mathbf{T}}}$ can be expressed in closed-form as in the two-microcrack interaction problem. Finally, it is noted that the computation of $\langle \hat{\mathbf{K}}' \rangle$ involves integration over the domain of all possible positions of two active neighboring microcracks around a specified penny-shaped microcrack (cf. Eq. (36)).

Following the same procedure presented in Sec. 3, it can be shown that $\langle \mathbf{S}^{*3} \rangle$ in Eq. (61) gives rise to the third-order terms (in ω^3) to overall compliances due to the third-order microcrack interactions. Therefore, a third-order statistical micromechanical model can actually be constructed. By repeating the foregoing procedure, we can formulate a complete (though very complicated) hierarchical family of statistical microcrack theories of arbitrary orders.

III.6. Conclusions

Based on the concept of ensemble-volume average and pairwise microcrack interaction, an innovative three-dimensional statistical micromechanical theory is proposed for brittle solids with many randomly located (but aligned), interacting microcracks. The effects of interaction-induced stress perturbations and random locations of microcracks are manifested by $\langle \tilde{\mathbf{T}} \rangle$. Approximate explicit (analytical) interaction solutions for two arbitrarily located, aligned microcracks are given in detail. Therefore, overall effective moduli of brittle solids with interacting microcracks can be formally derived on the ground of statistical and micromechanical informations. However, explicit closed-form solutions to arbitrarily located and arbitrarily oriented microcracks are very involved, and no reasonably compact explicit forms can be presented within normal page limit. In a forthcoming paper, nonetheless, general microcrack geometry will be fully accommodated through numerical computations of the "microcrack interaction matrix" $\boldsymbol{\alpha}$ and the ensemble average approach. In addition,, it is interesting to note that a physically "*nonlocal*" description of the material behavior can be obtained during the *ensemble averaging* process.

The proposed approach is fundamentally different from existing effective medium methods which do **not** depend on locations and configurations of microcracks. Further, the proposed microcrack interaction framework does *not* require the use of Monte Carlo simulations. Some numerical examples are presented to illustrate the behavior of the proposed model. The resulting predictions are compared with some existing methods. Finally, a higher-order microcrack interaction formulation is briefly summarized.

The proposed method provides a simple framework to accommodate statistical, micromechanical, and interaction aspects of distributed microcrack arrays. Applications may be made, for example, to aligned matrix cracks, fiber breaks, and interlaminar delaminations of brittle composite materials. Further research will be needed in the future to assess the applicability of the proposed method to practical engineering problems.

III.7. References

1. BATCHELOR, G. K., (1970), "The stress system in a suspension of force-free particles", *J. Fluid Mech.*, vol. 41, pp. 545–570.

2. BATCHELOR, G. K. AND GREEN, J. T., (1972), "The determination of the bulk stress in a suspension of spherical particles to order c^2", *J. Fluid Mech.*, vol. 56, part 3, pp. 401–427.

3. BENVENISTE, Y., (1986), "On the Mori-Tanaka's method in cracked bodies", *Mech. Res. Comm.*, vol. 13, pp. 193–201.

4. BUDIANSKY, B. AND O'CONNELL, R. J., (1976), "Elastic moduli of a cracked solid", *Int. J. Solids & Struct.*, vol. 12, pp. 81–97.

5. CHEN, H. S. AND ACRIVOS, A., (1978a), "The solution of the equations of linear elasticity for an infinite region containing two spherical inclusions", *Int. J. Solids & Struct.*, vol. 14, pp. 331–348.

6. CHEN, H. S. AND ACRIVOS, A., (1978b), "The effective elastic moduli of composite materials containing spherical inclusions at non-dilute concentrations", *Int. J. Solids & Struct.*, vol. 14, pp. 349–364.

7. CHEN, T. M. AND JU, J. W., (1991), "On effective elastic moduli of two-dimensional brittle solids with interacting microcracks. Part I : Basic formulations", *J. Appl. Mech.*, submitted for publication.

8. CHRISTENSEN, R. M., (1990), "A critical evaluation for a class of micromechanics models", *J. Mech. Phys. Solids*, vol. 38, no. 3 pp. 379–404.

9. CHRISTENSEN, R. M. AND LO, K. H., (1979), "Solutions for effective shear properties in three phase sphere and cylinder models", *J. Mech. Phys. Solids*, vol. 27, pp. 315–330.

10. CHOW, C. L. AND WANG, J., (1987), "An anisotropic theory of continuum damage mechanics for brittle fracture", *Eng. Fract. Mech.*, vol. 27, pp. 547–558.

11. ERINGEN, A. C. AND EDELEN, D. G. B., (1972), "On nonlocal elasticity", *Int. J. Eng. Sci.*, vol. 10, pp. 233–248.

12. FABRIKANT, V. I., (1987), "Close interaction of coplanar circular cracks in an elastic medium", *Acta Mechanica*, vol. 67, pp. 39–59.

13. FABRIKANT, V. I., (1989) "Applications of potential theory in mechanics: a selection of new results", Kluwer Academic Publishers, Dordrecht, The Netherlands.

14. FANELLA, D. AND KRAJCINOVIC, D., (1988), "A micromechanical model for concrete in compression", *Eng. Fract. Mech.*, vol. 29, no. 1, pp. 49–66.

15. GROSS, D., (1982), "Spannungsintensitatsfaktoren von ribsystemen (Stress intensity factors of systems of cracks)", *Ing.-Arch.*, vol. 51, pp. 301–310 (in German).

16. HASHIN, Z. AND SHTRIKMAN, S., (1962), "On some variational principles in anisotropic and nonhomogeneous elasticity", *J. Mech. Phys. Solids*, vol. 10, pp. 335–342.

17. HASHIN, Z. AND SHTRIKMAN, S., (1963), "A variational approach to the theory of the elastic behavior of multiphase materials", *J. Mech. Phys. Solids*, vol. 11, pp. 127–140.

18. HASHIN, Z., (1988), "The differential scheme and its application to cracked materials", *J. Mech. Phys. Solids*, vol. 36, pp. 719–734.

19. HILL, R., (1965), "A self-consistent mechanics of composite materials", *J. Mech. Phys. Solids*, vol. 13, pp. 213–222.

20. HINCH. E. J., (1977), "An averaged-equation approach to particle interactions in a fluid suspension", *J. Fluid Mech.*, vol. 83, pp. 695–720.

21. HORI, M. AND NEMAT-NASSER, S., (1987), "Interacting micro-cracks near the tip in the process zone of a macro-crack", *J. Mech. Phys. Solids*, vol. 35, pp. 601–629.

22. HORII, H. AND NEMAT-NASSER, S., (1983), "Overall moduli of solids with microcracks: load-induced anisotropy", *J. Mech. Phys. Solids*, vol. 331, pp. 155–171.

23. HORII, H. AND NEMAT-NASSER, S., (1985), "Elastic fields of interacting inhomogeneities", *Int. J. Solids & Struct.*, vol. 21, pp. 731–745.

24. HORII, H. AND SAHASAKMONTRI, K., (1990), "Mechanical properties of cracked solids: validity of the self-consistent method", in *Micromechanics and Inhomogeneity*, ed. by G. J. Weng, M. Taya and H. Abe, pp. 137–159, Springer-Verlag, New York.

25. HUDSON, J. A., (1980), "Overall properties of a cracked solid", *Math. Proc. Camb. Phil. Soc.*, vol. 88, pp. 371–384.

26. HUDSON, J. A., (1981), "Wave speeds and attenuation of elastic waves in material containing cracks", *Geophys. J. R. astr. Soc.*, vol. 64, pp. 133–150.

27. HUDSON, J. A., (1986), "A higher order approximation to the wave propagation constants for a cracked solid", *Geophys. J. R. astr. Soc.*, vol. 87, pp. 265–274.

28. JU, J. W., (1989a), "On energy-based coupled elastoplastic damage theories: constitutive modeling and computational aspects", *Int. J. Solids & Struct.*, vol. 25, no. 7, pp. 803–833.

29. JU, J. W., (1989b), "On energy-based coupled elastoplastic damage models at finite strains", *J. Eng. Mech.*, ASCE, vol. 115, no. 11, pp. 2507–2525.

30. JU, J. W., (1991a), "On two-dimensional self-consistent micromechanical damage models for brittle solids", *Int. J. Solids & Struct.*, vol. 27, no. 2, pp. 227–258.

31. JU, J. W., (1991b), "A micromechanical damage model for uniaxially reinforced composites weakened by interfacial arc microcracks", *J. Appl. Mech.*, ASME, vol. 58, no. 3, Sept. 1991.

32. JU, J. W. AND CHEN, T. M., (1991), "On effective elastic moduli of two-dimensional brittle solids with interacting microcracks. Part II : Evolutionary damage models", *J. Appl. Mech.*, submitted for publication.

33. JU, J. W. AND LEE, X., (1991), "On three-dimensional self-consistent micromechanical damage models for brittle solids. Part I: Tensile loadings", *J. Eng. Mech.*, ASCE, vol. 117, no. 7, pp. 1495–1515.

34. KACHANOV, M., (1985), "A simple technique of stress analysis in elastic solids with many cracks", *Int. J. Fract.*, vol. 28, pp. R11–R19.

35. KACHANOV, M., (1987), "Elastic solids with many cracks: a simple method of analysis", *Int J. Solids & Struct.*, vol. 23, pp. 23–43.

36. KACHANOV, M. AND MONTAGUT, E., (1986), "Interaction of a crack with certain microcrack arrays", *Eng. Fracture Mech.*, vol. 25, pp. 625–636.

37. KACHANOV, M. AND LAURES, J.-P., (1989), "Three-dimensional problems of strongly interacting arbitrarily located penny-shaped cracks", *Int. J. of Fract.*, vol. 41, pp. 289–313.

38. KRAJCINOVIC, D., (1989), "Damage mechanics", *Mech. Mater.*, vol. 8, no. 2-3 (Dec. 1989), pp. 117–197.

39. KRAJCINOVIC, D. AND FANELLA, D., (1986), "A micromechanical damage model for concrete", *Eng. Fract. Mech.*, vol. 25, pp. 585–596.

40. KRAJCINOVIC, D. AND SUMARAC, D., (1989), "A mesomechanical model for brittle deformation processes: Part I", *J. Appl. Mech.*, vol. 56, pp. 51–62.

41. LAURES, J.-P. AND KACHANOV, M., (1991), "Three-dimensional interactions of a crack front with arrays of penny shaped microcracks", *Int. J. Fract.*, to appear.

42. LAWS, N., DVORAK, G. J. AND HEJAZI, M., (1983), "Stiffness changes in unidirectional composites caused by crack systems", *Mech. of Mater.*, vol. 2, pp. 123–137.

43. LAWS, N. AND DVORAK, G. J., (1987), "The effect of fiber breaks and aligned penny-shaped cracks on the stiffness and energy release rates in unidirectional composites", *Int. J. Solids & Struct.*, vol. 23, no. 9, pp. 1269–1283.

44. LEE, X. AND JU, J. W., (1991), "On three-dimensional self-consistent micromechanical damage models for brittle solids. Part II: Compressive loadings", *J. Eng. Mech.*, ASCE, vol. 117, no. 7, pp. 1516–1537.

45. MCLAUGHLIN, R., (1977), "A study of the differential scheme for composite materials", *Int. J. Engng. Sci.*, vol. 15, pp. 237–244.

46. MONTAGUT, E. AND KACHANOV, M., (1988), "On modeling a microcracked zone by weakened elastic material and on statistical aspects of crack-microcrack interactions", *Int. J. Fract.*, vol. 37. R55–R62.

47. MORI, T. AND TANAKA, K., (1973), "Average stress in matrix and average elastic energy of materials with misfitting inclusions", *Acta Metallurgica*, vol. 21, pp. 571–574.

48. NEMAT-NASSER, S. AND HORI, M., (1990), "Elastic solids with microdefects", in *Micromechanics and Inhomogeneity*, pp. 297–320, ed. by G. J. Weng, M. Taya and H. Abe, Springer-Verlag, New York.

49. ROSCOE, R. A., (1952), "The viscosity of suspensions of rigid spheres", *Brit. J. Appl. Phys.*, vol. 3, pp. 267–269.

50. ROSCOE, R. A., (1973), "Isotropic composites with elastic or viscoelastic phases: general bounds for the moduli and solutions for special geometries", *Rheol. Acta*, vol. 12, pp. 404–411.

51. SAYERS, C. M. AND KACHANOV, M., (1991), "A simple technique for finding effective elastic constants of cracked solids for arbitrary crack orientation statistics", *Int. J. Solids & Struct.*, vol. 27, no. 6, pp. 671–680.

52. SUMARAC, D. AND KRAJCINOVIC, D., (1987), "A self-consistent model for microcrack-weakened solids", *Mech. Mater.*, vol. 6, pp. 39–52.

53. SUMARAC, D. AND KRAJCINOVIC, D., (1989), "A mesomechanical model for brittle deformation processes: part II", *J. Appl. Mech.*, vol. 56, pp. 57–62.

54. WENG, G. J., (1990), "The theoretical connection between Mori-Tanaka's theory and the Hashin-Shtrikman-Walpole bounds", *Int. J. Engng. Sci.*, vol. 28, no. 11, pp. 1111–1120.

55. WILLIS, J. R., (1977), "Bounds and self-consistent estimates for the overall properties of anisotropic composites", *J. Mech. Phys. Solids*, vol. 25, pp. 185–202.

56. WILLIS, J. R. AND ACTON, J. R., (1976), "The overall elastic moduli of a dilute suspension of spheres", *Quart. J. Mech. Appl. Math.*, vol. 29, part 2, pp. 163–177.

57. ZHAO, Y. H., TANDON, G. P. AND WENG, G. J., (1989), "Elastic moduli for a class of porous materials", *Acta Mechanica*, vol. 76, pp. 105–130.

Table 1. Two equal-sized coplanar microcracks under normal loading ($\nu = 0.25$)

$l/2a$	Present	Kachanov	Difference(%)
1.00025	1.0354	1.0837	4.46
1.005	1.0348	1.0779	4.00
1.05	1.0296	1.0529	2.21
1.1	1.0251	1.0398	1.41
1.15	1.0215	1.0315	0.97
1.25	1.0161	1.0214	0.52
1.5	1.0088	1.0104	0.16
2.0	1.0035	1.0038	0.03
2.5	1.0018	1.0019	0.01

Table 2. Two equal-sized coplanar microcracks under shear loading ($\nu = 0.5$)

$l/2a$	Present	Kachanov	Difference(%)
1.005	1.0681	1.1017	3.05
1.05	1.0580	1.0703	1.15
1.25	1.0317	1.0292	0.24
1.5	1.0174	1.0144	0.30
1.75	1.0106	1.0084	0.22
2.0	1.0070	1.0054	0.16
2.5	1.0035	1.0026	0.09
3.5	1.0013	1.0006	0.07

Table 3. Two equal-sized stacked microcracks under normal loading ($\nu = 0.25$)

$l/2a$	Present	Kachanov	Difference(%)
0.05	0.5004	0.5583	10.37
0.25	0.5383	0.6689	19.52
0.35	0.5836	0.7158	18.47
0.5	0.6667	0.7777	14.27
0.75	0.7928	0.8562	7.40
1.0	0.8754	0.9073	3.52
1.5	0.9505	0.9588	0.87

Table 4. Two equal-sized stacked microcracks under shear loading (ν = 0.25)

$l/2a$	Present	Kachanov	Difference(%)
0.05	0.5549	0.6613	16.09
0.25	0.8214	0.8886	7.56
0.5	1.0002	0.9837	1.68
0.75	1.0233	1.0053	1.79
1.0	1.0180	1.0084	0.95
1.25	1.0120	1.0072	0.48
1.5	1.0080	1.0055	0.25
2.0	1.0039	1.0031	0.08
2.5	1.0021	1.0026	0.05

Table 5. Convergence behavior of $\langle \hat{\mathbf{K}} \rangle$ vs. ξ_{max} (given $\xi_{min} = 2$)

$\xi_{max} = r_{max}/a$	$\langle \hat{K}_{13} \rangle$	$\langle \hat{K}_{26} \rangle = \langle \hat{K}_{35} \rangle$
4.0	0.150807	0.059503
6.0	0.168554	0.066656
8.0	0.173029	0.068467
10.0	0.174644	0.069121
20.0	0.176139	0.069728
40.0	0.176327	0.069804
80.0	0.176351	0.069828
160.0	0.176354	0.069829
320.0	0.176354	0.069829
640.0	0.176354	0.069829

Table 6. Numerical integration of $\langle \hat{\mathbf{K}} \rangle$ for different ξ_{min} (given $\xi_{max} = 20$)

$\xi_{min} = r_{min}/a$	$\langle \hat{K}_{13} \rangle$	$\langle \hat{K}_{26} \rangle = \langle \hat{K}_{35} \rangle$
2.0	0.176139	0.069728
1.75	0.305726	0.105974
1.5	0.601154	0.195689
1.25	0.850189	0.281202
1.125	0.975302	0.327491
1.1	1.049792	0.355988

III.8. Appendix I: Parameters for Eq. (22)

The parameters b_i, c_i and d_i in Eq. (22) can be shown to be:

$$
\begin{aligned}
b_1 &= \frac{2}{\pi}\left[(1+2\nu)k_1 + \frac{az^2}{g_2}k_2\right] \\
b_2 &= \frac{2}{\pi}ag_3^2\left[(1-2\nu)k_1 + \frac{z^2}{g_2}k_3\right]\cos 2\phi \\
b_3 &= \frac{2}{\pi}\left[k_1 - \frac{az^2}{g_2}k_2\right] \\
b_4 &= \frac{2}{\pi}ag_3^2\left[(1-2\nu)k_1 + \frac{z^2}{g_2}k_3\right]\sin 2\phi \\
b_5 &= -\frac{2}{\pi}zg_2g_3k_4\sin\phi \\
b_6 &= -\frac{2}{\pi}zg_2g_3k_4\cos\phi
\end{aligned}
\tag{62}
$$

$$
\begin{aligned}
c_1 &= f_3\cos\phi \\
c_2 &= f_4\cos\phi + f_5\cos 3\phi + f_6(\cos\phi + \cos 3\phi) \\
c_3 &= f_4\sin\phi + f_5\sin 3\phi + f_6(\sin 3\phi + \sin\phi) \\
c_4 &= -2f_6\cos\phi \\
c_5 &= f_7 + f_8\cos 2\phi \\
c_6 &= f_8\sin 2\phi
\end{aligned}
\tag{63}
$$

$$
\begin{aligned}
d_1 &= f_3\sin\phi \\
d_2 &= -f_4\sin\phi + f_5\sin 3\phi + f_6(\sin 3\phi - \sin\phi) \\
d_3 &= f_4\cos\phi - f_5\cos 3\phi + f_6(\cos\phi - \cos 3\phi) \\
d_4 &= -2f_6\sin\phi \\
d_5 &= f_8\sin 2\phi \\
d_6 &= f_7 - f_8\cos 2\phi
\end{aligned}
\tag{64}
$$

where

$$
\begin{aligned}
f_1 &= \frac{g_1}{g_5} \\
f_2 &= \frac{g_2}{g_5} \\
f_3 &= \frac{8}{\pi(2-\nu)}\left[-2(1+\nu)ag_3f_1 + zg_2g_3k_4\right] \\
f_4 &= -\frac{8(1-\nu)}{\pi(2-\nu)}ag_3f_1 \\
f_5 &= -\frac{8}{\pi(2-\nu)}zg_3f_2g_4^2 \\
f_6 &= \frac{2}{\pi(2-\nu)}zg_2g_3k_4 \\
f_7 &= \frac{2}{\pi}\left(k_1 + \frac{1}{2-\nu}zg_1k_2\right) \\
f_8 &= \frac{2}{\pi(2-\nu)}g_3^2(\nu af_2 + zg_1k_3)
\end{aligned}
\tag{65}
$$

$$
\begin{aligned}
g_1 &= (a^2 - l_1^2)^{1/2} \\
g_2 &= (l_2^2 - a^2)^{1/2} \\
g_3 &= \frac{l_1}{l_2} \\
g_4 &= \frac{a}{l_2} \\
g_5 &= l_2^2 - l_1^2
\end{aligned}
\tag{66}
$$

$$
\begin{aligned}
k_1 &= af_2 - \sin^{-1}(g_4) \\
k_2 &= \frac{l_1^4 + a^2(2a^2 + 2z^2 - 3\rho^2)}{g_5^3} \\
k_3 &= \frac{a^2(6l_2^2 - 2l_1^2 + \rho^2) - 5l_2^4}{g_5^3} \\
k_4 &= \frac{a^2(4l_2^2 - 5\rho^2) + l_1^4}{g_5^3}
\end{aligned}
\tag{67}
$$

III.9. Figure captions

Figure 1. Coordinate systems for two microcracks.

Figure 2. Comparison of overall longitudinal normal compliance $\overline{\langle S_{33} \rangle}$.

Figure 3. Comparison of overall longitudinal shear compliance $\overline{\langle S_{55} \rangle}$.

Figure 4. Comparison of normalized longitudinal Young's modulus.

Figure 5. Comparison of normalized longitudinal shear modulus.

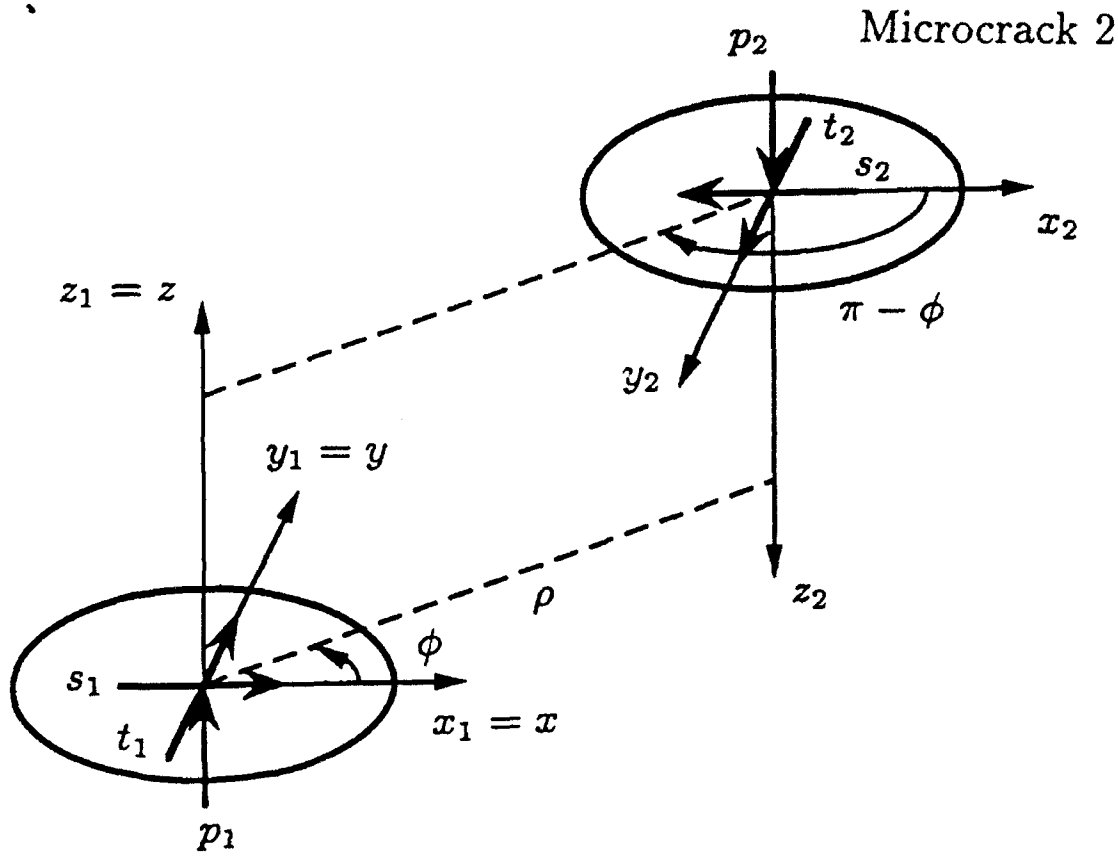

Figure 1. Coordinate systems for two microcracks.

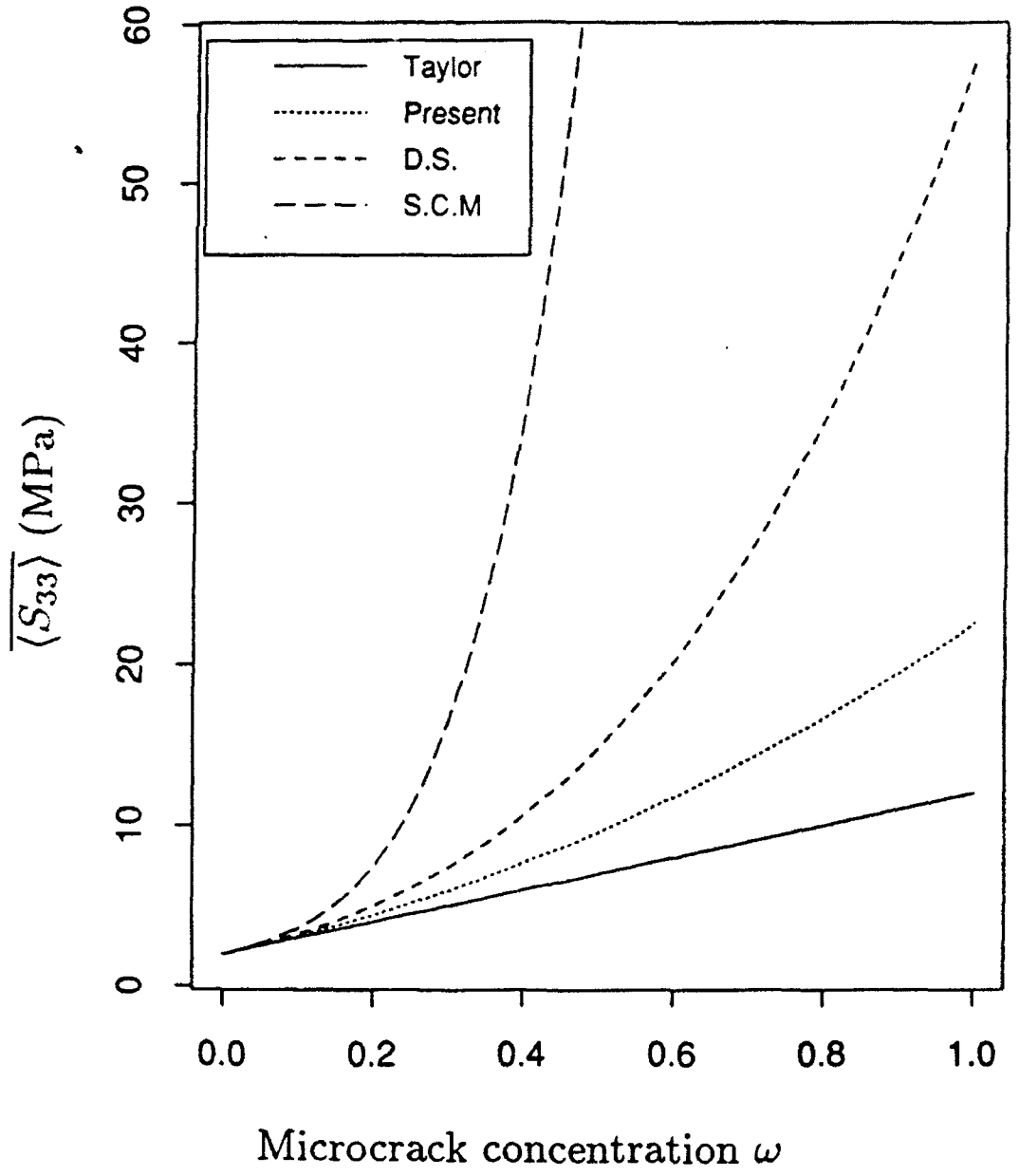

Figure 2. Comparison of overall longitudinal normal compliance $\overline{\langle S_{33} \rangle}$.

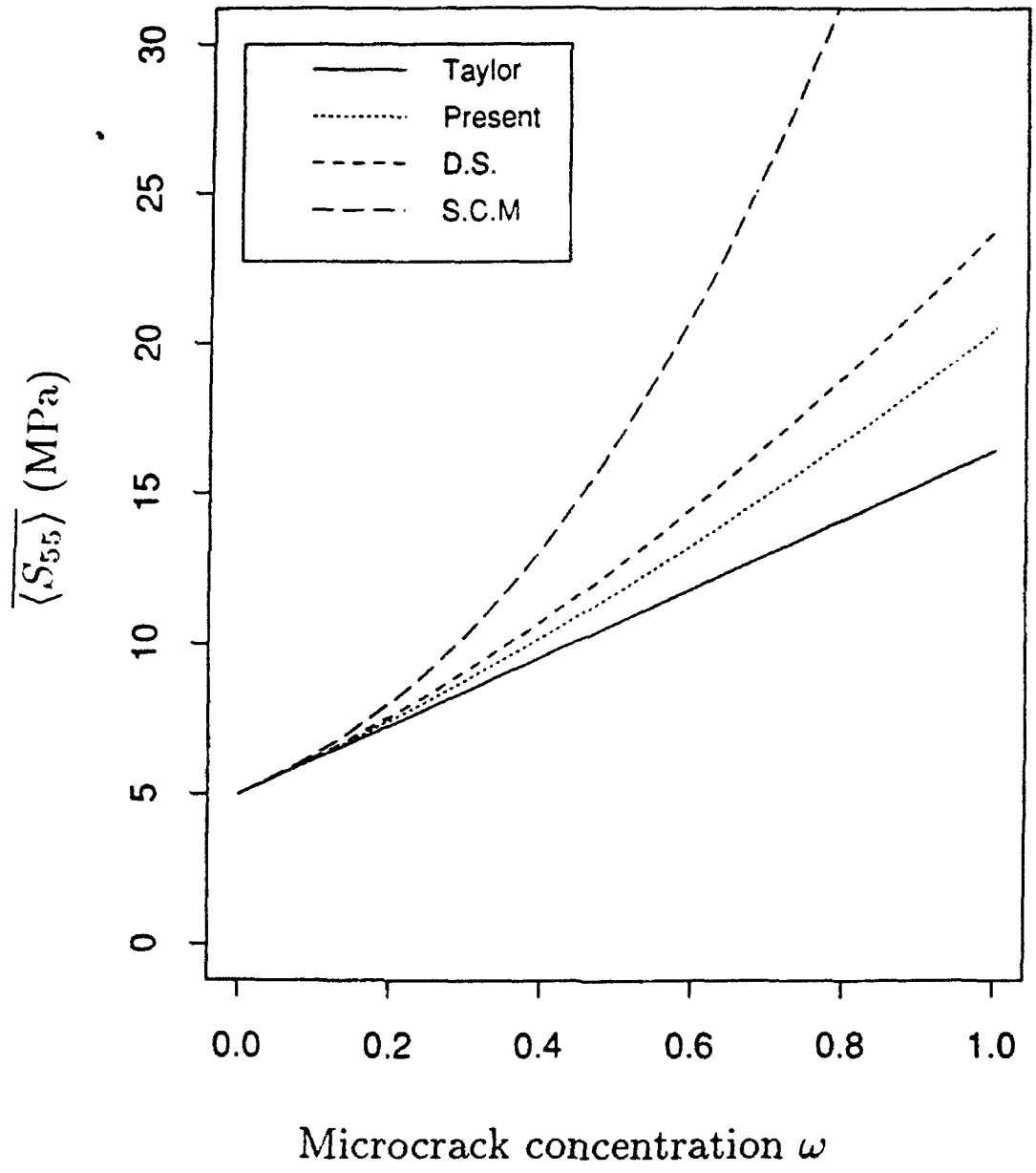

Figure 3. Comparison of overall longitudinal shear compliance $\overline{\langle S_{55} \rangle}$.

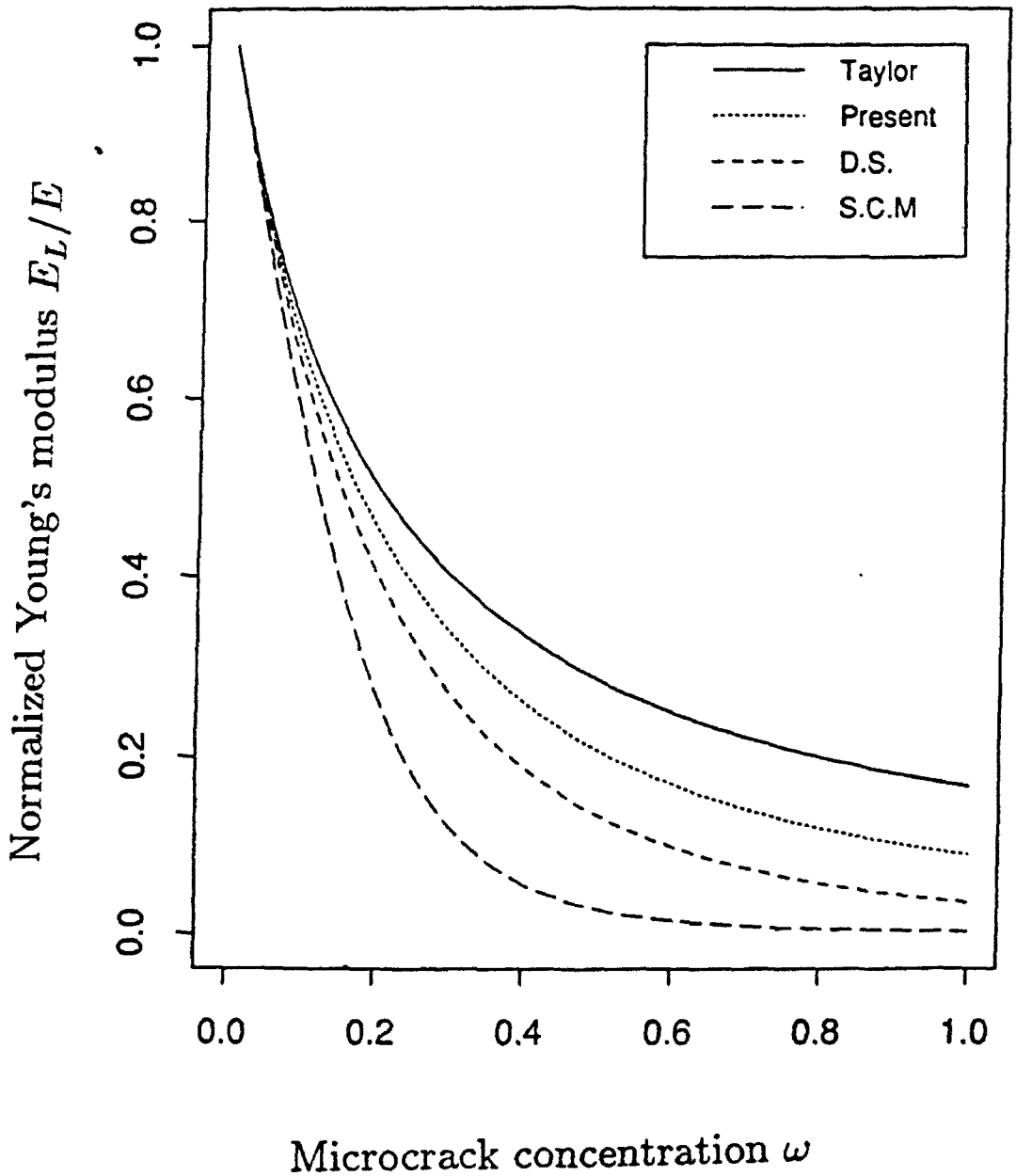

Figure 4. Comparison of normalized longitudinal Young's modulus.

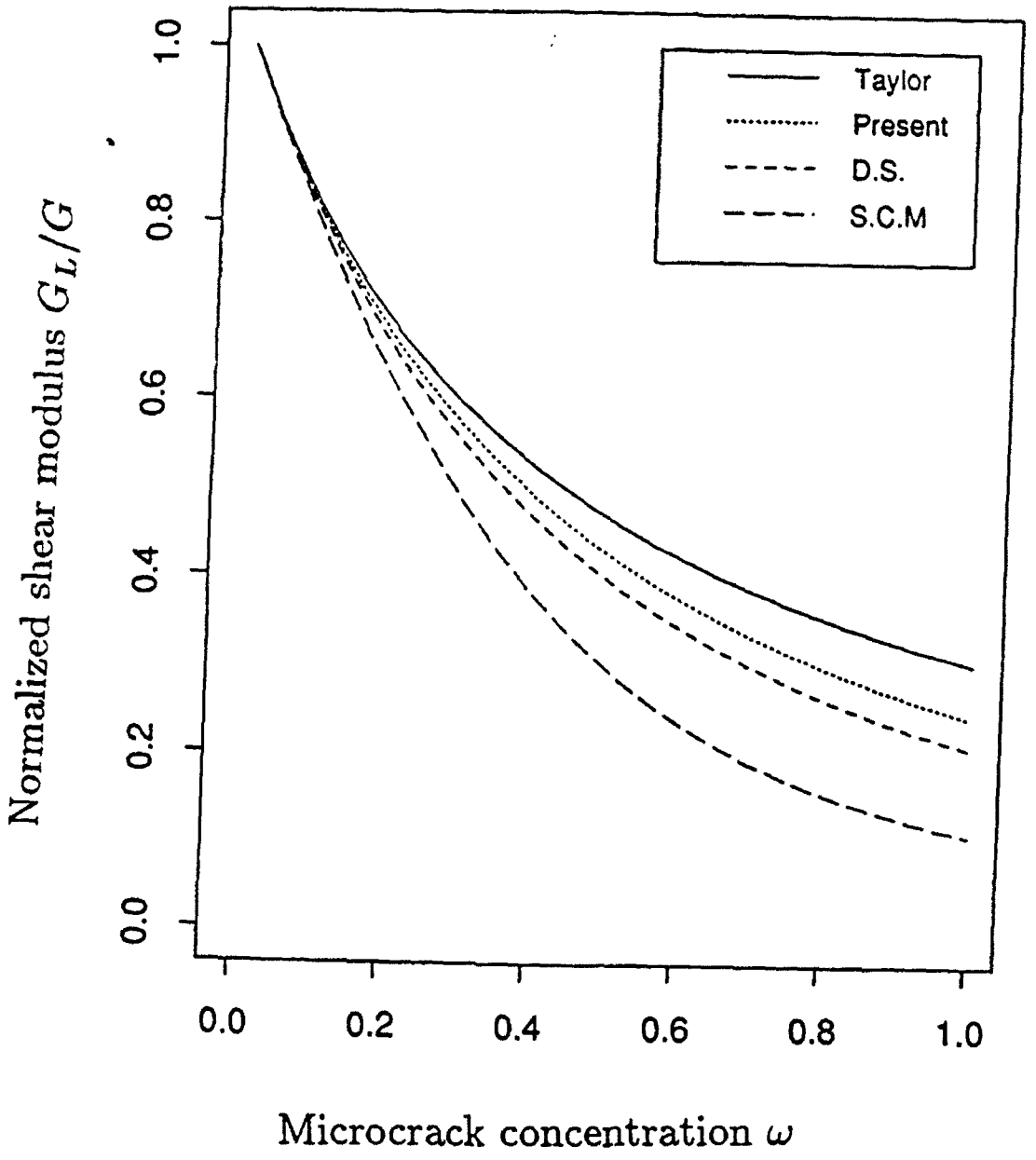

Figure 5. Comparison of normalized longitudinal shear modulus.

PART IV

An Improved Two-Dimensional Micromechanical Theory for Brittle Solids with Randomly Located Interacting Microcracks

IV.0. Abstract

This paper presents applications of accurate *orthogonal function* approximation methods to the two-dimensional problems of brittle solids containing **randomly** located and interacting microcracks within the framework of rigorous micromechanics and (probabilistic) ensemble average approach. The *random* two-crack interaction problems are solved by the highly accurate *Legendre* and *Tchebycheff* orthogonal polynomials to any desired orders. The complex stress potential method is subsequently employed to micromechanically derive microcrack opening displacements under complex loadings due to microcrack interaction effects — including concentrated loadings, arbitrary loadings and polynomial loadings. Improved local ensemble-averaged and overall effective elastic compliances due to microcracks and their interactions are systematically constructed by using the *pairwise* microcrack interaction mechanism and the ensemble average approach. A number of interesting analytical-numerical examples containing different random microcrack configurations are also presented to illustrate the capabilities of the proposed framework.

IV.1. Introduction

The effects of microcrack interactions on overall elastic moduli of brittle solids have been investigated by many researchers in the solid mechanics community. Among others, Ju and Chen (1991a,b) and Ju and Tseng (1992a) proposed two-dimensional and three-dimensional statistical micromechanical damage models to estimate effective elastic moduli of brittle solids containing many randomly dispersed and interacting microcracks. In particular, statistical aspects and microcrack interactions are explicitly accounted for. Based on a simplified stress interaction formulation, analytical closed-form solutions of microcrack interactions are derived by Ju and Chen (1991a) and Ju and Tseng (1992a) at the expense of some accuracy in local stresses. Gross (1982) and Horii and Nemat-Nasser (1985) proposed some asymptotic models for microcrack interaction problems. Embedded in their models is the restriction that microcracks are not too close to one another. On the other hand, accurate numerical, deterministic stress interaction approximations were introduced by Kachanov (1987) and Benveniste et al. (1989). Explicit analytical forms are not available in their models; however, higher accuracy in deterministic local stresses is achieved and stronger microcrack interactions are made possible.

In this study, numerical orthogonal function approximations are employed to improve the accuracy of local stresses of microcrack interactions and therefore the accuracy of the overall ensemble averaged effective elastic moduli. In Section 2 of this paper, orthogonal function approximations are applied to solve the arbitrary (probabilistic) local two-microcrack interaction problems. In particular, Legendre and Tchebycheff polynomial families are implemented to assess their effectiveness. Other approximation methods are discussed and compared with the orthogonal function approximation method in Section 4. Applications of complex stress potentials on microcrack interaction problems are discussed in Section 4. Stress potentials for concentrated loading conditions are integrated for arbitrary loading cases. Microcrack opening displacements and strains for polynomial loadings of any arbitrary order are also presented. In Section 5, overall effective elastic moduli are derived by taking the ensemble-volume averages in the *probability space* over all possible microcrack realizations. Finally, some numerical examples are presented to illustrate the proposed theory in Section 6.

IV 2. Orthogonal function approximations of two-crack interaction problems

IV.2.1. Two-crack interaction problems

The problem of two interacting microcracks embedded in an elastic solid loaded by far field stress σ^{∞} has been studied by various methods in the literature. In particular, $\sigma^{\infty} \equiv (\sigma^{\infty}_{xx}, \sigma^{\infty}_{yy}, \sigma^{\infty}_{xy})^T$ in two-dimension; see **Figure 1** for a schematic plot of coordinate systems.

Let p and q denote the local normal and shear tractions on the surface of a microcrack, respectively. A system of equations for the tractions on two arbitrary, interacting microcracks can be set up by decomposing the original problem into three subproblems. The boundary conditions that microcrack surfaces are traction-free lead to

$$\begin{aligned} p_1(x_1) &= p_1^{\infty} + \tilde{p}_1(x_1) \quad ; \quad q_1(x_1) = q_1^{\infty} + \tilde{q}_1(x_1) \\ p_2(x_2) &= p_2^{\infty} + \tilde{p}_2(x_2) \quad ; \quad q_2(x_2) = q_2^{\infty} + \tilde{q}_2(x_2) \end{aligned} \tag{1}$$

where x_1 and x_2 are local horizontal coordinates along the microcrack lines. Further, subscripts 1 and 2 denote microcrack 1 and microcrack 2, respectively. Local tractions due to far field loading only are p^{∞} and q^{∞}. Traction perturbation due to *inter-crack interactions only* are denoted by $(\tilde{p}_1, \tilde{q}_1, \tilde{p}_2, \tilde{q}_2)$. Assuming that a_1 and a_2 are the half-lengths of the two microcracks, respectively, Eq. (1) are valid for $-a_1 < x_1 < a_1$ and $-a_2 < x_2 < a_2$. Following Kachanov (1987), Benveniste et al. (1989) and Ju and Chen (1991a), it is assumed further that microcracks do not intersect each other arbitrarily.

Following Benveniste et al. (1989), we let $P_n(x), n = 0, 1, 2, ..., N$ denote a family of orthogonal functions defined in $[-1, 1]$. The tractions $p_1(x_1)$, $q_1(x_1)$, $p_2(x_2)$, and $q_2(x_2)$ can be approximated by the base function set as:

$$\begin{aligned} p_1(x_1) &= \sum_{n=0}^{N} p_1^n P_n\left(\frac{x_1}{a_1}\right) \quad ; \quad q_1(x_1) = \sum_{n=0}^{N} q_1^n P_n\left(\frac{x_1}{a_1}\right) \\ p_2(x_2) &= \sum_{n=0}^{N} p_2^n P_n\left(\frac{x_2}{a_2}\right) \quad ; \quad q_2(x_2) = \sum_{n=0}^{N} q_2^n P_n\left(\frac{x_2}{a_2}\right) \end{aligned} \tag{2}$$

Accordingly, the perturbed tractions, $\tilde{p}_1(x_1)$, $\tilde{q}_1(x_1)$, $\tilde{p}_2(x_2)$, and $\tilde{q}_2(x_2)$ are linear combinations of

perturbations on one crack when the other crack is loaded by the base functions:

$$\begin{aligned}
\tilde{p}_1(x_1) &= \sum_{n=0}^{N} p_2^n F_{pp}^{12(n)}(x_1) + \sum_{n=0}^{N} q_2^n F_{pq}^{12(n)}(x_1) \\
\tilde{q}_1(x_1) &= \sum_{n=0}^{N} p_2^n F_{qp}^{12(n)}(x_1) + \sum_{n=0}^{N} q_2^n F_{qq}^{12(n)}(x_1) \\
\tilde{p}_2(x_2) &= \sum_{n=0}^{N} p_1^n F_{pp}^{21(n)}(x_2) + \sum_{n=0}^{N} q_1^n F_{pq}^{21(n)}(x_2) \\
\tilde{q}_2(x_2) &= \sum_{n=0}^{N} p_1^n F_{pp}^{21(n)}(x_2) + \sum_{n=0}^{N} q_1^n F_{pq}^{21(n)}(x_2)
\end{aligned} \tag{3}$$

where

$$\begin{aligned}
F_{pp}^{\alpha\beta(n)} &= \textit{normal traction on crack } \alpha \textit{ due to normal loading } P_n\left(\frac{x_\alpha}{a_\alpha}\right) \textit{ on crack } \beta \\
F_{pq}^{\alpha\beta(n)} &= \textit{normal traction on crack } \alpha \textit{ due to shear loading } P_n\left(\frac{x_\alpha}{a_\alpha}\right) \textit{ on crack } \beta \\
F_{qp}^{\alpha\beta(n)} &= \textit{shear traction on crack } \alpha \textit{ due to normal loading } P_n\left(\frac{x_\alpha}{a_\alpha}\right) \textit{ on crack } \beta \\
F_{qq}^{\alpha\beta(n)} &= \textit{shear traction on crack } \alpha \textit{ due to shear loading } P_n\left(\frac{x_\alpha}{a_\alpha}\right) \textit{ on crack } \beta
\end{aligned} \tag{4}$$

Substituting Eq. (2) and Eq. (3) into Eq. (1), we obtain

$$\begin{aligned}
\sum_{n=0}^{N} p_1^n P_n\left(\frac{x_1}{a_1}\right) &= p_1^\infty + \sum_{n=0}^{N} p_2^n F_{pp}^{12(n)}(x_1) + \sum_{n=0}^{N} q_2^n F_{pq}^{12(n)}(x_1) \\
\sum_{n=0}^{N} q_1^n P_n\left(\frac{x_1}{a_1}\right) &= q_1^\infty + \sum_{n=0}^{N} p_2^n F_{qp}^{12(n)}(x_1) + \sum_{n=0}^{N} q_2^n F_{qq}^{12(n)}(x_1) \\
\sum_{n=0}^{N} p_2^n P_n\left(\frac{x_2}{a_2}\right) &= p_2^\infty + \sum_{n=0}^{N} p_1^n F_{pp}^{21(n)}(x_2) + \sum_{n=0}^{N} q_1^n F_{pq}^{21(n)}(x_2) \\
\sum_{n=0}^{N} q_2^n P_n\left(\frac{x_2}{a_2}\right) &= q_2^\infty + \sum_{n=0}^{N} p_1^n F_{qp}^{21(n)}(x_2) + \sum_{n=0}^{N} q_1^n F_{qq}^{21(n)}(x_2)
\end{aligned} \tag{5}$$

The property of *orthogonality* of P_n is then applied to arrive at the following system of equa-

tions:

$$
\begin{aligned}
\left(P_n\left(\frac{x_1}{a_1}\right), P_n\left(\frac{x_1}{a_1}\right)\right)_w p_1^n &= \left(p_1^\infty, P_n\left(\frac{x_1}{a_1}\right)\right)_w + \sum_{n=0}^{N}\left(F_{pp}^{12(n)}(x_1), P_n\left(\frac{x_1}{a_1}\right)\right)_w p_2^n + \\
&\quad \sum_{n=0}^{N}\left(F_{pq}^{12(n)}(x_1), P_n\left(\frac{x_1}{a_1}\right)\right)_w q_2^n \quad \text{for } n = 0, 1, 2, \ldots, N \\
\left(P_n\left(\frac{x_1}{a_1}\right), P_n\left(\frac{x_1}{a_1}\right)\right)_w q_1^n &= \left(q_1^\infty, P_n\left(\frac{x_1}{a_1}\right)\right)_w + \sum_{n=0}^{N}\left(F_{qp}^{12(n)}(x_1), P_n\left(\frac{x_1}{a_1}\right)\right)_w p_2^n + \\
&\quad \sum_{n=0}^{N}\left(F_{qq}^{12(n)}(x_1), P_n\left(\frac{x_1}{a_1}\right)\right)_w q_2^n \quad \text{for } n = 0, 1, 2, \ldots, N \\
\left(P_n\left(\frac{x_2}{a_2}\right), P_n\left(\frac{x_2}{a_2}\right)\right)_w p_2^n &= \left(p_2^\infty, P_n\left(\frac{x_2}{a_2}\right)\right)_w + \sum_{n=0}^{N}\left(F_{pp}^{21(n)}(x_2), P_n\left(\frac{x_2}{a_2}\right)\right)_w p_1^n + \\
&\quad \sum_{n=0}^{N}\left(F_{pq}^{21(n)}(x_2), P_n\left(\frac{x_2}{a_2}\right)\right)_w q_1^n \quad \text{for } n = 0, 1, 2, \ldots, N \\
\left(P_n\left(\frac{x_2}{a_2}\right), P_n\left(\frac{x_1}{a_1}\right)\right)_w q_2^n &= \left(q_2^\infty, P_n\left(\frac{x_1}{a_1}\right)\right)_w + \sum_{n=0}^{N}\left(F_{qp}^{21(n)}(x_2), P_n\left(\frac{x_2}{a_2}\right)\right)_w p_1^n + \\
&\quad \sum_{n=0}^{N}\left(F_{qq}^{21(n)}(x_2), P_n\left(\frac{x_2}{a_2}\right)\right)_w q_1^n \quad \text{for } n = 0, 1, 2, \ldots, N
\end{aligned}
\tag{6}
$$

in which $(f, g)_w$ denotes the weighted norm of f and g.

All the norms in Eq. (6) are simple constants after carrying out the integrations. The system of $4(N + 1)$ equations is sufficient to solve for the $4(N + 1)$ unknowns, p_1^n, q_1^n, p_2^n, and q_2^n. In the case of $N = 4$, there are 20 equations in terms of 20 unknowns. For more accurate solutions, the number N can be increased.

The total tractions accounting for microcrack interactions are obtained by substituting the solved unknowns back into Eq. (2). However, another choice exists as we look at Eq. (3). That is, in addition to the left-hand side of Eq. (2), the right-hand side provides another (better) approximation [Benveniste et al. (1989)]. The difference between these two choices is that, with the former choice, tractions on each crack are solved directly from the system of equations while for the latter tractions on one crack are the sum of tractions due to the far field applied loadings and the perturbations induced by the interaction with the other crack. This stress perturbation is the amount of tractions on one crack while the other crack is loaded by the total tractions. In another words, the total tractions solved from Eq. (6) are **projected** onto the other crack. This process is embedded

in Eq. (3). Stress projections are equivalent to the evaluations of those influence functions, $F_{pp}^{\alpha\beta}$, $F_{pq}^{\alpha\beta}$, $F_{qp}^{\alpha\beta}$, and $F_{qq}^{\alpha\beta}$.

IV.2.2. Legendre and Tchebycheff polynomials

Among the orthogonal function sets, Legendre and Tchebycheff polynomials are widely used in various applications. Both polynomials are tested in this study. The definitions of Legendre Polynomials are

$$L_0(x) = 0, \qquad L_n(x) = \frac{1}{2^n n!}\frac{d^n}{dx^n}[(x^2-1)^n] \tag{7}$$

with the following orthogonal property

$$(L_n, L_j)_{w_L} = \begin{cases} \frac{2}{2n+1}, & \text{for } n = j \\ 0, & \text{otherwise} \end{cases} \tag{8}$$

The weighting function for Legendre polynomials is $w_L(x) = 1$. The system of equations for two-crack interaction with the application of Legendre polynomials is as follows

$$\begin{aligned}
&\frac{2a_1}{2n+1}p_1^n - \sum_{n=0}^{N}\left(F_{pp}^{12(n)}(x_1), L_n\left(\frac{x_1}{a_1}\right)\right)p_2^n - \sum_{n=0}^{N}\left(F_{pq}^{12(n)}(x_1), L_n\left(\frac{x_1}{a_1}\right)\right)q_2^n \\
&\qquad = 2a_1 p_1^{\infty}\delta_{n0}, \quad \text{for } n = 0,1,2,\ldots,N \\
&\frac{2a_1}{2n+1}q_1^n - \sum_{n=0}^{N}\left(F_{qp}^{12(n)}(x_1), L_n\left(\frac{x_1}{a_1}\right)\right)p_2^n - \sum_{n=0}^{N}\left(F_{qq}^{12(n)}(x_1), L_n\left(\frac{x_1}{a_1}\right)\right)q_2^n \\
&\qquad = 2a_1 q_1^{\infty}\delta_{n0}, \quad \text{for } n = 0,1,2,\ldots,N \\
&-\sum_{n=0}^{N}\left(F_{pp}^{21(n)}(x_2), L_n\left(\frac{x_2}{a_2}\right)\right)p_1^n - \sum_{n=0}^{N}\left(F_{pq}^{21(n)}(x_2), L_n\left(\frac{x_2}{a_2}\right)\right)q_1^n + \frac{2a_2}{2n+1}p_2^n \\
&\qquad = 2a_2 p_2^{\infty}\delta_{n0}, \quad \text{for } n = 0,1,2,\ldots,N \\
&-\sum_{n=0}^{N}\left(F_{qp}^{21(n)}(x_2), L_n\left(\frac{x_2}{a_2}\right)\right)p_1^n - \sum_{n=0}^{N}\left(F_{qq}^{21(n)}(x_2), L_n\left(\frac{x_2}{a_2}\right)\right)q_1^n + \frac{2a_2}{2n+1}q_2^n \\
&\qquad = 2a_2 q_2^{\infty}\delta_{n0}, \quad \text{for } n = 0,1,2,\ldots,N
\end{aligned} \tag{9}$$

where $\delta_{ij} = 0$ for $i = j$ and 0, otherwise.

On the other hand, the triangle family of orthogonal polynomials, Tchebycheff polynomials, is defined as

$$\begin{aligned}
&T_0(x) = 1, \qquad T_1(x) = x \\
&T_{n+1}(x) = 2xT_n(x) - T_{n-1}(x)
\end{aligned} \tag{10}$$

with the orthogonal property

$$(T_i, T_j)_{w_T} = \begin{cases} \pi, & \text{for } i = j = 0 \\ \frac{\pi}{2}, & \text{for } i = j \neq 0 \\ 0, & \text{otherwise} \end{cases} \tag{11}$$

The weighting function for Tebycheff family is $w_T(x) = (1-x^2)^{-1/2}$. If this family is applied, we have the following equations for the two-crack interaction problem:

$$\begin{aligned}
&\frac{\pi a_1}{2-\delta_{n0}}p_1^n - \sum_{n=0}^{N}\left(F_{pp}^{12(n)}(x_1), T_n\left(\frac{x_1}{a_1}\right)\right)_{w_T} p_2^n - \sum_{n=0}^{N}\left(F_{pq}^{12(n)}(x_1), T_n\left(\frac{x_1}{a_1}\right)\right)_{w_T} q_2^n \\
&\qquad = \pi a_1 p_1^\infty \delta_{n0}, \text{ for } n = 0, 1, 2, ..., N \\
&\frac{\pi a_1}{2-\delta_{n0}}q_1^n - \sum_{n=0}^{N}\left(F_{qp}^{12(n)}(x_1), T_n\left(\frac{x_1}{a_1}\right)\right)_{w_T} p_2^n - \sum_{n=0}^{N}\left(F_{qq}^{12(n)}(x_1), T_n\left(\frac{x_1}{a_1}\right)\right)_{w_T} q_2^n \\
&\qquad = \pi a_1 q_1^\infty \delta_{n0}, \text{ for } n = 0, 1, 2, ..., N \\
&-\sum_{n=0}^{N}\left(F_{pp}^{21(n)}(x_2), T_n\left(\frac{x_2}{a_2}\right)\right)_{w_T} p_1^n - \sum_{n=0}^{N}\left(F_{pq}^{21(n)}(x_2), T_n\left(\frac{x_2}{a_2}\right)\right)_{w_T} q_1^n + \frac{\pi a_2}{2-\delta_{n0}}p_2^n \\
&\qquad = \pi a_2 p_2^\infty \delta_{n0}, \text{ for } n = 0, 1, 2, ..., N \\
&-\sum_{n=0}^{N}\left(F_{qp}^{21(n)}(x_2), T_n\left(\frac{x_2}{a_2}\right)\right)_{w_T} p_1^n - \sum_{n=0}^{N}\left(F_{qq}^{21(n)}(x_2), T_n\left(\frac{x_2}{a_2}\right)\right)_{w_T} q_1^n + \frac{\pi a_2}{2-\delta_{n0}}q_2^n \\
&\qquad = \pi a_2 q_2^\infty \delta_{n0}, \text{ for } n = 0, 1, 2, ..., N
\end{aligned} \tag{12}$$

Due to the fact that base functions of Legendre and Tchebycheff approximations are polynomials, if no stress projection is performed, the tractions obtained by solving either Eq. (9) or Eq. (12) and substituting the coefficients into Eq. (2) can be rearranged by collecting the terms of the same power of x.

$$\begin{aligned}
p_1(x_1) &= p_1^\infty + \sum_{n=0}^{N}\mathcal{P}_1^n\left(\frac{x_1}{a_1}\right)^n \quad ; \quad q_1(x_1) = q_1^\infty + \sum_{n=0}^{N}\mathcal{Q}_1^n\left(\frac{x_1}{a_1}\right)^n \\
p_2(x_2) &= p_2^\infty + \sum_{n=0}^{N}\mathcal{P}_2^n\left(\frac{x_2}{a_2}\right)^n \quad ; \quad q_2(x_2) = q_2^\infty + \sum_{n=0}^{N}\mathcal{Q}_2^n\left(\frac{x_2}{a_2}\right)^n
\end{aligned} \tag{13}$$

Tractions with the operations of stress projection are similarly obtained by the right-hand side of Eq. (5).

$$\begin{aligned}
p_1(x_1) &= p_1^\infty + \sum_{n=0}^{N}\mathcal{P}_2^n\mathcal{F}_{pp}^{12(n)}(x_1) + \sum_{n=0}^{N}\mathcal{Q}_2^n\mathcal{F}_{pq}^{12(n)}(x_1) \\
q_1(x_1) &= q_1^\infty + \sum_{n=0}^{N}\mathcal{P}_2^n\mathcal{F}_{qp}^{12(n)}(x_1) + \sum_{n=0}^{N}\mathcal{Q}_2^n\mathcal{F}_{qq}^{12(n)}(x_1) \\
p_2(x_2) &= p_2^\infty + \sum_{n=0}^{N}\mathcal{P}_1^n\mathcal{F}_{pp}^{21(n)}(x_2) + \sum_{n=0}^{N}\mathcal{Q}_1^n\mathcal{F}_{pq}^{21(n)}(x_2) \\
q_2(x_2) &= q_2^\infty + \sum_{n=0}^{N}\mathcal{P}_1^n\mathcal{F}_{qp}^{21(n)}(x_2) + \sum_{n=0}^{N}\mathcal{Q}_1^n\mathcal{F}_{qq}^{21(n)}(x_2)
\end{aligned} \tag{14}$$

in which influence functions are similar to those defined in Eq. (4)

$$\begin{aligned}
\mathcal{F}_{pp}^{\alpha\beta(n)} &= \textit{normal traction on crack } \alpha \textit{ due to normal loading } \left(\frac{x_\alpha}{a_\alpha}\right)^n \textit{ on crack } \beta \\
\mathcal{F}_{pq}^{\alpha\beta(n)} &= \textit{normal traction on crack } \alpha \textit{ due to shear loading } \left(\frac{x_\alpha}{a_\alpha}\right)^n \textit{ on crack } \beta \\
\mathcal{F}_{qp}^{\alpha\beta(n)} &= \textit{shear traction on crack } \alpha \textit{ due to normal loading } \left(\frac{x_\alpha}{a_\alpha}\right)^n \textit{ on crack } \beta \\
\mathcal{F}_{qq}^{\alpha\beta(n)} &= \textit{shear traction on crack } \alpha \textit{ due to shear loading } \left(\frac{x_\alpha}{a_\alpha}\right)^n \textit{ on crack } \beta
\end{aligned} \tag{15}$$

IV.2.3. Comparisons of Legendre and Tchebycheff approximations

Both Legendre and Tchebycheff approximations employ polynomials as the base functions. They are both orthogonal and have the same symmetry property:

$$L_n(x) = (-1)^n P_n(-x) \qquad ; \qquad T_n(x) = (-1)^n T_n(-x) \tag{16}$$

The leading orders of the n^{th} functions, $L_n(x)$ and $T_n(x)$, are both equal to n. The shapes of base functions of the same order are quite similar. Weighting functions are, perhaps, the most noticeable difference. For the Legendre family, the weighting function is simply 1. The weighting function for the Tchebycheff family is singular at the two crack tips.

To compare the effectiveness of two approximation function sets on the problem of two-crack interaction, let us consider the stress intensity factors (SIF) at crack tips. For Mode I loadings, SIFs at both crack tips can be calculated by integrating over the crack line on the product of total traction $p(x)$ and the SIF for a unit concentrated normal loading [Tada et al. (1973)]:

$$\mathbf{K}_\mathbf{I}^{\pm} = \frac{1}{\sqrt{\pi a}} \int_{-a}^{+a} \sqrt{\frac{a \pm t}{a \mp t}}\, p(t)\, dt \tag{17}$$

For the cases in which $p(x)$ are simple polynomials, analytical SIF can be obtained. Assuming that $p(x) = (\frac{t}{a})^n$, it can be shown that [by carrying out the integration in Eq. (17)]

$$\mathbf{K}_\mathbf{I}^{\pm(n)} = c^n \sqrt{\pi a} \tag{18}$$

where c^n is a simple constant which can be easily calculated by symbolic mathematical softwares like MAPLE, MATHEMATICA, or MACSYMA for any number of n. Manuals for these softwares are provided in the reference. **Table 1** shows c^n for n ranging from 0 to 8. The authors like to point out that the applications of symbolic computation softwares in various research fields are becoming

Table 1. Constants for SIFs of polynomial loadings

n	0	1	2	3	4	5	6	7	8
c^n	1	$\pm\frac{1}{2}$	$\frac{1}{2}$	$\pm\frac{3}{8}$	$\frac{3}{8}$	$\pm\frac{5}{16}$	$\frac{5}{16}$	$\pm\frac{35}{128}$	$\frac{35}{128}$

popular as the capability of computers improved by the modern technology. Ioakimidis (1990) applied these power tools to the crack problems in fracture mechanics. More references about the so-called semi-analytical/numerical (SAN) method can be found in Ioakimidis (1992) in which the numerical and symbolic computations are combined to solve the singular integral equations commonly found in fracture mechanics.

These simple results are applicable to the problems of solving crack tip SIFs for two-crack interaction *without* stress projection. Combining Eq. (13), Eq. (17), and Eq. (18), SIFs of the two microcracks can be expressed by simple summations on the coefficients solved from the system of equations

$$\mathbf{K}_{\mathrm{I}_1}^{\pm(N)} = \mathbf{K}_{\mathrm{I}_{0_1}}(1 + \sum_{n=0}^{N} c^n \mathcal{P}_1^n) \quad ; \quad \mathbf{K}_{\mathrm{I}_2}^{\pm(N)} = \mathbf{K}_{\mathrm{I}_{0_2}}(1 + \sum_{n=0}^{N} c^n \mathcal{P}_2^n) \tag{19}$$

where the SIFs for non-interacting case are defined by

$$\mathbf{K}_{\mathrm{I}_{0_1}} \equiv p_1^{\infty}\sqrt{\pi a} \quad ; \quad \mathbf{K}_{\mathrm{I}_{0_2}} \equiv p_2^{\infty}\sqrt{\pi a} \tag{20}$$

Table 2. Comparison of normalized SIFs for two interacting collinear cracks

	Inner tip			Outer tip		
k	Exact	Legendre	Tchebycheff	Exact	Legendre	Tchebycheff
0.9	1.0004	1.0004	1.0004	1.0003	1.0003	1.0003
0.75	1.0028	1.0028	1.0028	1.0024	1.0024	1.0024
0.5	1.0176	1.0176	1.0176	1.0125	1.0125	1.0125
0.25	1.0804	1.0804	1.0804	1.0409	1.0410	1.0409
0.2	1.1125	1.1124	1.1125	1.0517	1.0517	1.0517
0.1	1.2551	1.2539	1.2551	1.0863	1.0870	1.0863
0.05	1.4729	1.4650	1.4733	1.1198	1.1229	1.1198
0.02	1.9046	1.8593	1.9132	1.1589	1.1727	1.1595
0.01	2.3716	2.2475	2.4201	1.1841	1.2149	1.1864
0.001	5.3947	4.0501	10.6993	1.2443	1.4029	1.3654
0.0001	13.3456	6.0830	-4.7501	1.2808	1.6190	1.0973
10^{-6}	93.0293	7.9860	-1.2083	1.3212	1.8234	1.1646

Tables 2, 3, and **4** show the comparisons of crack tip SIFs for the three cases depicted in **Figure 2.** Since the two microcracks are parallel to each other in all the three cases, SIFs of both microcracks are identical. The non-interacting SIF, $\mathbf{K}_{I_0}$, is used to normalize all SIFs in the three tables. Normalized SIFs in **Table 2** are always greater than one. This is in agreement with the physical observation since two collinear cracks intuitively enhance the tractions for each other. On the contrary, two stacked cracks act against each other from opening the crack lines and therefore SIFs given in **Table 3** are all less than one.

Table 3. Comparison of normalized SIFs for two stacked cracks

r/a	Inner/Outer tip	
	Legendre	Tchebycheff
100	1.000	1.000
10	0.986	0.986
5	0.951	0.951
2	0.843	0.843
1	0.774	0.788
0.4	0.772	0.721
0.2	0.677	0.696
0.1	0.628	0.674
0.05	0.588	0.654
0.01	0.535	0.620
0.005	0.524	0.610
0.001	0.506	0.596

Note that SIFs at the two crack tips for stacked cases are identical. Both Legendre and Tchebycheff family lead to very close results in the stacked cases even when the distance between the two crack is very small. For the third (aligned) case in **Table 4,** significant differences are observed only at the inner tips when the two cracks are very close to each other. Exact solutions given by Erdogan (1962) are included in **Table 2** for comparison for the first case in which two cracks are collinear. **Table 1** shows that if the cracks are very close, Legendre family still works well while Tchebycheff family results in negative SIFs at the inner tips which are actually unreasonable. Both sets yield nearly identical results if two cracks are far away from each other. It is interesting to observe that except those unreasonable results, Tchebycheff method tends to over-estimate the interaction effect. Consequently, SIFs at the inner tips calculated through Tchebycheff method are larger than

the exact values. On the contrary, the interaction effects are under-estimated by the Legendre approximation and the inner-tip SIFs are less than the exact ones. **Table 2** also shows that if the two collinear crack are not too close, $k > 0.01$ for example, Tchebycheff method appears to be a better approximation to the exact solution than the Legendre method though the approximation by the later is actually quite close to the exact result. However, in the cases which two collinear cracks are extremely close, Legendre method seems to be a better choice since the Tchebycheff method behaves unreasonably. One possible reason for the poor approximation of Tchebycheff family at extremely close distance is the singularities at both crack tips. In the collinear cases, tractions at the inner crack tips rise sharply as the distance between the two cracks decreases. This fast growth is amplified by the weighting function which is singular at crack tips. The comparisons above show that Legendre family is a more robust choice for the crack problems especially when cracks are very close and collinear.

Table 4. *Comparison of normalized SIFs for two aligned cracks*

	Inner tip		Outer tip	
r/a	Legendre	Tchebycheff	Legendre	Tchebycheff
100	1.000	1.000	1.000	1.000
10	1.004	1.004	1.005	1.005
5	1.010	1.010	1.020	1.020
2	0.847	0.847	1.078	1.077
1	0.481	0.478	1.087	1.091
0.4	0.234	0.235	1.050	1.044
0.2	0.180	0.183	1.016	1.011
0.1	0.152	0.168	0.986	0.990
0.05	0.135	0.162	0.964	0.977
0.01	0.115	0.158	0.936	0.962
0.005	0.113	0.160	0.931	0.959
0.001	0.126	0.162	0.932	0.955

Table 5 compares the crack-tip SIFs calculated by fourth order Legendre approximation method with and without the stress projection. The two interacting cracks are collinear as in the first case of **Figure 2**. The numerical experiments show that the stress projection is not important if the two cracks are not very close. In **Table 5**, SIFs with and without stress projection are quite close for k greater or equal to 0.01. However, when the two cracks are extremely close, the operation of stress

projection appears to be necessary if the accuracy is concerned. The approximated SIFs are much improved toward the exact solution for the cases of $k = 0.001, 0.0001$, and 10^{-6} in which cracks are extremely close.

Table 5. Comparison of normalized SIFs for two interacting collinear cracks by the fourth order Legendre approximation with and without stress projection.

	Inner tip			Outer tip		
k	Exact Solution	No Projection	Exact Projection	Exact Solution	No Projection	Exact Projection
0.9	1.0004	1.0004	1.0004	1.0003	1.0003	1.0003
0.75	1.0028	1.0028	1.0028	1.0024	1.0024	1.0024
0.5	1.0176	1.0176	1.0176	1.0125	1.0125	1.0125
0.25	1.0804	1.0804	1.0804	1.0409	1.0410	1.0409
0.2	1.1125	1.1124	1.1125	1.0517	1.0517	1.0517
0.1	1.2551	1.2539	1.2551	1.0863	1.0870	1.0863
0.05	1.4729	1.4650	1.4733	1.1198	1.1229	1.1198
0.02	1.9046	1.8593	1.9093	1.1589	1.1727	1.1595
0.01	2.3716	2.2475	2.3899	1.1841	1.2149	1.1858
0.001	5.3947	4.0501	5.5333	1.2443	1.4029	1.2614
0.0001	13.3456	6.0830	11.6430	1.2808	1.6190	1.3244
10^{-6}	93.0293	7.9860	26.3239	1.3212	1.8234	1.3785

IV.3. Other approximation methods

IV.3.1. The zeroth-order approximations

Several approximation techniques have been proposed in the literature to solve Eq. (1). For example, Ju and Chen (1991),for simplicity, expanded the traction functions in terms of polynomials with respect to the *center* of microcracks, and (for computational simplicity only) took only the *zeroth-order terms* which were constants for specified microcrack locations and orientations. Therefore, Eq. (1) can be recast as

$$\begin{aligned} p_1 &= p_1^{\infty} + \tilde{p}_1 \\ q_1 &= q_1^{\infty} + \tilde{q}_1 \\ p_2 &= p_2^{\infty} + \tilde{p}_2 \\ q_2 &= q_2^{\infty} + \tilde{q}_2 \end{aligned} \tag{21}$$

By employing Sneddon and Lowengrub (1969) solutions, Ju and Chen (1991) obtained approximate, analytical solutions

$$\begin{Bmatrix} \tilde{p}_1 \\ \tilde{q}_1 \\ \tilde{p}_2 \\ \tilde{q}_2 \end{Bmatrix} = \begin{bmatrix} 0 & 0 & \alpha_1 & \alpha_2 \\ 0 & 0 & \alpha_3 & \alpha_4 \\ \alpha_5 & \alpha_6 & 0 & 0 \\ \alpha_7 & \alpha_8 & 0 & 0 \end{bmatrix} \begin{Bmatrix} p_1 \\ q_1 \\ p_2 \\ q_2 \end{Bmatrix} \tag{22}$$

Definitions for α_i's can be found in the Appendix of Ju and Chen (1991).

For compactness, let us define $\mathbf{T}_{1-2} \equiv (p_1, q_1, p_2, q_2)^T$, $\mathbf{T}_{1-2}^{\infty} \equiv (p_1^{\infty}, q_1^{\infty}, p_2^{\infty}, q_2^{\infty})^T$, and $\tilde{\mathbf{T}}_{1-2} = (\tilde{p}_1, \tilde{q}_1, \tilde{p}_2, \tilde{q}_2)^T$. Therefore, Eq. (21) and Eq. (22) are rewritten in matrix and vectorial forms

$$\begin{aligned} \mathbf{T}_{1-2} &= \mathbf{T}_{1-2}^{\infty} + \tilde{\mathbf{T}}_{1-2} \\ \tilde{\mathbf{T}}_{1-2} &= \boldsymbol{\alpha} \cdot \mathbf{T}_{1-2} \end{aligned} \tag{23}$$

where $\boldsymbol{\alpha}$ denotes the 4 by 4 matrix in Eq. (22). The perturbed tractions due to two-microcrack interaction are solved from Eq. (23)

$$\tilde{\mathbf{T}}_{1-2} = \boldsymbol{\alpha} \cdot (\mathbf{I} - \boldsymbol{\alpha})^{-1} \cdot \mathbf{T}_{1-2}^{\infty} \tag{24}$$

Definition of $\mathbf{K}_{1-2} \equiv \boldsymbol{\alpha} \cdot (\mathbf{I} - \boldsymbol{\alpha})^{-1}$ and transformation of the far field loading $\boldsymbol{\sigma}^{\infty}$ into the local microcrack coordinates then render

$$\tilde{\mathbf{T}}_{1-2} = \mathbf{K}_{1-2} \cdot \mathbf{G}_{1-2} \cdot \boldsymbol{\sigma}^{\infty} \tag{25}$$

where

$$\mathbf{G}_{1-2} \equiv \begin{bmatrix} \sin^2\theta & \cos^2\theta & -\sin 2\theta \\ -\frac{1}{2}\sin 2\theta & \frac{1}{2}\sin 2\theta & \cos 2\theta \\ \sin^2(\theta+\phi) & \cos^2(\theta+\phi) & -\sin 2(\theta+\phi) \\ -\frac{1}{2}\sin 2(\theta+\phi) & \frac{1}{2}\sin 2(\theta+\phi) & \cos 2(\theta+\phi) \end{bmatrix} \tag{26}$$

Moreover, we define $\tilde{\mathbf{T}}_1 \equiv (\tilde{p}_1, \tilde{q}_1)^T$ and $\tilde{\mathbf{T}}_2 \equiv (\tilde{p}_2, \tilde{q}_2)^T$. Therefore, Eq. (25) can be rephrased for two microcracks as follows

$$\tilde{\mathbf{T}}_1 = \mathbf{K}_1 \cdot \mathbf{G}_{1-2} \cdot \boldsymbol{\sigma}^{\infty} \tag{27}$$

$$\tilde{\mathbf{T}}_2 = \mathbf{K}_2 \cdot \mathbf{G}_{1-2} \cdot \boldsymbol{\sigma}^{\infty} \tag{28}$$

where $\mathbf{K}_1$ contains the first two rows of $\mathbf{K}_{1-2}$ and $\mathbf{K}_2$ the last two rows.

In addition to the aforementioned zeroth-order polynomial expansion at microcrack *centers*, Kachanov (1985, 1987) proposed a more accurate approximation which also led to a system of equations in terms of some constants. Eq. (1) are first averaged over the microcrack lines. In essence, traction perturbations on one microcrack due to the *interaction* with another microcrack loaded by an averaged traction are averaged over the microcrack line. Accordingly, the following system of equations can be obtained (Kachanov, 1985)

$$\begin{aligned}
\overline{p}_1 &= p_1^{\infty} + \Lambda_{12}^{pp}\,\overline{p}_2 + \Lambda_{12}^{pq}\,\overline{q}_2 \\
\overline{q}_1 &= q_1^{\infty} + \Lambda_{12}^{qp}\,\overline{p}_2 + \Lambda_{12}^{qq}\,\overline{q}_2 \\
\overline{p}_2 &= p_2^{\infty} + \Lambda_{21}^{pp}\,\overline{p}_1 + \Lambda_{21}^{pq}\,\overline{q}_1 \\
\overline{q}_2 &= q_2^{\infty} + \Lambda_{21}^{qp}\,\overline{p}_1 + \Lambda_{21}^{qq}\,\overline{q}_1
\end{aligned} \tag{29}$$

For a given deterministic microcrack configuration, transmission factors Λ_{ij}^{kl} must be computed by numerical integrations. With pre-computed transmission factors, Eq. (29) become a system of simultaneous equations in terms of constants only, which can be solved for the unknown average tractions. Note that the matrix operation in Eq. (24) serves the same purpose as the solutions of simultaneous equations in Eq. (29). Certainly, Eq. (29) are more accurate than (24). However, much less computational efforts are required for the analytical zeroth-order polynomial expansion since no transmission factors involving numerical integrations are needed. Further, Eq. (24) are expressed in close-form. The efficiency of analytical expressions over numerical computations might not be very significant for a very few deterministic microcracks. Nevertheless, for ensemble-averaged effective compliance computations of *statistical* microcrack arrays (involving hundreds of random microcracks), the computational efficiency and simplicity of the zeroth-order polynomial expansion are more favorable.

IV.3.2. Other higher order approximations

There are a number of methods in the literature which involve higher-order approximations of microcrack interaction problems. Emanating from Eq. (1), the traction functions were expanded

into Fourier series in Horii and Nemat-Nasser (1985). Moreover, Gross (1982) approximated traction functions by Tchebycheff polynomials. Both methods involve choosing a parameter which represents the ratio of the distances between microcrack centers to microcrack lengths. Higher-order terms involving a chosen parameter are asymptotically dropped such that the number of terms corresponding to expanded tractions becomes *finite*. A system of equations containing the unknown coefficients of the expansion and known constants are then constructed. Approximate tractions are computed by substituting those coefficients solved from simultaneous equations back into the traction expansions. Significant errors are observed for the foregoing two methods when microcracks are closely located.

IV.3.3. Comparisons of SIFs for zeroth order approximation

For the case of two collinear interacting cracks in **Figure 2**, the SIFs solved by applying the zeroth order approximation at center points are listed in **Table 6** and **Table 7** for the inner and outer tips, respectively. Results by Kachanov and Gross are also compared with the exact values given by Erdogan (1962). Kachanov's method which is a special case of Benveniste's method appears to be the best approximation in both tables. If no projection is performed in the center-point approximation, the results are no better than Gross'. However, with a simple stress projection, the center-point method becomes better than the fourth order asymptotic method of Gross. Actually, center-point zeroth order approximation with stress projections is comparable to the method proposed by Kachanov.

Although center-point zeroth order approximation method is improved by the operation of stress projection, the orthogonal function approximation method employed in this paper is shown to be better when **Table 6** and **Table 7** are compared with **Table 2**. Another advantage for the orthogonal function approximation method is that higher accuracy may be achieved by simply increasing the number of order used in the numerical implementation. The entire formulation is highly systematic so that the computer implementation for any order of approximation is easy and straightforward.

Table 6. Comparison of normalized inner-tip SIFs for two interacting collinear cracks

k	Exact	Kachanov	Gross	Zeroth Order Approximation	
				No Projection	Exact Projection
0.9	1.0004		1.0004	1.0004	1.0004
0.75	1.0028		1.0028	1.0026	1.0028
0.5	1.0176		1.0173	1.0144	1.0176
0.25	1.0804		1.0696	1.0507	1.0797
0.2	1.1125	1.112	1.0911	1.0646	1.1109
0.1	1.2551	1.251	1.1564	1.1061	1.2423
0.05	1.4729	1.452	1.2062	1.1380	1.4200
0.02	1.9046	1.809	1.2441	1.1630	1.7039
0.01	2.3716	2.134**	1.2583	1.1727	1.9410
0.001	5.3947	3.401*	1.2719	1.1819	2.7825
0.0001	13.3456	4.731*	1.2733	1.1829	3.6462
10^{-6}	93.0293	7.309*	1.2734	1.1830	5.3798

* from Benveniste et al. (1989) ** 2.138 from Benveniste et al. (1989)

IV.4. Applications of complex stress potentials to crack interaction problems

IV.4.1. Concentrated loadings

Consider the problem of a single crack with half-length a loaded at $x = b$ by normal and shear forces, P and Q, as shown in **Figure 3**. Complex stress potentials which solve this problem completely are readily given in Tada et al.(1973):

$$\left\{ \begin{array}{c} Z_I(z) \\ Z_{II}(z) \end{array} \right\} = \frac{1}{\pi} \left\{ \begin{array}{c} P \\ Q \end{array} \right\} \frac{\sqrt{a^2 - b^2}}{(z-b)\sqrt{z^2 - a^2}} \tag{30}$$

where $z = x + iy$ and $i = \sqrt{-1}$. For normal loading (Mode I) the stresses and displacements are

$$\begin{aligned} \sigma_{xx} &= ReZ_I - yImZ_I' \\ \sigma_{yy} &= ReZ_I + yImZ_I' \\ \tau_{xy} &= -yReZ_I' \end{aligned} \tag{31}$$

and

$$\begin{aligned} 2Gu &= (1-2\nu)Re\overline{Z}_I - yImZ_I \\ 2Gv &= 2(1-\nu)Im\overline{Z}_I - yReZ_I \end{aligned} \tag{32}$$

Table 7. Comparison of normalized outer-tip SIFs for two interacting collinear cracks

k	Exact	Kachanov	Gross	Zeroth Order Approximatic	
				No Projection	Exact Projection
0.9	1.0003		1.0003	1.0004	1.0003
0.75	1.0024		1.0024	1.0026	1.0024
0.5	1.0125		1.0126	1.0144	1.0125
0.25	1.0409		1.0426	1.0507	1.0406
0.2	1.0517	1.052	1.0540	1.0646	1.0510
0.1	1.0863	1.086	1.0880	1.1061	1.0828
0.05	1.1198	1.118	1.1136	1.1380	1.1096
0.02	1.1589	1.154	1.1332	1.1630	1.1339
0.01	1.1841	1.175	1.1406	1.1727	1.1451
0.001	1.2443	1.214*	1.1476	1.1819	1.1591
0.0001	1.2808	1.227*	1.1484	1.1829	1.1613
10^{-6}	1.3212	1.233*	1.1484	1.1830	1.1616

* from Benveniste et al. (1989)

where

$$\overline{Z}_I = \int Z_I(z)\,dz \qquad \text{and} \qquad Z_I' = \frac{dZ_I(z)}{dz}$$

In the case of shear loading (Mode II),

$$\begin{aligned} \sigma_{xx} &= 2ImZ_{II} + yReZ_{II}' \\ \sigma_{yy} &= -yReZ_{II}' \\ \tau_{xy} &= ReZ_{II} - yImZ_{II}' \end{aligned} \tag{33}$$

and

$$\begin{aligned} 2Gu &= 2(1-\nu)Im\overline{Z}_{II} + yReZ_{II} \\ 2Gv &= -(1-2\nu)Re\overline{Z}_{II} - yImZ_{II} \end{aligned} \tag{34}$$

where

$$\overline{Z}_{II} = \int Z_{II}(z)\,dz \qquad \text{and} \qquad Z_{II}' = \frac{dZ_{II}(z)}{dz}$$

Shear modulus and Poisson's ratio are denoted by G and ν, respectively in Eq. (32) and Eq. (34). The displacements in x and y direction are u and v, respectively.

When a microcrack is loaded by only normal pressure, the problem becomes symmetric with respect to the x-axis. Relative horizontal opening displacements vanish and relative vertical opening

displacements are simply twice the vertical displacements along the microcrack line. By contrast, in the case of shear loading, the problem becomes anti-symmetric with respect to the microcrack line. Therefore, the relative vertical opening displacements vanish and the relative horizontal opening displacements are simply two times the horizontal displacement along the microcrack line. See **Figure 4** for a schematic representation.

Accordingly, the effects of normal and shear loadings to vertical and horizontal opening displacements are *uncoupled*. Stress potentials are calculated by Eq. (30). The displacement components along the microcrack line are then obtained through Eq. (32) or Eq. (34). Therefore, for normal loading, we have

$$[\![u]\!] = 0 \qquad \text{and} \qquad [\![v]\!] = 2v|_{y=0} \tag{35}$$

and for shear loading

$$[\![v]\!] = 0 \qquad \text{and} \qquad [\![u]\!] = 2u|_{y=0} \tag{36}$$

Assuming that the total volume of the solid containing the microcrack to be V, with the application of divergent theorem, the average microcrack-induced strain can be written as [Horii and Nemat-Nasser (1983)]

$$\overline{\epsilon^*} = \frac{1}{V}\int_{S_I} ([\![\mathbf{u}]\!] \otimes \mathbf{n} + \mathbf{n} \otimes [\![\mathbf{u}]\!])\, dS_I \tag{37}$$

where $\mathbf{n}$ denotes the normal of the crack lines S_I and vector $[\![\mathbf{u}]\!] = ([\![u]\!], [\![v]\!])^T$ the crack opening displacements. Substituting Eq. (30) into Eq. (32) and Eq. (34) and by the nature of symmetry and anti-symmetry, respectively, of Mode I and Mode II loadings discussed above the induced strains are

$$\begin{Bmatrix} \overline{\epsilon^*_{22}} \\ \overline{\gamma^*_{12}} \end{Bmatrix} = \frac{4(1-\nu^2)}{VE}\sqrt{a^2-b^2}\begin{Bmatrix} P \\ Q \end{Bmatrix} \tag{38}$$

in which the Young's modulus is denoted by E.

IV.4.2. Arbitrary loadings

For any arbitrary forms of loadings $P(x)$ or $Q(x)$, the concept of the famous Green's function is applied to derive to the stress potentials and the strains. The stress potentials given by Eq. (30) and the corresponding strains given by Eq. (38) are for the case of a crack subjected to the concentrated loading applied at a point on the two-dimensional crack line. When a normal or shear loading in the form of an arbitrary function apllied on the crack line, the two equations serve as the Green's

function for this problem. Strains are therefore related to the loadings by integrating the product of loading functions and Eq. (38) over the entire crack line

$$\left\{ \begin{array}{c} \overline{\epsilon_{22}^*} \\ \overline{\gamma_{12}^*} \end{array} \right\} = \frac{4(1-\nu^2)}{VE} \int_{-a}^{+a} \sqrt{a^2 - x^2} \left\{ \begin{array}{c} P(x) \\ Q(x) \end{array} \right\} dx \tag{39}$$

Following the same logic, the corresponding stress potentials can be derived from Eq. (30)

$$\left\{ \begin{array}{c} Z_I(z) \\ Z_{II}(z) \end{array} \right\} = \frac{1}{\pi} \int_{-a}^{+a} \frac{\sqrt{a^2 - x^2}}{(z-x)\sqrt{z^2 - a^2}} \left\{ \begin{array}{c} P(x) \\ Q(x) \end{array} \right\} dx \tag{40}$$

and the corresponding stresses and displacements are obtained by the substitution of stress potentials calculated from Eq. (40) into Eqs. (31) to (34).

IV.4.3. Polynomial loadings

Consider the special cases where loadings are simple polynomials. Assuming that $P(x) = P_n(\frac{x}{a})^n$ and $Q(x) = Q_n(\frac{x}{a})^n$, the integration in Eq. (39) is an Euler integration of the first kind by a change of variable. With the help of the Beta function, strains are written as

$$\left\{ \begin{array}{c} \overline{\epsilon_{22}^*} \\ \overline{\gamma_{12}^*} \end{array} \right\} = \frac{4(1-\nu^2)}{VE} \left\{ \begin{array}{c} P_{2n} \\ Q_{2n} \end{array} \right\} a^2 B(\frac{3}{2}, n + \frac{1}{2}) \tag{41}$$

where the Beta function is defined in terms of the Gamma function $\Gamma(x)$:

$$B(p,q) \equiv \int_0^1 x^{p-1}(1-x)^{q-1}\, dx = \frac{\Gamma(p)\Gamma(q)}{\Gamma(p+q)} \tag{42}$$

Similarly, stress potentials for polynomial loadings can be derived. Listed below are stress potentials for the polynomial loadings up to the fourth order:

$$\begin{aligned}
Z_I^{(0)}(z) = Z_{II}^{(0)}(z) &= \frac{z - \sqrt{z^2 - a^2}}{\sqrt{z^2 - a^2}} \\
Z_I^{(1)}(z) = Z_{II}^{(1)}(z) &= \frac{z^2 - z\sqrt{z^2 - a^2} - a^2/2}{a\sqrt{z^2 - a^2}} \\
Z_I^{(2)}(z) = Z_{II}^{(2)}(z) &= \frac{z^3 - z^2\sqrt{z^2 - a^2} - za^2/2}{a^2\sqrt{z^2 - a^2}} \\
Z_I^{(3)}(z) = Z_{II}^{(3)}(z) &= \frac{z^4 - z^3\sqrt{z^2 - a^2} - z^2a^2/2 - a^4/8}{a^3\sqrt{z^2 - a^2}} \\
Z_I^{(4)}(z) = Z_{II}^{(4)}(z) &= \frac{z^5 - z^4\sqrt{z^2 - a^2} - z^3a^2/2 - za^4/8}{a^4\sqrt{z^2 - a^2}}
\end{aligned} \tag{43}$$

Microcrack opening displacements for a microcrack subjected to polynomial normal and shear loadings

$$\left\{ \begin{array}{c} P(x) \\ Q(x) \end{array} \right\} = \left(\frac{x}{a}\right)^n \cdot \left\{ \begin{array}{c} P_n \\ Q_n \end{array} \right\} \tag{44}$$

can thus be derived by method outlined in this section:

$$[\![\mathbf{u_n}]\!] \equiv \left\{ \begin{array}{c} [\![u_n]\!](x) \\ [\![v_n]\!](x) \end{array} \right\} \equiv A_n(x) \cdot \left\{ \begin{array}{c} P_n \\ Q_n \end{array} \right\} \tag{45}$$

where $A_n(x)$ for $n = 0, 1, 2, 3, 4$ for plane strain are

$$\begin{aligned} A_0(x) &= \frac{4(1-\nu^2)}{E}\sqrt{a^2-x^2} \\ A_1(x) &= \frac{4(1-\nu^2)}{E}\sqrt{a^2-x^2}\left(\frac{x}{2a}\right) \\ A_2(x) &= \frac{4(1-\nu^2)}{E}\sqrt{a^2-x^2}\left(\frac{1}{6}+\frac{x^2}{3a^2}\right) \\ A_3(x) &= \frac{4(1-\nu^2)}{E}\sqrt{a^2-x^2}\left(\frac{x}{8a}+\frac{x^3}{4a^3}\right) \\ A_4(x) &= \frac{4(1-\nu^2)}{E}\sqrt{a^2-x^2}\left(\frac{3}{40}+\frac{x^2}{10a^2}+\frac{x^4}{5a^4}\right) \end{aligned} \tag{46}$$

The factor $(1-\nu^2)$ should be removed from Eq. (46) for plane stress problems. It is noted that microcrack opening displacements corresponding to even-order polynomial loadings are *even* functions. On the other hand, the odd-order polynomial loadings result in *odd* microcrack opening displacement functions. That is,

$$A_n(-x) = (-1)^n A_n(x) \tag{47}$$

for non-negative integers k. Derivations of Eq. (43) and Eq. (46) are carried out with the assistance of symbolic mathematical softwares MAPLE and MATHEMATICA. Similar results may be obtained for any number of n.

Now, assume that there are N cracks which are all aligned such that their normal directions coincide the y-axis. Further, we assume that tensile and shearing forces are applied homogeneously over the solids. By neglecting the interaction effects, the volume average compliances due to the presence of microcracks can be derived by letting $n = 0$ in Eq. (41) and summing over N cracks:

$$\begin{aligned} \frac{\overline{\epsilon^*_{22}}}{P_0} = \frac{\overline{\gamma^*_{12}}}{Q_0} &= \frac{Na^2}{V}\frac{4(1-\nu^2)}{E}B(\frac{3}{2},\frac{1}{2}) \\ &= \frac{1-\nu^2}{E}2\pi\omega \end{aligned} \tag{48}$$

Note that the well-known Taylor's model is recovered by Eq. (48).

IV.5. Local and overall effective elastic moduli

IV.5.1. Local ensemble averaged moduli

Assuming that the distribution of microcracks satisfies reasonable randomness and local homogeneity [Hinch (1977)] and that no microcracks intersect one another, statistical tractions at a local material point are obtained by considering the effect of two-crack interaction and averaging the effect over all possible microcrack configurations. See Ju and Tseng (1992b) for a more detailed discussion. Let $\mathbf{T}(x) = (p(x), q(x))^T$ be the vector of local tractions. Ensemble averaged tractions at a local point are the sum of far field loading-induced component and the component due to two-crack interaction:

$$\langle \mathbf{T} \rangle (\mathbf{x}_1, a_1, \theta_1) = \{ \mathbf{K}_0(\mathbf{x}_1, a_1, \theta_1) + f(\mathbf{x}_1, a_1, \theta_1) \langle \mathbf{K} \rangle (\mathbf{x}_1, a_1, \theta_1) \} \cdot \boldsymbol{\sigma}^{\infty} \tag{49}$$

where the transformation matrix is defined by

$$\mathbf{K}_0(\mathbf{x}_1, a_1, \theta_1) \equiv \begin{bmatrix} \sin^2\theta_1 & \cos^2\theta_1 & -\sin 2\theta_1 \\ -\frac{1}{2}\sin 2\theta_1 & \frac{1}{2}\sin 2\theta_1 & \cos 2\theta_1 \end{bmatrix} \tag{50}$$

and (in the probability space)

$$\langle \mathbf{K} \rangle (\mathbf{x}_1, a_1, \theta_1) \equiv \int_{\Gamma} \mathbf{K}(\mathbf{x}_1, a_1, \theta_1; \mathbf{x}_2, a_2, \theta_2)\, d\mathbf{x}_2 da_2 d\theta_2 \tag{51}$$

in which $\mathbf{K}$ *denotes a two by three matrix whose components are solved from the system of equations described in Section 2. Each column of* $\mathbf{K}$ represents a specific loading condition. The first, second, and third column correspond to the cases in which the solid is loaded only by σ^{∞}_{xx}, σ^{∞}_{yy}, and τ^{∞}_{xy}, respectively. The two components in each column are the normal and shear tractions solved from the system of equations. Local tractions are once again statistically averaged over all possible crack configurations at that material point. With the help of Eq. (39), ensemble averaged local strain takes the form

$$\langle \epsilon^* \rangle (\mathbf{x}) = f(\mathbf{x}) \frac{2(1-\nu^2)}{E} \int_A \int_{\Theta} \int_{-a}^{+a} \sqrt{a^2 - t^2}\, \mathbf{g} \cdot \langle \mathbf{T} \rangle f(a, \theta)\, dt\, da\, d\theta \tag{52}$$

where $\mathbf{g}$ is local-global transformation matrix. Note that the ensemble operator is performed in the probability space, not in the physical space.

Local statistical compliances are then obtained by substituting Eq. (49) into Eq. (52). The microcrack-induced compliances are separable into two parts:

$$\begin{aligned} \langle \mathbf{S}^{*1} \rangle (\mathbf{x}) &= f(\mathbf{x}) \frac{2(1-\nu^2)}{E} \int_A \int_{\Theta} \int_{-a}^{+a} \sqrt{a^2 - t^2}\, \mathbf{g} \cdot \mathbf{K}_0 f(a, \theta)\, dt\, da\, d\theta \\ \langle \mathbf{S}^{*2} \rangle (\mathbf{x}) &= f(\mathbf{x}) \frac{2(1-\nu^2)}{E} \int_A \int_{\Theta} \int_{-a}^{+a} \sqrt{a^2 - t^2}\, \mathbf{g} \cdot \langle \mathbf{K} \rangle f^2(a, \theta)\, dt\, da\, d\theta \end{aligned} \tag{53}$$

IV.5.2. Overall ensemble averaged effective elastic moduli

We assume that *statistical homogeneity* holds. Therefore, the volume average is equal to the ensemble average. Accordingly, the ensemble-volume averaged microcrack-induced compliances take the form

$$\begin{aligned}\overline{\langle \mathbf{S}^{*1} \rangle} &= \frac{(1-\nu^2)}{E}\omega\frac{2}{\pi}\int_A\int_\Theta\int_{-1}^{+1}\sqrt{1-\xi^2}\mathbf{g}\cdot\mathbf{K}_0\, d\xi\, da\, d\theta \\ \overline{\langle \mathbf{S}^{*2} \rangle} &= \frac{(1-\nu^2)}{E}\frac{\omega^2}{\pi}\frac{2}{\pi}\int_A\int_\Theta\int_{-1}^{+1}\sqrt{1-\xi^2}\mathbf{g}\cdot\langle\hat{\mathbf{K}}\rangle\, d\xi\, da\, d\theta\end{aligned} \tag{54}$$

where $\omega = \frac{Na^2}{A}$ denotes the microcracks density parameter. Note that $\overline{\langle \mathbf{S}^{*1} \rangle}$ represents the first-order effects due to the presence of microcracks. Microcrack interaction effects are represented by $\overline{\langle \mathbf{S}^{*2} \rangle}$ which is of the second-order in ω. It is emphasized that our second-order compliance formulation is completely different from the dubious second-order stiffness formulation proposed by Hudson.

Following the Voigt's notation for strains, the ensemble-volume averaged overall constitutive equation is

$$\overline{\langle \mathbf{e} \rangle} = \overline{\langle \mathbf{S} \rangle} \cdot \boldsymbol{\sigma}^\infty \tag{55}$$

where $\mathbf{e} = (\epsilon^*_{xx}, \epsilon^*_{yy}, 2\epsilon^*_{xy})^T$. The overall ensemble-volume averaged compliance consists of three components:

$$\overline{\langle \mathbf{S} \rangle} = \mathbf{S}^\circ + \overline{\langle \mathbf{S}^{*1} \rangle} + \overline{\langle \mathbf{S}^{*2} \rangle} \tag{56}$$

in which, since the solid is assumed to be isotropic linear elastic, the elastic compliance is

$$\mathbf{S}^\circ = \frac{(1+\nu)}{E}\begin{bmatrix} 1-\nu & -\nu & 0 \\ -\nu & 1-\nu & 0 \\ 0 & 0 & 2 \end{bmatrix} \tag{57}$$

Remark 5.2.1: The effective properties normally relate the average strains with the average average stresses or mathematically, $\overline{\langle \mathbf{e} \rangle} = \overline{\langle \mathbf{S} \rangle} \cdot \overline{\langle \boldsymbol{\sigma} \rangle}$. However, in Eq. 55, the relations between the average strains and the far field applied stresses are established. This defines a set of slightly different effective properties. In case that the average stresses are very close to the far filed applied stresses ($\boldsymbol{\sigma}^\infty \simeq \overline{\langle \boldsymbol{\sigma} \rangle}$), the two definitions are equivalent. ∎

IV.6. Some numerical examples

For simplicity, all microcracks are assumed to be of equal size and uniformly distributed in locations. Legendre polynomials of the fourth order are adopted as base functions. The number N in Eq. (9) is therefore set to 4. Twenty unknowns are solved from twenty equations for each two-crack interaction problem. Two categories of problems with different orientation distributions are considered. In the first category, all microcracks are assumed to be alinged (parallel) yet randomly located. The compliance matrix due to the presence of microcracks is

$$\overline{\langle \mathbf{S}^{*1} \rangle} = \frac{1-\nu^2}{E} 2\pi\omega \begin{bmatrix} 0 & 0 & 0 \\ 0 & 1 & 0 \\ 0 & 0 & 1 \end{bmatrix} \tag{58}$$

which is in consistent with the Taylor's model given by Eq. (48). On the other hand, only two components in the 3 by 3 microcrack-interaction induced compliance matrix are non-zero:

$$\overline{\langle \mathbf{S}^{*2} \rangle} = \frac{1-\nu^2}{E} \pi\omega^2 \begin{bmatrix} 0 & 0 & 0 \\ 0 & r_1 & 0 \\ 0 & 0 & r_2 \end{bmatrix} \tag{59}$$

The constants r_1 and r_2 are given in **Table 8** for two cases with and without stress projections. To ensure that no microcracks intersect each other, a small elliptical probabilistic region surrounding a microcrack is excluded when performing the numerical Gauss integration. Major axis of the elliptical probabilistic region coincides the crack line. The lengths of major axes for all computations are twice the crack size. The parameter h is defined as the ratio of minor axis to the crack size. See **Figure 5** for a schematic illustration. A smaller h value implies that stronger interacting microcracks are allowed to appear in the neighborhood of a given microcrack.

Table 8. Results for aligned microcracks by using the fourth order Legendre polynomials.

	r_1		r_2	
h	No Projection	Exact Projection	No Projection	Exact Projection
2.0	1.253	1.253	0.489	0.489
1.5	0.721	0.721	0.572	0.572
1.0	0.248	0.248	0.618	0.618
0.5	-0.006	-0.006	0.528	0.528

Randomly oriented and located microcracks are considered in the second category of examples. Much more computational efforts are required in these cases.

$$\overline{\langle \mathbf{S}^{*1} \rangle} = \frac{1-\nu^2}{E} \pi\omega \begin{bmatrix} 1 & 0 & 0 \\ 0 & 1 & 0 \\ 0 & 0 & 2 \end{bmatrix} \tag{60}$$

Table 11. Results for microcracks with random orientation by using the center point.

h	s_1		s_2		s_3	
	No Projection	Exact Projection	No Projection	Exact Projection	No Projection	Exact Projection
2.0	3.685	3.497	0.405	0.364	6.559	6.265
1.75	3.443	3.928	0.236	0.430	6.411	6.995
1.5	3.279	4.487	0.063	0.509	6.432	7.956

There are three non-zero independent components in the microcrack-interaction induced compliance:

$$\overline{\langle \mathbf{S}^{*2} \rangle} = \frac{1-\nu^2}{\pi E}\omega^2 \begin{bmatrix} s_1 & s_2 & 0 \\ s_2 & s_1 & 0 \\ 0 & 0 & s_3 \end{bmatrix} \tag{61}$$

Since the orientations of the microcracks are random and the original material is isotropic, the overall compliance should be isotropic. In this case, the three components of the overall compliance matrix Eqs. (57), (60), and (61) are all isotropic. Therefor, the property of isotropy is preserved in the ensemble-volume averaging process. Numerical results of s_1, s_2, and s_3 for cases with and without the operation of stress projection are shown in **Table 9**.

Table 9. Results for microcracks with random orientation by using the fourth order Legendre.

h	s_1		s_2		s_3	
	No Projection	Exact Projection	No Projection	Exact Projection	No Projection	Exact Projection
2.0	1.036	1.036	0.014	0.014	2.046	2.046
1.75	-0.364	-0.364	-0.257	-0.257	1.243	1.243
1.5	-1.098	-1.098	-0.573	-0.573	0.408	0.408

As a comparison, **Tables 10** and **11** display the results for the two categories by using only the crack-center points approximations [see Ju and Chen (1991a)].

Table 10. Results for aligned microcracks by using the center point interaction.

h	r_1		r_2	
	No Projection	Exact Projection	No Projection	Exact Projection
2.0	1.173	1.116	0.481	0.447
1.0	0.364	0.022	0.686	0.542
0.5	0.640	-0.398	0.688	0.372

From **Tables 8–11**, we observe that there is no difference on the overall compliances with or without the stress projection procedure when the fourth order Legendre family is employed to approximate the interactions. It suggests that the fourth-order Legendre approximation itself is accurate enough so that a further stress projection dose not affect the results. On the other hand, center point interaction approximation appears to be less accurate. Different results are obtained for the two categories with or without a stress projection. It is observed that the column r_1 in **Table 8** exhibits a decrease as h becomes smaller. Since microcracks are aligned in this case, a decrease in the h value allows more interaction effects from the random second crack which is likely to be approximately stacked on top of the given first crack. As mentioned in Section 2, stacked cracks tend to interact against each other. A shielding effect which decreases the value of r_1 should be expected. Therefore, the trend in the r_1 column in **Table 8** is rational.

IV.7. Conclusions

Accurate microcrack interaction method is incorporated into the framework of statistical micromechanical model to estimate the effective elastic moduli of brittle solids. A linear system of equations is obtained through the numerical function approximation method by using the family of orthogonal base functions. The proposed method is capable of solving the problems of very strongly interacting microcracks. Higher accuracy is achieved by increasing the order used in the approximation and solving the resulting larger system of equations. The system of equations for many-microcrack interaction problems can be constructed in a similar manner.

Complex stress potentials are shown to be a useful tool for the crack-interaction and compliance problems. Based on the single crack stress potentials corresponding to concentrated loads, relevant quantities such as stresses, strains, displacements and complainces are derived for any arbitrary loadings. Simple and useful results are obtained for the special cases of polynomial loadings. Extensive numerical computations are required for the overall ensemble-volume averaged elastic moduli. Numerical examples show that the fourth order Legendre approximation is accurate enough so that further stress projection is not necessary. However, the stress projection should be applied to improve the accuracy if center-point interaction approximation is used.

IV.8. References

1. BENVENISTE, Y., DVORAK, J. Z., AND WUNG, E. C. J., (1989) "On interacting cracks and complex crack configurations in linear elastic media," *Int. J. Solids & Struct.*, vol. 25, pp. 1279–1293.

2. ERDOGAN, F., (1962) "On the stress distribution in plates with collinear cuts under arbitrary loads," *Proceedings, Fourth U. S. National Congress of Applied Mechanics*, pp. 547–553.

3. HASHIN, Z., (1988) "The differential scheme and its application to cracked materials", *J. Mech. Phys. Solids.*, vol. 36, pp. 719–734.

4. GOTTESMAN, T., HASHIN, Z., AND BRULL, M. A., , "Effective elastic moduli of cracked fiber composites", *Advances in Composites Materials*, Proc. ICCM 3, Pergamon Press, Oxford, New York.

5. IOAKIMIDIS, N. I., (1990) "Symbolic computations: A powerful method for the solution of crack problems in fracture mechanics," *Int. J. Frac.*, vol. 43, R39-R42.

6. IOAKIMIDIS, N. I., (1992) "Application of computer algebra to the iterative solution of singular equations", *Comp. Meth. Appl. Mech. Eng.*, vol. 94, pp. 229–237.

7. JU, J. W. AND CHEN, T. M., (1991a), "On effective elastic moduli of two-dimensional brittle solids with interacting microcracks. Part I : Basic formulations", *J. Appl. Mech.*, to appear.

8. JU, J. W. AND CHEN, T. M., (1991b), "On effective elastic moduli of two-dimensional brittle solids with interacting microcracks. Part II : Evolutionary damage models", *J. Appl. Mech.*, to appear.

9. JU, J. W. AND TSENG, K. H., (1992a), "A three-dimensional statistical micromechanical theory for brittle solids with interacting microcracks", *Int. J. Damage Mech.*, vol. 1, pp. 102–131.

10. JU, J. W. AND TSENG, K. H., (1992b), "Recent development in Two-dimensional micromechanical theories for elastic solids with interacting microcracks," in *Recent advances in damage mechanics and plasticity, edited by Ju, J. W., ASME, New York*, pp. 91–101.

11. GROSS, D., (1982), "Spannungsintensitatsfaktoren von ribsystemen (Stress intensity factors of systems of cracks)", *Ing.-Arch.*, vol. 51, pp. 301–310 (in German).

12. HINCH. E. J., (1977), "An averaged-equation approach to particle interactions in a fluid suspension," *J. Fluid Mech.*, vol. 83, pp. 695–720.

13. HORII, H. AND NEMAT-NASSER, S., (1983) "Overall moduli of solids with microcracks: load-induced anisotropy", *J. Mech. Phys. Solids*, vol. 31, pp. 155–171.

14. HORII, H. AND NEMAT-NASSER, S., (1985), "Elastic fields of interacting inhomogeneities", *Int. J. Solids & Struct.*, vol. 21, pp. 731–745.

15. KACHANOV, M., (1985), "A simple technique of stress analysis in elastic solids with many cracks", *Int. J. Fract.*, vol. 28, pp. R11–R19.

16. KACHANOV, M., (1987), "Elastic solids with many cracks: a simple method of analysis", *Int J. Solids & Struct.*, vol. 23, pp. 23–43.

17. MACSYMA, *"MACSYMA reference manual, Version 13*, 1988, Symbolics, Inc., Massachusetts.

18. MAPLE, *"MAPLE reference manual, 5th ed.* by Char, B. W., Geddes, K. O., Gonnet, G. H., Monagan, M. B., and Watt, S. M., Symbolic Computation Group, Department of Computer Science, University of Waterloo, 1988, and Waterloo Maple Publishing, Waterloo, Ontario, Canada, 1990.

19. MATHEMATICA, *"Mathematica: A system for doing mathematics by computer", 2nd ed.* by Wolfram, S., 1991, Addison-Welsley, California.

20. SNEDDON, I. N., AND LOWENGRUB, M., (1969) *"Crack problems in the classical theory of elasticity", John Wiley & Sons, Inc, New York*

21. TADA, H., PARIS, P., AND IRWIN, G., (1974) *"The stress analysis of cracks handbook," Del Research Corp., Pennsylvania*, p. 5.9

IV.9. Figure captions

Figure 1. Coordinate systems for two microcracks.

Figure 2. Three cases of two-crack interaction configurations.

Figure 3. A single crack subjected to a pair of concentrated normal and shear loads.

Figure 4. Symmetry and anti-symmetry for normal and shear loadings.

Figure 5. Active integration domain.

Figure 6. Four cases of microcrack configurations.

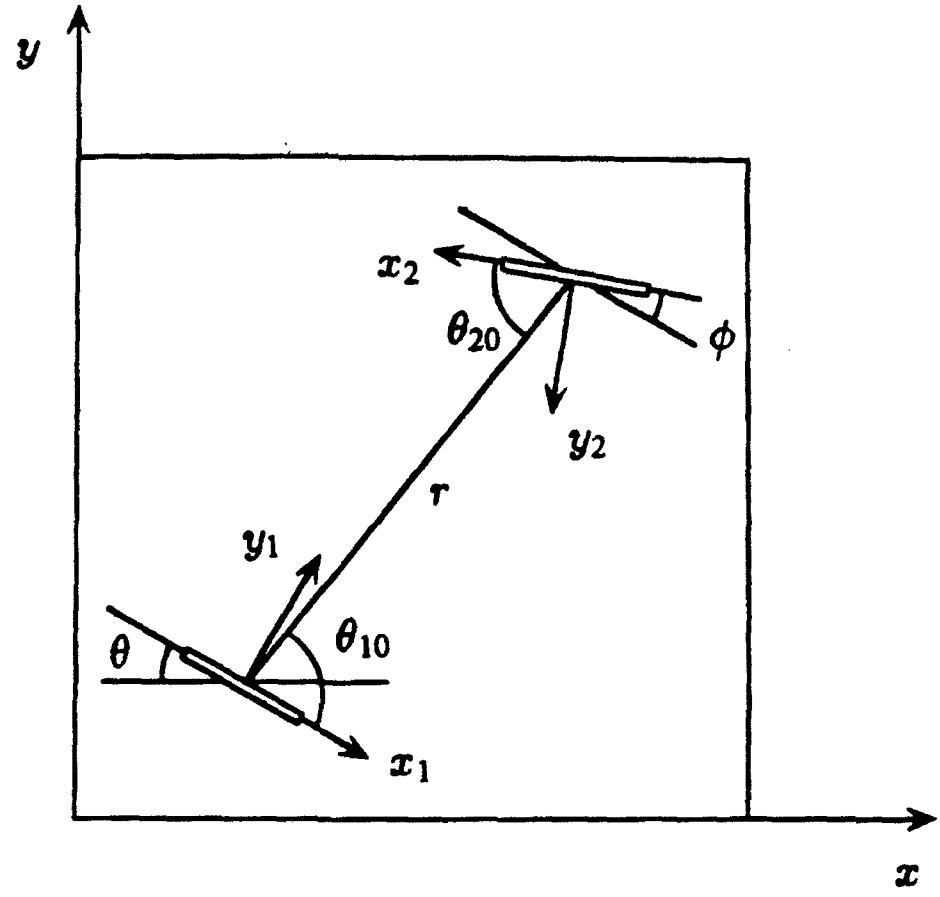

Figure 1. Coordinate systems for two microcracks.

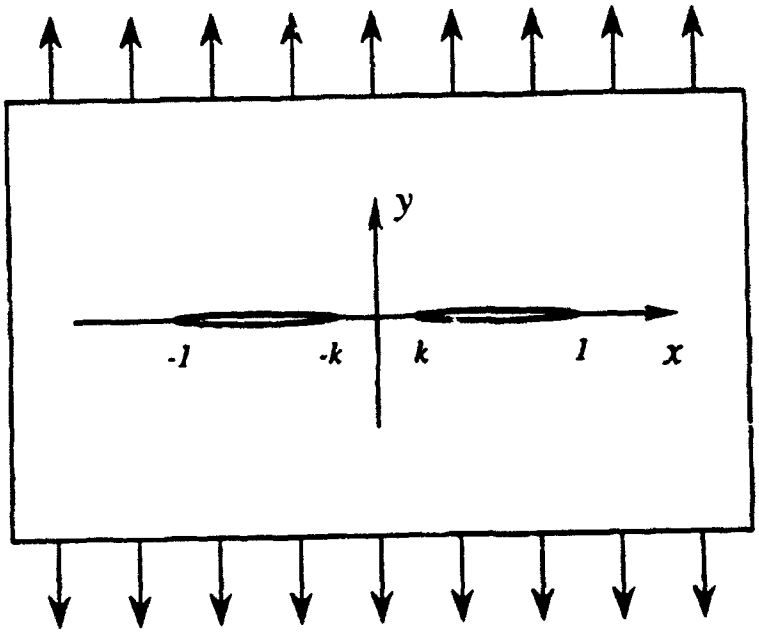

Case 1. Two collinear cracks

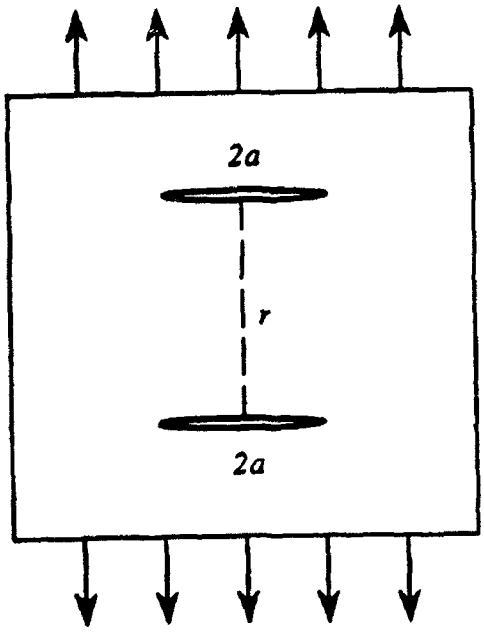

Case 2. Two stacked cracks

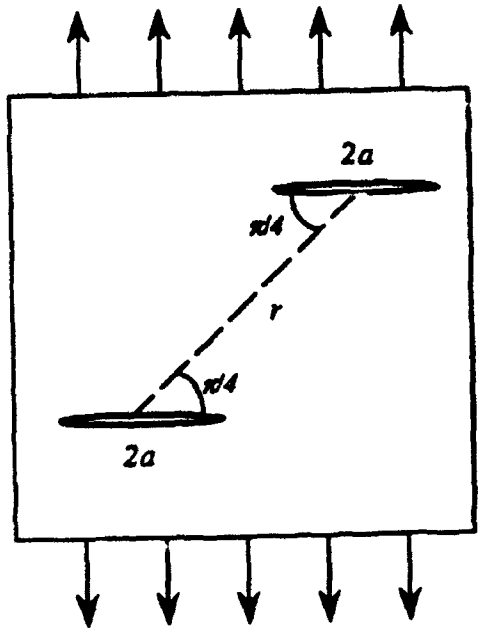

Case 3. Two offset aligned cracks

Figure 2. Three cases of two-crack interaction configurations.

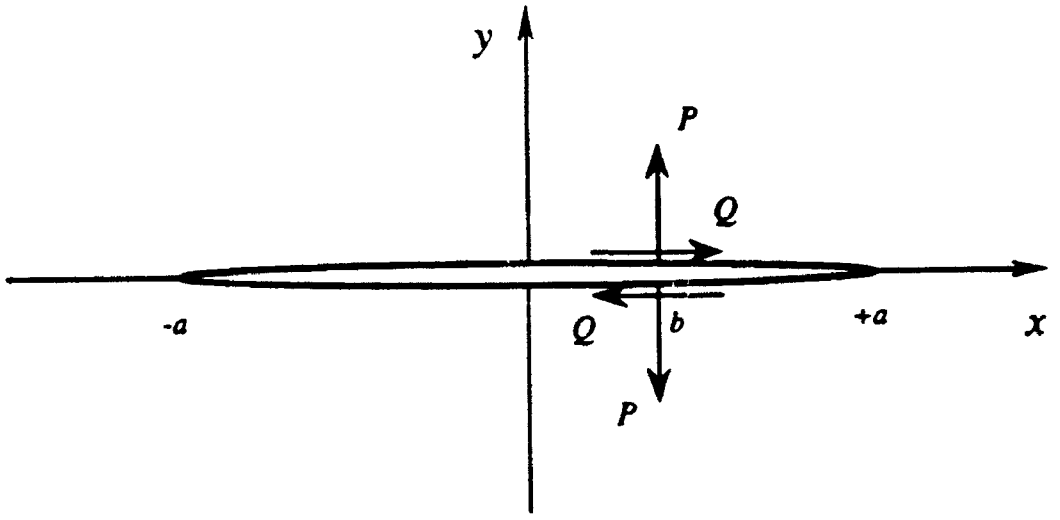

Figure 3. A single crack subjected to a pair of concentrated normal and shear loads.

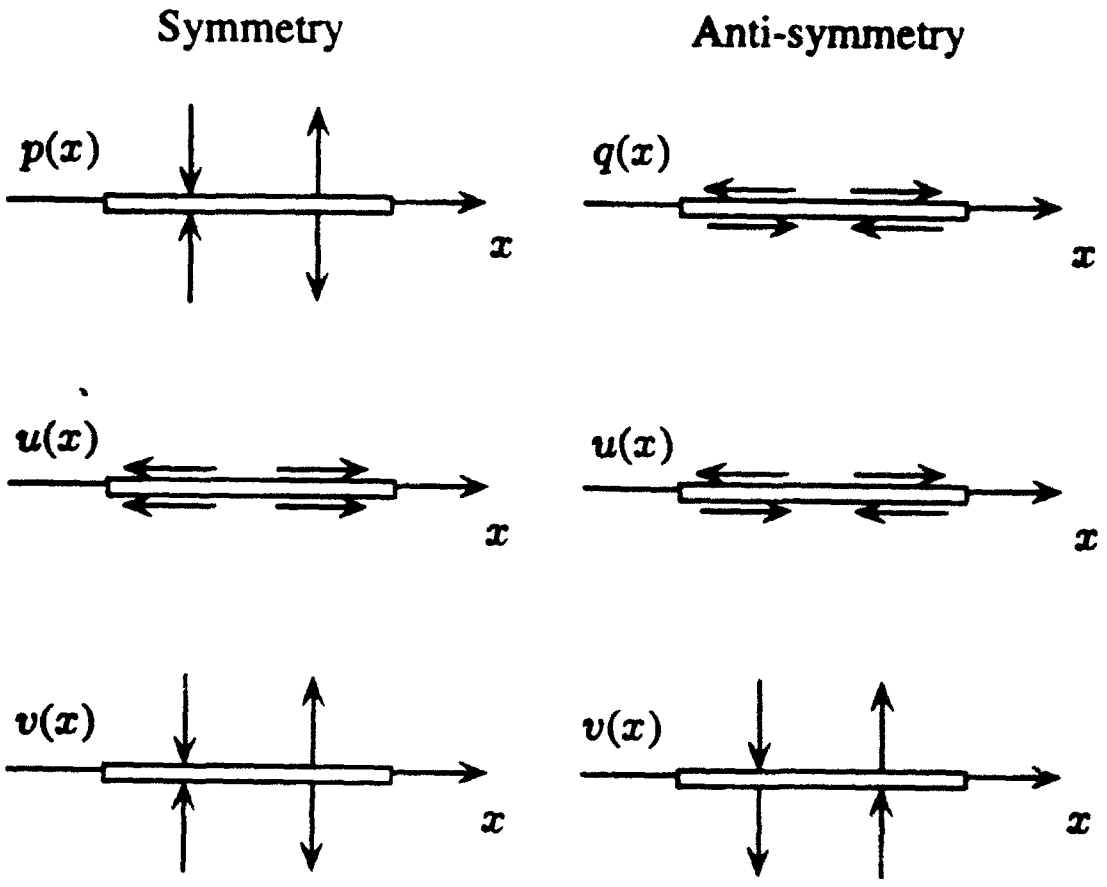

Figure 4. Symmetry and anti-symmetry for normal and shear loadings.

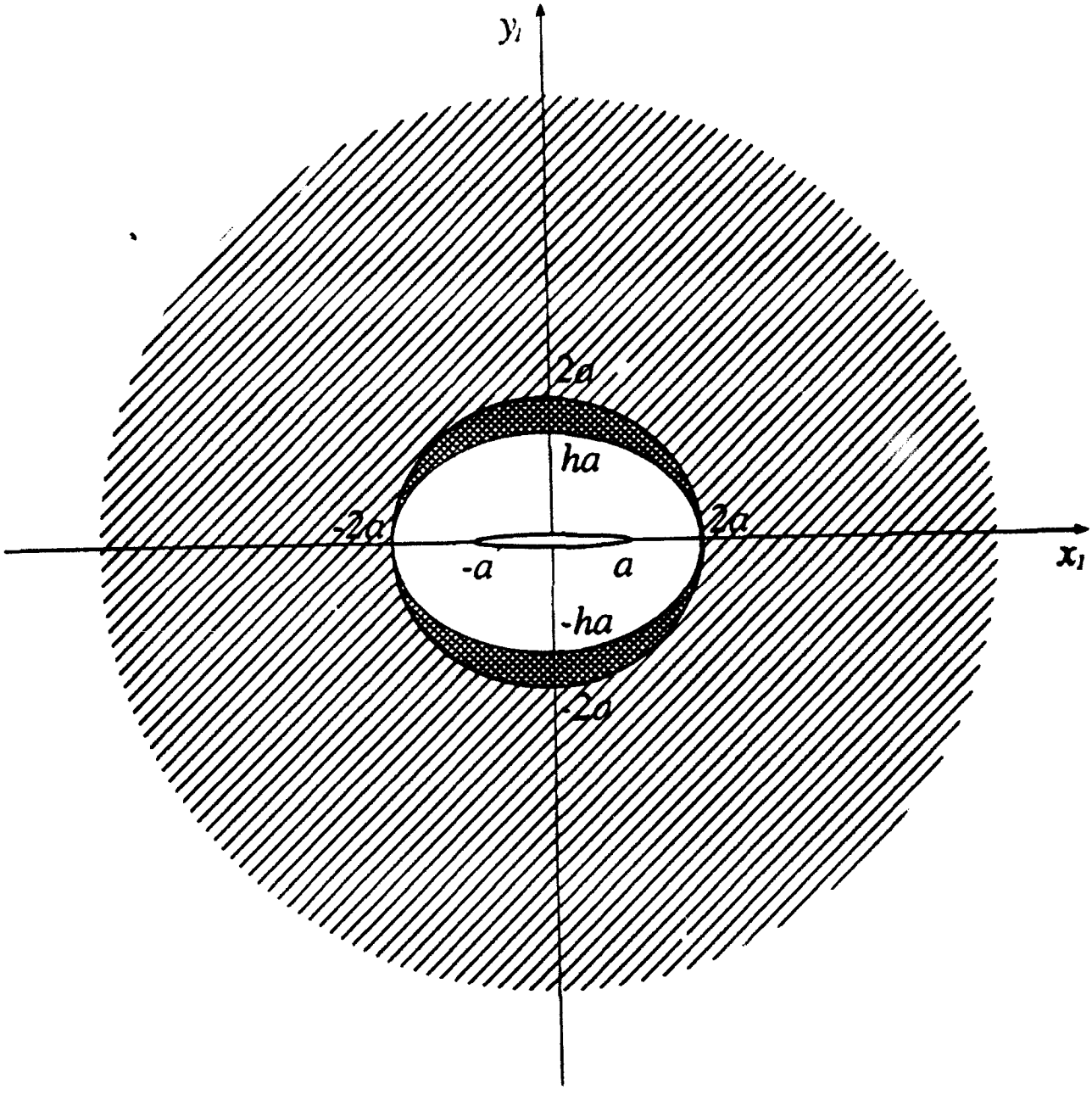

Figure 5. Active integration domain.

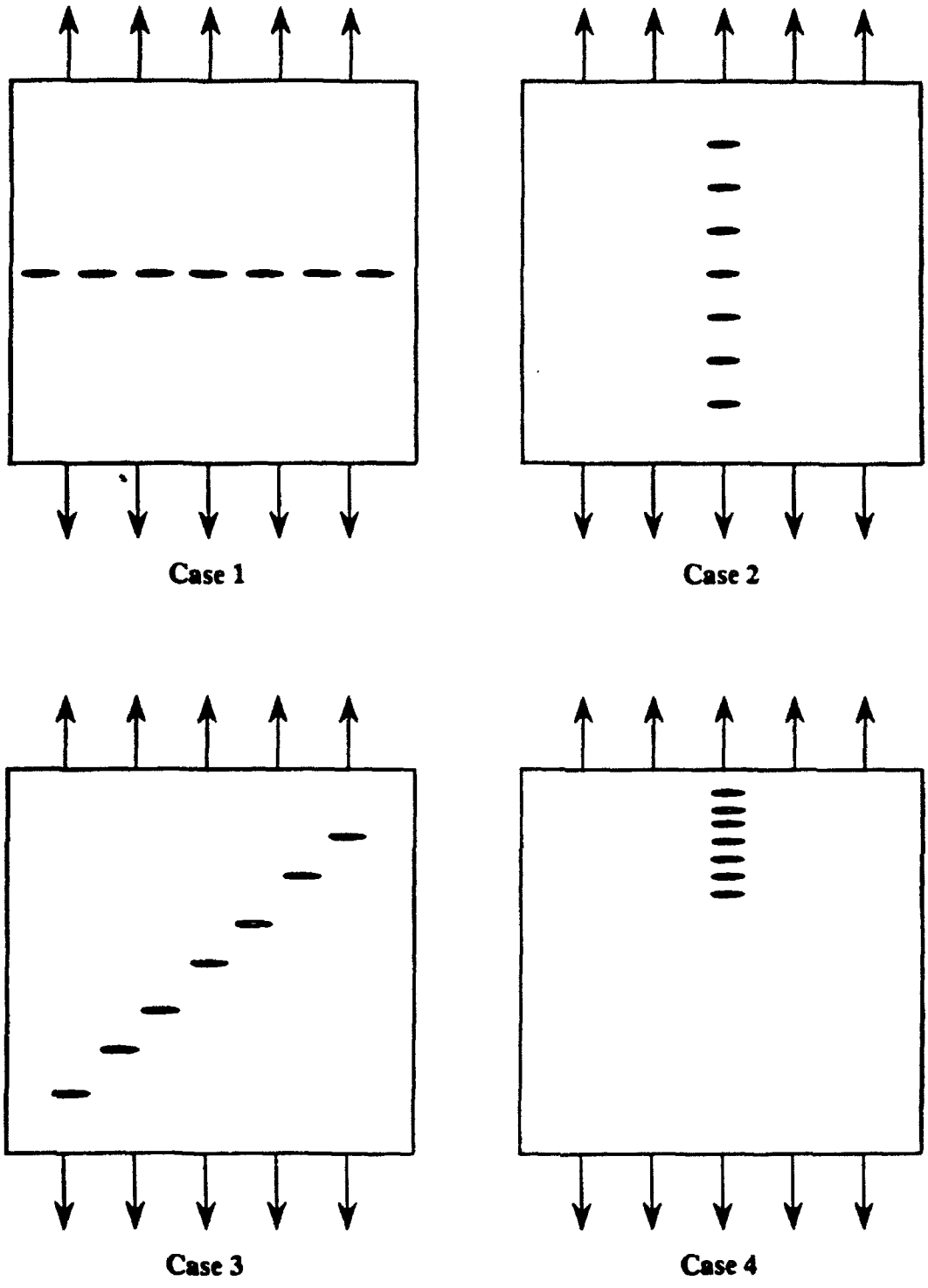

Figure 6. Four cases of microcrack configurations.